

Summer 8-28-2014

# Targeting GRP78 in Cancer with Nucleic Acid Bioconjugates

Pradeepkumar L. Patel  
pradeepkumar.patel@student.shu.edu

Follow this and additional works at: <https://scholarship.shu.edu/dissertations>

 Part of the [Biochemistry Commons](#)

---

## Recommended Citation

Patel, Pradeepkumar L., "Targeting GRP78 in Cancer with Nucleic Acid Bioconjugates" (2014). *Seton Hall University Dissertations and Theses (ETDs)*. 1993.  
<https://scholarship.shu.edu/dissertations/1993>

# **Targeting GRP78 in Cancer with Nucleic Acid Bioconjugates**

*A thesis submitted to Seton Hall University in partial fulfillment of the requirements for the degree of Doctor of Philosophy*

By

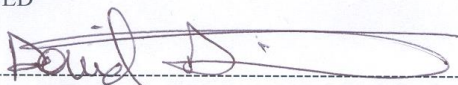
**Pradeepkumar L. Patel**

August 2014

Department of Chemistry and Biochemistry  
Seton Hall University  
South Orange, NJ, USA

We certify that we have read this dissertation and that in our opinion it is adequate to scientific scope and quality as a dissertation for the degree of Doctor of Philosophy.

APPROVED

  
-----

David Sabatino, Ph.D

Research Mentor, Department of Chemistry and Biochemistry, Seton Hall University

  
-----

Cosimo Antonacci, Ph.D

Member of the Dissertation Committee, Department of Chemistry and Biochemistry, Seton Hall University

  
-----

Uri Samuni, Ph.D

Member of the Dissertation Committee, Queens College, CUNY

  
-----

Nicholas H. Snow, Ph.D

Chair, Department of Chemistry and Biochemistry, Seton Hall University

*I dedicate this thesis to  
my parents, Lavjibhai and Indumati, and my wife, Bansi,  
for their constant support and unconditional love.*

## ABSTRACT

Nucleic acid bioconjugates have gained widespread use in medicinal chemistry research programs aimed at fighting human malignancies such as cancer, diabetes, genetic and infectious diseases. Their popularity stems from their ability to accelerate the drug development process by conjugating chemical functionality that may improve the pharmacology of a bioactive nucleoside. Moreover, this strategy has been proven to be effective with small molecule nucleoside analogs and those derived from lengthy oligonucleotide sequences. Considering these fruitful applications, my research and this thesis aims to explore the synthesis, characterization and therapeutic potential of novel classes of nucleic acid bioconjugates.

These are based on, aminoacyl nucleolipids, from which a simple, versatile and efficient synthesis strategy has been developed for this new class of DNA binding molecules as described in Chapter 2 of this thesis. This bioconjugate exhibited GRP78 oncogene binding affinity ( $K_D$ : 0.25 mM) as characterized by PAGE gel shift assays. Its binding affinity towards the GRP78 oncogene was also confirmed using circular dichroism spectroscopy, and thermal denaturation experiments. Moreover, dynamic light scattering experiments also demonstrated increases in particle sizes after binding of this molecule to the GRP78 oncogene. In a single dose (10  $\mu$ M) screen against a panel of 60 cancer cell lines, the aminoacyl nucleolipid demonstrated selective anti-leukemic activity, highlighting its potential in anti-cancer research programs.

In Chapter 3, the synthesis, biophysical properties and GRP78 DNA cleavage activity of a phthalocyanine-linked oligonucleotide will be highlighted for photodynamic oncogene therapy applications. The synthesis and characterization of cancer-targeting oligonucleotide (CTO) and its bio-conjugation to a chemically resilient photosensitizer, a carboxy-derived perfluorophthalocyanine (Pc), enabled the production of a unique bioconjugate for potential anti-

cancer applications. In this study, the Pc-CTO demonstrated the ability to hybridize to complementary GRP78 DNA and mRNA oncogenes. In a photochemical oxidative cleavage assay, the Pc-CTO triggered significant degradation of the GRP78 oncogenes underscoring its potential in GRP78-targeting photodynamic therapy.

In Chapter 4, a study into the design, synthesis and structure-function relationships of a new class of nucleic acid bioconjugates is presented. The diacylhydrazine-linked dinucleosides represent a novel class of nucleic acid bioconjugates that are proposed to improve the structural stability of turn conformations in DNA or RNA hairpin secondary structures. My advances in the synthesis, structure elucidation and biological evaluation of these putative hairpin mimics will be described. In sum, this thesis will serve to highlight my contributions to the flourishing field of nucleic acid bioconjugation for GRP78-targeting for anti-cancer applications.

## ACKNOWLEDGEMENTS

Each and every event, either small or big in nature is itself a new creation. As one flower makes no garland, this research would not have been fulfilled and reaped as a healthy fruit without the whole hearted encouragement, faith and active involvement of my mentors, friends and well-wishers. Thank you is a very small word to describe what I wanted to say about my mentor, Dr. Sabatino and my friends. I would like to express the deepest gratitude to my mentor, Dr. David Sabatino for accepting me in his group and giving me opportunity to gain a doctorate degree under his guidance. I would like to acknowledge the continuous encouragement and help extended to me by Dr. David Sabatino for his mentorship on my thesis work. He has been my sole guide and philosopher throughout the period of my work. Without his spontaneous support and expert guidance this project would not have come to fruition. I would like to thank him for all of his guidance, encouragement and support in personal and professional life at my happiest and darkest points. Dr. Sabatino remains my best role model for a scientist, mentor, teacher and person. He has the great attitude (to teach at all levels), and element of genius. Without his guidance and persistence help this dissertation would not have been possible. In short, I can say that I found “**ELEMENT # 119 in Periodic Table: SABATINONIUM**”.

I would also like to thank Dr. Sergiu Gorun, Dr. Cecilia Marzabadi, Dr. Uri Samuni and Reeta Yadav for being my co-mentors in my collaborative projects. I could not complete my projects without their infinite support and guidance. I would like to express my gratitude to Dr. Antonacci for being a part of my dissertation committee. I will always remember his scientific advice, knowledge and many insightful discussions and suggestions.

My special thank you goes to Dr. Murphy for his teaching and guidance on the NMR. I will forever be thankful to Professors Nicholas Snow, Yuri Kazakevich, John Sowa and Stephen Kelty. They have been helpful in providing advice many times. I would like to thank Maureen and Rose for always going out of their way to assist me.

A true friend is greatest of all blessing; a journey becomes easier when you travel together, especially surviving and staying in a grad school. I consider myself as a lucky fellow to be a member of what we call “CLUB 419” and refer to Mayur Patel, Niki Rana, Lathamol Kurian, Mariana Philips, Emily Borland, Chris Cultrara, Dan Goldman, Eric Carrion and adopted member of club 419, Lauren Ridley, Hemant Patel, Emi Hanawa. These friends mean a lot to me. I could not have survived without them. We all are like different bio-active molecules and attached through Dr. Sabatino’s secret bond to form the best bioconjugate group at Seton Hall.

I especially thank you my hard working parents. I would like to thank their infinite sacrifices, their unconditional love and care. I love them so much and I could not do it without their physical, mental and financial support. My dad is my best friend and I would like to thank him for all his advice and support. Special thanks to the newest member of my family, Bansi, my lovely wife and her family who have all been supportive and caring. I would like to also thank my aunts, uncles and cousins. You all have pushed me and believed in me. Special thanks to my aunt Juliet and uncle Sheldon for without you none of this would be possible.

I am extremely thankful and grateful to my wife Bansi for her patience, support, encouragement and love. I am married to the best person out there for me. I thank her for putting up with me, I know it is not easy. These past several months have not been easy, both personally and educationally. I truly thank Bansi for sticking by my side, giving me encouragement and



having faith in me. At last, I also thank my friends back home (too many to list here but you know who you are!) for providing support and friendship that I needed. If I am forgetting you, you know you're in my heart always. "*Micchami Dukkadam*"

## TABLE OF CONTENTS

DEDICATION	iii
ABSTRACT	iv
ACKNOWLEDGEMENTS	vi
TABLE OF CONTENTS	ix
ABBREVIATIONS AND SYMBOLS	xii
LIST OF FIGURES	xxi
LIST OF SCHEME	xxvi
LIST OF TABLES	xxviii
<b>CHAPTER 1: ANTI-CANCER APPLICATIONS OF NUCLEIC ACID</b>	<b>1</b>
<b>BIOCONJUGATES:</b>	
1.1 GENERAL INTRODUCTION OF NUCLEIC ACID BIOCONJUGATES AND THEIR RELEVANCE IN CANCER THERAPY	1
1.2 SMALL MOLECULE-NUCLEIC ACID BIOCONJUGATES IN CANCER THERAPY	3
1.3 CANCER-TARGETING THERAPY WITH OLIGONUCLETIDE BIOCONJUGATES	7
1.3.1 Synthesis of oligonucleotides	8
1.3.2 Synthesis and anti-cancer applications of antisense oligonucleotide bioconjugates	11
1.3.3 Synthesis and anti-cancer applications of aptamer oligonucleotide	18

bioconjugates	
1.3.4 Synthesis and anti-cancer applications of short-interfering RNA (siRNA)	20
bioconjugates	
1.4 THESIS OBJECTIVES	24
1.5 REFERENCES	25
<b>CHAPTER 2: SYNTHESIS, DNA BINDING AND ANTI-LEUKEMIC ACTIVITY</b>	<b>28</b>
<b>OF AN AMINOACYL NUCLEOLIPID</b>	
2.1 GENERAL INTRODUCTION	28
2.2 CHAPTER OBJECTIVE	30
2.3 SYNTHESIS, DNA BINDING AND ANTI-LEUKEMIC ACTIVITY OF AN	33
AMINOACYL NUCLEOLOPID	
2.3.1 Abstract	34
2.3.2 Introduction	34
2.3.3 Results and discussion	35
2.3.4 Synthesis of an aminoacyl nucleolipid	35
2.3.5 DNA binding studies of aminoacyl nucleolpid, <b>2.6</b>	39
2.3.6 Anti-cancer activity of aminoacyl nucleolipid, <b>2.6</b>	44
2.3.7 Conclusions	45
2.3.8 Experimental section	46
2.4 REFERENCES	61

<b>CHAPTER 3: PHTHALOCYANINE-NUCLEIC ACID BIOCONJUGATES AND THEIR APPLICATIONS IN CANCER</b>	<b>64</b>
3.1 GENERAL INTRODUCTION	64
3.2 CHAPTER OBJECTIVES	66
3.3 CHEMICALLY ROBUST FLUOROALKYL PHTHALOCYANINE- OLIGONUCLEOTIDE BIOCONJUGATES AND THEIR GRP78 ONCOGENE PHOTOCLEAVAGE ACTIVITY	68
3.3.1 Abstract	68
3.3.2. Introduction	69
3.3.3 Results and Discussion	72
3.3.4. Conclusions	80
3.3.5. Experimental section	80
3.4 REFERENCES	91
<b>CHAPTER 4: PROGRESS TOWARDS THE SYNTHESIS, STRUCTURAL ANALYSIS AND GRP78 BINDING OF A DIACYLHYDRAZINE LINKED DINUCLEOSIDE</b>	<b>94</b>
4.1 GENERAL INTRODUCTION	94
4.2 CHAPTER OBJECTIVES	98
4.3 STABILIZING TURN CONFORMATIONS IN DNA HAIRPINS BY DIACYLHYDRAZINE-LINKED NUCLEIC ACIDS	100

4.3.1 Abstract	100
4.3.2. Introduction	101
4.3.3. Results and discussion	105
4.3.4. Conclusions	113
4.3.5. Experimental section	114
4.4 REFERENCES	120
<b>CHAPTER 5: CONCLUSIONS AND CONTRIBUTIONS TO KNOWLEDGE</b>	123
5.1 CONCLUSIONS AND CONTRIBUTIONS TO KNOWLEDGE MADE IN THIS THESIS	123
5.1.1 Aminoacyl Nucleolipids as DNA Binding Molecules with Anti-Leukemic Activity	123
5.1.2 A Fluoroalkyl Phthalocyanine-Cancer Targeting Oligonucleotide Bioconjugate and its Oncogene Photocleavage Activity	124
5.1.3 The Diacylhydrazine DNA Turn	125
5.2 PUBLICATIONS, INVENTION DISCLOSURES AND CONFERENCE PRESENTATIONS	126

## ABBREVIATIONS AND SYMBOLS

$\mu\text{g}$	Microgram
$\mu\text{L}$	Microliter
$\mu\text{M}$	Micromolar
$^{18}\text{F}$	Fluorine
5FU	5-flourouracil
$^{64}\text{Cu}$	Copper
A or Ala	Alanine
Abs	UV absorbance measured at 260 nm
AchR	Acetylcholine receptor
ADCC	Antibody dependent cell cytotoxicity
ADTT	3-amino-1,2,4-dithiazole 5 thione
ANOVA	Analysis of variance
AON	Antisense oligonucleotide
Arg	Arginine
aRNA	Antisense RNA
BAIB	(Diacetoxiyodo)benzene
BSA	Bovine serum albumin
C or Cys	Cysteine
$\text{Ca}^{2+}$	Calcium ion
CATB	Cetyl triethylammonium bromide
CCD-11Lu	Human lung fibroblast

CD	Circular dichroism
CD-21	Cluster of differentiation 21 (glycoprotein)
CO <sub>2</sub>	Carbon dioxide
COSY	Correlation spectroscopy
CPG	Controlled pore glass
CTO	Cancer targeting oligonucleotide
CTP	Cancer targeting peptide
CuAAC	Copper catalyzed azide alkyne cycloaddition
D or Asp	Aspartate
DCH	Doxorubicine conjugated hairpin
DCM	Dichloromethane
DIC	<i>N,N'</i> -diisopropylcarbodiimide
DIEA	<i>N,N'</i> -diisopropylethylamine
DLS	Dynamic light scattering
DMAP	Dimethoxyaminopyridine
DMEM	Dulbecco's modified eagle medium
DMF	Dimethylformamide
DMF	<i>N,N'</i> -dimethyl formamide
DMSO	Dimethyl sulfoxide
DMSO	Dimethylsulfoxide
DMT	Dimethoxytrityl
DNA	2'-deoxyribonucleic acid
DOTA	1,4,7,10-tetraazacyclododecane-1,4,7,10-tetraacetic acid

DOX	Doxorubicin
DTPA	Diethylenetriaminepentaacetic acid
DTT	Dithioreitol
DU145	Prostate cancer cell line
EDC	1-Ethyl-3-(3-dimethylaminopropyl)carbodiimide
EDTA	Ethylene-diamine tetraacetate dehydrate
EEDQ	N-Ethoxycarbonyl-2-ethoxy-1,2-dihydroquinoline
EEDQ	N-Ethoxycarbonyl-2-ethoxy-1,2-dihydroquinoline
EGCG	Epigallocatechin gallate
EM	Emission
ER	Endoplasmic reticulum
ER	Endoplasmic reticulum
ESI-MS	Electrospray ionization mass spectrometry
EtOH	Ethanol
ETT	5-ethylthiotetrazole
FA	Folic acid
FA	Formic acid
FBOA	<i>P</i> -fluorobenzyloxime acetyl
FBS	Fetal bovine serum
FDA	Food and drug administration
FGF-R	Fibroblast growth factor receptor
FITC	Fluorescein isothiocyanate
Fmoc	Fluorenylmethyloxycarbonyl



g	Gram	
G or Gly	Glycine	
g/mol	Grams pre mole	
GRP78	Glucose regulated protein 78 kda	
G-tetrads	G-tetraplexes	
H	Hours	
HATU	(1-[Bis(dimethylamino)methylene]-1H-1,2,3-triazolo[4,5-b]pyridinium hexafluorophosphate)	3-oxid
HB	Hepatoblastoma	
HCTU	O-(1H-6-Chlorobenzotriazole-1-yl)-1,1,3,3-tetramethyluronium hexafluorophosphate	
HDFa	Human dermal fibroblast	
HepG2	Human hepatocellular liver carcinoma cell line	
HER-2	Human epidermal growth factor receptor 2	
HIF-1	Hypoxia-inducible factor 1	
HNK	Honokiol	
HOBt	1-hydroxybenzotriazole	
hPTN	Human pleiotrophin	
HRMS	High resolution mass spectrometry	
HRP	Horseradish peroxidase	
HSP	Heat shock protein	
HSP70	Heat shock protein 70 kda	
HYD-1	Hybrid peptide	
IC <sub>50</sub>	Concentration of inhibitor which causes 50% inhibition	

ID-PFG	Indirect Pulse field gradient
Ile	Isoleucine
Ile	Isoleucine
IR	Infrared
KBr	Potassium bromide
KCl	Potassium chloride
K <sub>D</sub>	Binding affinity
kDa	Kilodalton
KSP	Kinesin spindle protein
LC/MS	Liquid chromatography mass spectrometry
Leu	Leucine
LH-RH	Luteinizing hormone releasing hormone
LNP	Lipid nanoparticle
M.W.	Molecular weight
<i>m/z</i>	Mass to charge ratio
mAb	Monoclonal antibody
MDR	Multi drug resistance
Me6652/4	Melanoma cells
MeCN	Acetonitrile
MeOH	Methanol
mg	Milligram
MgCl <sub>2</sub>	Magnesium chloride

MHC	Major histocompatibility complex
mM	Millimolar
mol	Mole
MONs	Modified oligonucleotide
mRNA	Messenger RNA
MS	Mass spectrometry
MW	Microwave
N:P	Nitrogen to phosphate ratio
NaCl	Sodium chloride
NaHPO <sub>4</sub>	Sodium hydrogen phosphate
NaOAc	Sodium acetate
NBO	Natural bond orbital
nBu-OH	N-Butanol
NCI	National cancer institute
NH <sub>4</sub> OH	Ammonium hydroxide
NIR	Near infrared
NK	Natural killer
NMM	<i>N</i> -methylmorpholine
NMP	<i>N</i> -methylpyrrolidinone
NMR	Nuclear magnetic resonance
NOTA	1,4,7-triazacyclononane-1,4,7-triacetic acid
OBOC	One-bead one compound
Oh	Hydrodynamic radii

PAGE	Polyacrylamide gel electrophoresis
Pbf	Ng-2,2,4,6,7-pentamethyldihydrobenzofuran-5-sulfonyl
PBS	Phosphate buffered saline
Pc	Phthalocyanine
PDA	Photodiode array
PDT	Photodynamic therapy
Pep42-QD	Pep42- quantum dots
PET	Positron emission tomography
P-gp	P-glycoprotein
pIII	Filamentous phage protein III
PNA	Peptide nucleic acid
Pro	Proline
PS-DVB	Poly(styrene/divinyl benzene)
PSI	Peptide scientific inc.
PVDF	Polyvinylidene difluoride
pVIII	Filamentous phage protein VIII
R	Arginine
RGD	Arginine-glycine-aspartic acid
RIF-1	Radiation induced fibrosarcoma
RIPA	Radioimmunoprecipitation assay
RISC	RNA-induced silencing complex
RNA	Ribonucleic acid
RNAi	RNA interference

RP-HPLC	Reverse-phase high performance liquid chromatography
RT	Retention time
SEM	Standard error of the mean
Sf-9	Spodoptera frugiperda 9
shDNA	Small hairpin dna
shRNA	Small hairpin DNA
siRNA	Small interfering RNA
SJSA-1	Osteosarcoma cells
SPPS	Solid phase peptide synthesis
SRB	Sulforhodamine B
ssDNA	Single strand DNA
T or Thr	Threonine
TAE	Tris-acetate-EDTA
TBE	Tris/boric acid/EDTA buffer
<i>t</i> -Bu	Tertiary butyl
TE2A	Tetraazamacrocycles
TEA	Triethylamine
TEM	Transmission electron microscopy
TEMPO	(2,2,6,6-Tetramethylpiperidin-1-yl)oxy
TES	Triethylsilane
TETA	1,4,8,11-tetraazacyclotetradecane-1,4,8,11-tetraacetic acid
TFA	Trifluoroacetic acid
TFE	2,2,2-trifluoroethanol

TGF- $\beta$	Transforming growth factor beta
TGGE	Temperature gradient gel electrophoresis
THF	Trihydroflouride
Thr	Threonine
TLC	Thin layer chromatography
TM	Trademark
TMB	3,3',5,5'tetramethylbenzidine
Tris-HCl	<b>Tris(hydroxymethyl)aminomethane hydrochloride</b>
Tyr	Tyrosine
UPR	Unfolded protein response
UV-Vis	Ultraviolet-visible
v/v	Volume per volume
Val	Valine
VEGF	Vascular endothelial growth factor
$\epsilon$ -Ahx	Aminohexanoic acid
$\Theta$	Molar ellipticity
$\Lambda$	Wavelength

## LIST OF FIGURES

### CHAPTER 1

<b>Figure 1.1</b>	siRNA:LNP complexes for combination therapy in human cancer clinical trials.	2
<b>Figure 1.2</b>	Terminal hydroxyl groups (2', 3' and 5'-OH) on the nucleic acid core that can serve as possible points of attachment with other bio-active molecules or functional groups.	3
<b>Figure 1.3</b>	General structural and chemical modifications of nucleoside and nucleotide analogues.	4
<b>Figure 1.4</b>	Chemical structures of anticancer nucleoside and nucleotide analogues in clinical applications.	6
<b>Figure 1.5</b>	Rational design of an oligonucleotide bioconjugate	8
<b>Figure 1.6</b>	Antisense mechanism of inhibiting mRNA protein translation	12
<b>Figure 1.7</b>	5'-Cholesterol conjugate antisense phosphorothioate oligonucleotide, 1.14.	14
<b>Figure 1.8</b>	Potent anti-cancer drugs used in combination or conjugated to antisense oligonucleotides	15
<b>Figure 1.9</b>	In vivo effects of RGD-antisense oligonucleotide (623).	16
<b>Figure 1.10</b>	Structures and models of DCH.	19
<b>Figure 1.11</b>	The RNAi mechanism of action.	21

### CHAPTER 2

<b>Figure 2.1</b>	Structures of synthetic aminoacyl nucleolipids	30
<b>Figure 2.2</b>	Chemical structure and DNA-binding interactions of aminoacyl nucleolipid, 2.6.	32
<b>Figure 2.3</b>	Graphical abstract describing the binding of an aminoacyl nucleolipid bioconjugate to the oncogene GRP78 DNA sequence.	33

<b>Figure 2.4</b>	CD spectrum of <b>2.6</b> (0.2-3.9 mM) in phosphate buffer at 25 °C.	39
<b>Figure 2.5</b>	HPLC chromatograms (260 nm) and corresponding mass spectra data of GRP78 DNA (A) sense (ss) and (B) antisense (as) strands	40
<b>Figure 2.6</b>	Gel shift assay for GRP78 DNA with <b>2.6</b> .	41
<b>Figure 2.7</b>	Thermal denaturation curves. Changes in % hyperchromicity at 260 nm versus temperature of GRP78 DNA (1.1 μM) in the presence of ligand <b>2.6</b> (0.2-3.9 mM).	42
<b>Figure 2.8</b>	Circular Dichorism (CD) spectrum of GRP78 DNA (1.1 μM) with complexing ligand <b>2.6</b> (0-3.9 mM) in phosphate buffer.	43
<b>Figure 2.9</b>	Cell death of human leukemia cell lines following treatment with <b>2.6</b> (10 μM) for 48 h.	46
<b>Figure 2.10</b>	NCI 60 cancer cell line one-dose screen.	60
 <b>CHAPTER 3</b>		
<b>Figure 3.1</b>	MPcs-nucleic acid conjugates for applications in detection and photodynamic therapy	66
<b>Figure 3.2</b>	Mechanism of action of Pc-CTO bioconjugates.	68
<b>Figure 3.3</b>	Graphical abstract representation of A. journal cover art image of perfluorophthalocyanine-GRP78 DNA photo-oxidation and cleavage activity, in addition to, B. perfluorophthalocyanine-GRP78 mRNA aerobic illumination and cleavage pattern at oxidized sites.	69
<b>Figure 3.4</b>	F <sub>48</sub> H <sub>7</sub> PcZn-GRP78 cancer-targeting oligonucleotide (CTO) bioconjugate, <b>3.14</b> .	72
<b>Figure 3.5</b>	UV-Vis electronic absorption spectra of F <sub>48</sub> H <sub>7</sub> (COOH)PcZn, <b>3.10</b>	74
<b>Figure 3.6</b>	a) Photooxidation of β-citronellol in EtOH by <b>3.10</b> , ("ZnPc").	75
<b>Figure 3.7</b>	Thermal denaturation curves of PcDNA-DNA ( <b>3.14:3.15</b> ), PcDNA-RNA ( <b>3.14:3.16</b> ), DNA-DNA ( <b>3.17:3.15</b> ), RNA-DNA ( <b>3.17:3.16</b> ) hybrids	77
<b>Figure 3.8</b>	CD spectra of PcDNA-DNA ( <b>3.14:3.15</b> ), PcDNA-RNA ( <b>3.14:3.16</b> ), DNA-DNA ( <b>3.17:3.15</b> ), RNA-DNA ( <b>3.17:3.16</b> ) hybrid	78



<b>Figure 3.9</b>	24% PAGE for the photo-oxidation and piperidine cleavage pattern of a) <b>3.14:3.15</b> and b) <b>3.14:3.16</b> .	79
<b>Figure 3.10</b>	Schematic representation of the catalytic oxidation equipment.	83
<b>Figure 3.11</b>	UV-Vis electronic absorption spectra of F <sub>48</sub> H <sub>7</sub> PcZn-CTO bioconjugate, <b>3.14</b> .	85
<b>Figure 3.12</b>	HPLC trace of GRP78 CTO, <b>3.13</b> .	86
<b>Figure 3.13</b>	HPLC trace of GRP78 DNA, <b>3.15</b> .	86
<b>Figure 3.14</b>	HPLC trace of GRP78 mRNA, <b>3.16</b> .	87
<b>Figure 3.15</b>	HPLC trace of F <sub>48</sub> H <sub>7</sub> PcZn-CTO bioconjugate, <b>3.14</b> .	87
<b>Figure 3.16</b>	24% PAGE for the photo-oxidation and piperidine cleavage reactions.	90

#### CHAPTER 4

<b>Figure 4.1</b>	General structure of a DNA hairpin.	94
<b>Figure 4.2</b>	Structures of nonionic backbone modified oligonucleotides.	96
<b>Figure 4.3</b>	Structures of loop-modified shDNA.	98
<b>Figure 4.4</b>	Structures of phosphodiester, <b>4.18</b> and diacylhydrazine, <b>4.19</b> , linked T:A dimer	102
<b>Figure 4.5</b>	Small molecule GRP78 inhibitors [31-34].	104
<b>Figure 4.6</b>	Structures and models of A. (ApT), native DNA, <b>4.18</b> and B. 3',5'-diacylhydrazine linked T:A, <b>4.19</b> .	106
<b>Figure 4.7</b>	Docking of diacylhydrazine linked T:A dimer, <b>4.19</b> on the GRP78:ATP complex (PDB: 3LDL).	108
<b>Figure 4.8</b>	Expansion of the docking interaction of diacylhydrazine linked T:A dimer, <b>4.19</b> on the GRP78:ATP complex (PDB: 3LDL).	109

## LIST OF SCHEMES

### CHAPTER 1

- Scheme 1.1** Automated solid phase oligonucleotide synthesis cycle. 10
- Scheme 1.2** Bioconjugation strategies for the preparation of RGD peptide-oligonucleotide conjugates. 17
- Scheme 1.3** Reductive amination of Dox at localized Gua 12 and 15 on DNA hairpin, **1.26**. 18
- Scheme 1.4** Click reaction of oligonucleotide alkynes with azido ligands to produce bioconjugates, **1.43-1.48**. 22
- Scheme 1.5** Michael addition of a trivalent cyclic RGD, **1.51**, with a maleimide-derived siRNA, **1.49**, to produce the bioconjugate, **1.50**. 23

### CHAPTER 2

- Scheme 2.1** Synthesis of *N*-isobutyryl 5'-carboxy 2',3'-bis-*O*-(carbobenzyloxy) guanosine, **2.10**. 36
- Scheme 2.2** Synthesis of aminoacyl nucleolipid, **2.6**. 38

### CHAPTER 3

- Scheme 3.1** Microwave-assisted solution-phase synthesis of  $F_{48}H_7(COOH)PcZn$ , **3.10**. 73
- Scheme 3.2** Conjugation of **3.10** to an antisense GRP78 deoxyoligonucleotide bound to a solid support, **3.13**. 76

### CHAPTER 4

- Scheme 4.1** Synthesis of *N*-acetyl 5'-semicarbazide 3'-carboxybenzyloxy 111

	deoxyadenosine, <b>4.28</b> .	
<b>Scheme 4.2</b>	Synthesis of 5'- <i>O</i> -(4-dimethoxytrityl) 3'- <i>O</i> -(carboxymethylene) thymidine, <b>4.32</b> .	112
<b>Scheme 4.3</b>	Proposed synthesis of the 3',5'-diacylhydrazine linked T:A dimer, <b>4.19</b> .	113

## LIST OF TABLES

### CHAPTER 2

<b>Table 2.1</b>	Bioconjugation of aminoacyl and lipid nucleosides.	37
<b>Table 2.2</b>	Hydrodynamic Radii (Rh, nm) of aminoacyl nucleolipid, <b>2.6</b> , and DNA+ <b>2.6</b> at 25 °C.	44

### CHAPTER 3

<b>Table 3.1</b>	Electron spray mass spectrometry data for oligonucleotides <b>3.13-3.17</b> .	88
------------------	---	----

### CHAPTER 4

<b>Table 4.1</b>	Energy minimized conformations of <b>4.19</b> bound to GRP78.	107
------------------	---	-----

# **CHAPTER 1: ANTI-CANCER APPLICATIONS OF NUCLEIC ACID BIOCONJUGATES**

## **1.1 GENERAL INTRODUCTION OF NUCLEIC ACID BIOCONJUGATES AND THEIR RELEVANCE IN CANCER THERAPY**

Genetic mutations can be the origin of tumorigenesis, unleashing a myriad of signaling pathways that leads to protein overexpression, unregulated cell growth and differentiation. This aberrant activity is followed by tumor invasion and metastatic spread to a variety of tissues and organs. At this stage, tumors are typically too lethal to treat by common surgical procedures or localized chemotherapy and radiation treatments [1]. Therefore, combination approaches are rapidly emerging in a last ditch effort to save patients that have been diagnosed with *incurable* forms of tumors. Combination therapy is based on prescribing multiple chemotherapeutic drugs or combining chemotherapy with other treatment methods such as radiation and related photodynamic therapies. These synergistic approaches have proven to be highly effective by compromising multiple pathways of tumor progression, triggering cancer cells death while minimizing toxicities, drug resistance and tumor recurrence [2]. In recent years, modified nucleic acids have gained widespread use as cancer therapeutics. This trend has chemical origins, which facilitates the incorporation of modification without restriction to improve the *therapeutic* properties of the bioactive nucleic acids. For example, small molecule-nucleoside conjugates, small interfering RNA (siRNA), antisense oligonucleotides (AON), and short hairpin DNA/RNA (shDNA/RNA) have all been successfully applied for cancer therapy *in-vivo* [3–5]. Historically, the majority of this research has focused on targeting a single oncogene or oncoprotein limiting the full potential of modified nucleic acids in cancer therapy. In order to improve the power of nucleic acids in cancer therapy, bioconjugation approaches have been explored and developed. These include the combination of modified nucleic acids with small molecule drugs, or other

treatment and/or imaging modalities [3,5]. In this manner, modified nucleic acids own the potential for targeting multiple biological markers in tumors leading to synergistic anti-tumor responses. Consequently, tumor resistance and recurrence is limited en route towards an effective form of cancer therapy. For the widespread adoption of nucleic acids in clinical applications, effective delivery strategies are necessary to shield nucleic acids from ubiquitous nuclease degradation and to facilitate cellular penetration. Towards this effect nucleic acid delivery systems based on polyplexes, nanoparticles, liposomes, and micelles, have been formulated to enhance their pharmacokinetic properties [6]. Recent advances in materials design and synthesis has facilitated the production of biocompatible nanocarriers that are capable of delivering drug–nucleic acid combinations with exquisite cancer cell selectivity and controlled delivery for potent anti-cancer responses [7]. This has led to the first human clinical trials (**Figure 1.1**) of siRNA:lipid nanoparticles (siRNA:LNP) targeting the vascular endothelial growth factor (VEGF) and kinesin spindle protein (KSP) in humans diagnosed with liver cancer [8].



**Figure 1.1.** siRNA:LNP complexes for combination therapy in human cancer clinical trials. Figure adapted from Tabernero, J.; Shapiro, G.I.; LoRusso, P.M.; Cervantes, A.; Schwartz, G.K.; Weiss, G.J.; Paz-Ares, L.; Cho, D.C.; Infante, J.R.; Alsina, M.; Gounder, M.M.; Falzone,

R.; Harrop, J.; White, A.C.; Toudjarska, I.; Bumcrot, D.; Meyers, R.E.; Hinkle, G.; Svrtikapa, N.; Hutabarat, R.M.; Clausen, V.A.; Cehelsky, J.; Nochur, S.V.; Gamba-Vitalo, C.; Vaishnav, A.K.; Sah, D.W.; Gollob, J.A.; Burris, H.A. *Cancer Discov.* **2013**, 3, 406-417.  
[8].

## 1.2 SMALL MOLECULE NUCLEIC ACID BIOCONJUGATES IN CANCER THERAPY

Recent advances in chemical methods for nucleic acid synthesis has enabled the development of nucleic acid bioconjugates. In this presentation, nucleic acids encompass the core of the bioconjugate, with the terminal hydroxyl groups (2', 3' and 5'-OH) presenting the points of attachment with other bio-active molecules or functional groups (**Figure 1.2**).

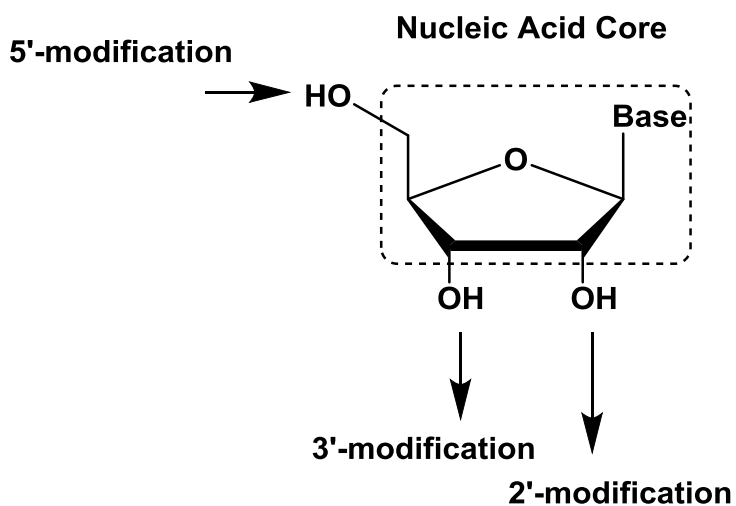


**Figure 1.2.** Terminal hydroxyl groups (2', 3' and 5'-OH) on the nucleic acid core that can serve as possible points of attachment with other bio-active molecules or functional groups..

Furthermore, the hydroxyl groups may also be selectively modified to other functional groups (amino, thiol, carbonyl and carboxylic acids) to facilitate conjugation with stable or reversible covalent bonds [9]. The latter has been especially useful in the development of nucleic acid pro-drug approaches [10]. Other synthetic approaches have been developed, incorporating

chemical modifications on the nucleobases using azide-alkyne Huisgen cycloaddition chemistry [11], ring-opening reactions of the carbohydrate [12], and replacement of the phosphate group through various functional group transformation reactions [13]. Thus, nucleic acids may be readily derivitized by chemical synthesis to yield bio-active compounds for cancer therapy [14]

**Figure 1.3.**

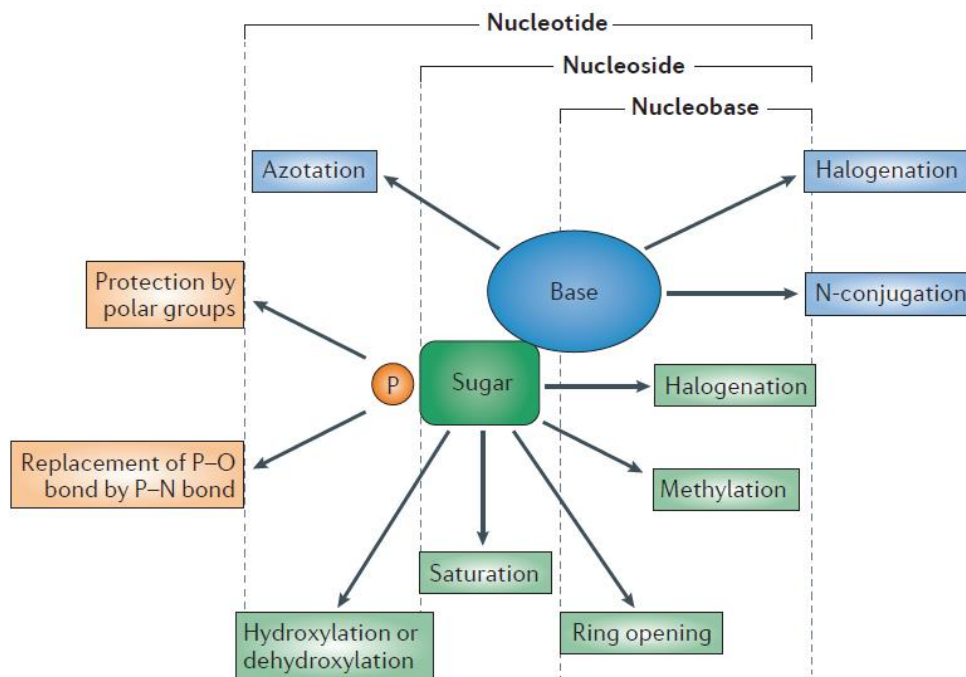


**Figure 1.3.** General structural and chemical modifications of nucleoside and nucleotide analogues. Nucleoside and nucleotide analogues consist of a nucleobase (a purine or pyrimidine derivative) and nucleotides have a phosphate group (P) linked to sugar moiety. The chemical diversity of these compounds is based on chemical reactions including halogenation, azotation, protection by polar groups and other chemical modifications (Figure adapted from reference 14).

For example, adenine deoxynucleosides cladribine (2CdA, **1.1**) and fludarabine (FAraA, **1.2**) have been shown to damage DNA by interfering with DNA replication and repair

mechanisms leading to caspase-dependent apoptosis by activation of the mitochondrial cell death pathways in rapidly proliferating lymphoid cells [15]. Modified thymidine-based nucleoside, sapacitabine (**1.3**) has been used in human clinical trials for the treatment of acute myeloid leukemia [16]. In the bone marrow of peripheral blood acute myeloid leukemia cells, sapacitabine, **1.3**, has been shown to induce cell cycle arrest in the G2 phase following a delayed S phase [19]. Its mechanism of action is based on kinase activation and incorporation within DNA during DNA polymerase assisted chain elongation. The electron withdrawing C2'-cyano group triggers the elimination of the vicinal 3'-OH group, preventing DNA polymerization and inducing a strand scission which is minimally repaired by DNA polymerase leading to cell death. Gemcitabine (**1.4**) has been used to treat lethal forms of solid pancreatic tumors, often with success when used in combination with other chemotherapeutics such as 5-fluorouracil (**1.5**), [17]. Its mechanism of action is partly based on its high accumulation within cells. This results in efficient substrate-level phosphorylation, where it acts as an inhibitor of ribonucleotide reductase and a substrate for DNA polymerase where it terminates DNA synthesis and thereby stimulating apoptosis [20]. The pro-drug cytidine-based phosphoramidate, NUC-1031 (**1.6**) has been administered to cancer patients that have grown resistant to gemcitabine (**1.4**) [18]. In this instance, tumor resistance towards gemcitabine (**1.4**) can be intrinsically acquired or developed with prolonged treatment methods. The intracellular uptake of gemcitabine (**1.4**) and related nucleosides is dependent on the cell surface overexpression of nucleoside transporters (*eg.* hENT-1), which have been found to be suppressed in gemcitabine (**1.4**) resistant tumor cell lines [21]. Overcoming tumor resistance with the incorporation of chemical modification has recently enabled an analog of gemcitabine (**1.4**), NUC-1031 (**1.6**), to exhibit significant reduction in tumor volumes in pancreatic cancer xenograft mice models. This analog is currently in Phase I/II



clinical testing and presents itself as a promising lead in resistant tumor models [22]. Thus, chemical modifications in small molecule nucleoside analogs have been successful in translating biologically active nucleosides from pre-clinical to bed side use in cancer therapy (**Figure 1.4**). Despite their growing clinical potential, they are still plagued by widespread toxicology profiles as these types of non-specific chemotherapeutics are dispersed in all tissue types. Therefore, the need for new and improved forms of cancer therapy are currently in high demand, in the hope of eradicating the most morbid and resilient types of tumors with cancer-targeting approaches.

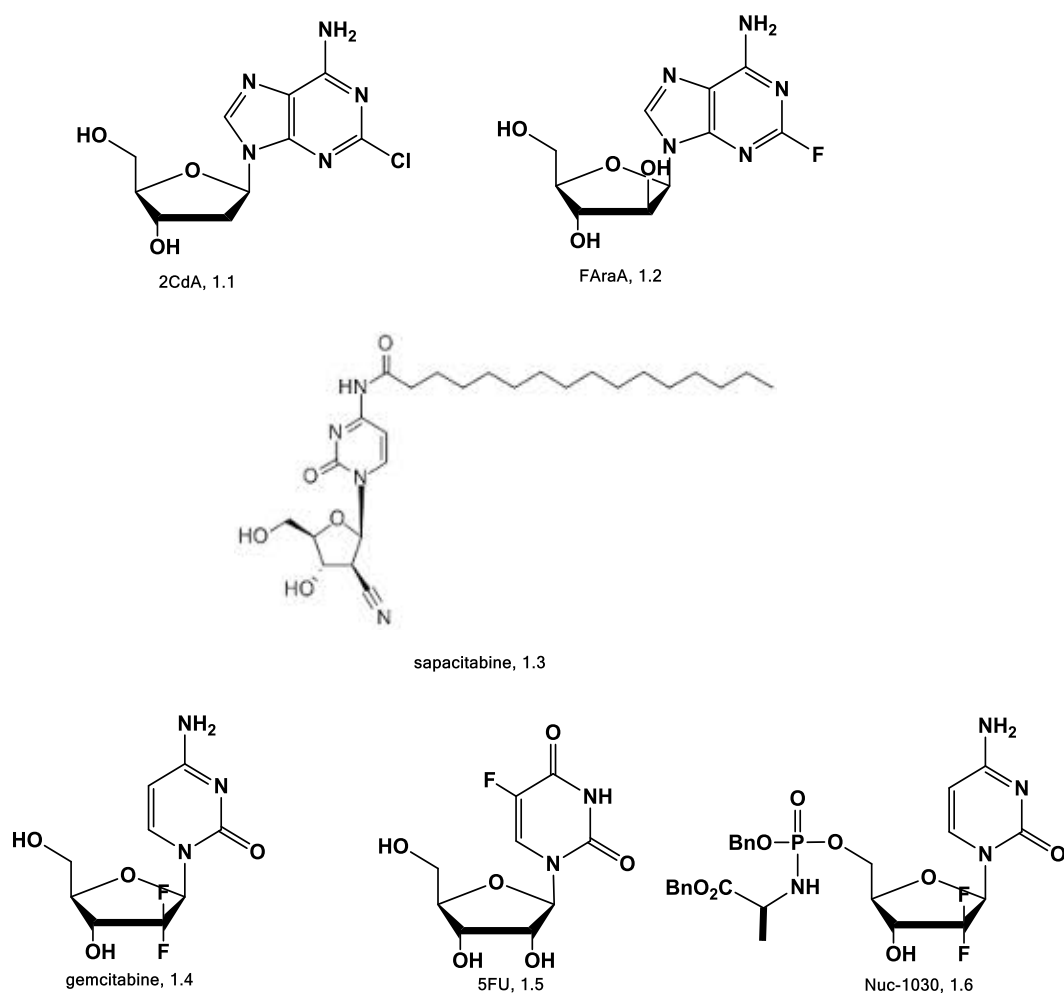


**Figure 1.4.** Chemical structures of anticancer nucleoside and nucleotide analogues in clinical applications. 2CdA, **1.1**, FAraA, **1.2** and 5FU, **1.5** are nucleoside analogs; sapacitabine, **1.3** is a

nucleoside-fatty acid conjugate; NUC-1031, **1.6**, is a prodrug bioconjugate of gemcitabine, **1.4** [15-18].

### **1.3 CANCER-TARGETING THERAPY WITH OLIGONUCLETIDE BIOCONJUGATES**

Bioconjugation approaches of oligonucleotides have gained widespread interest due to the unrestricted ability to introduce chemical or biological functionality that may improve the therapeutic properties of modified oligonucleotides (MONs). These types of nucleic acid bioconjugates are based on an oligonucleotide scaffold (natural or modified) and a linker that functions to connect the oligonucleotide moiety to the bio- or chemically active component (**Figure 1.5**). Moreover, the oligonucleotide strand may be composed of base sequences that enable specific recognition and binding to a complementary RNA, DNA or nucleic acid binding proteins. In this manner, the oligonucleotide functions as a targeting vector for the selective treatment of oncogene or oncoproteins in cancer. The choice of the linker is also very important because its length and composition typically influences the biological activity of the conjugated components. Additionally, the linker may also impart favorable solubility properties, such as fine tuning the hydrophobicity of the polar ionic oligonucleotide strand. It may also effect oligonucleotide flexibility or rigidity, respectively based on the linear or cyclic linker moieties. In spite of the linker's utility, the power of oligonucleotide bioconjugates ultimately resides within the oligonucleotide targeting vector and the conjugated components which functions in a synergistic manner to improve the therapeutic potential of oligonucleotides.

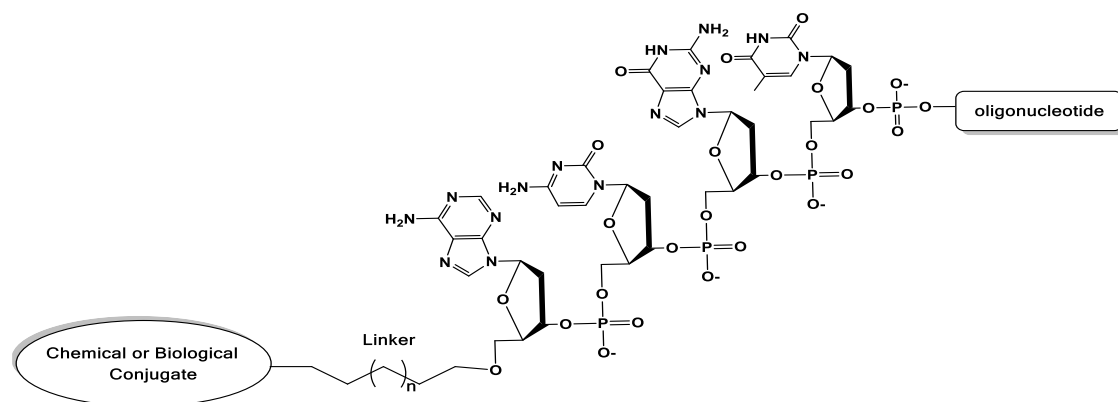


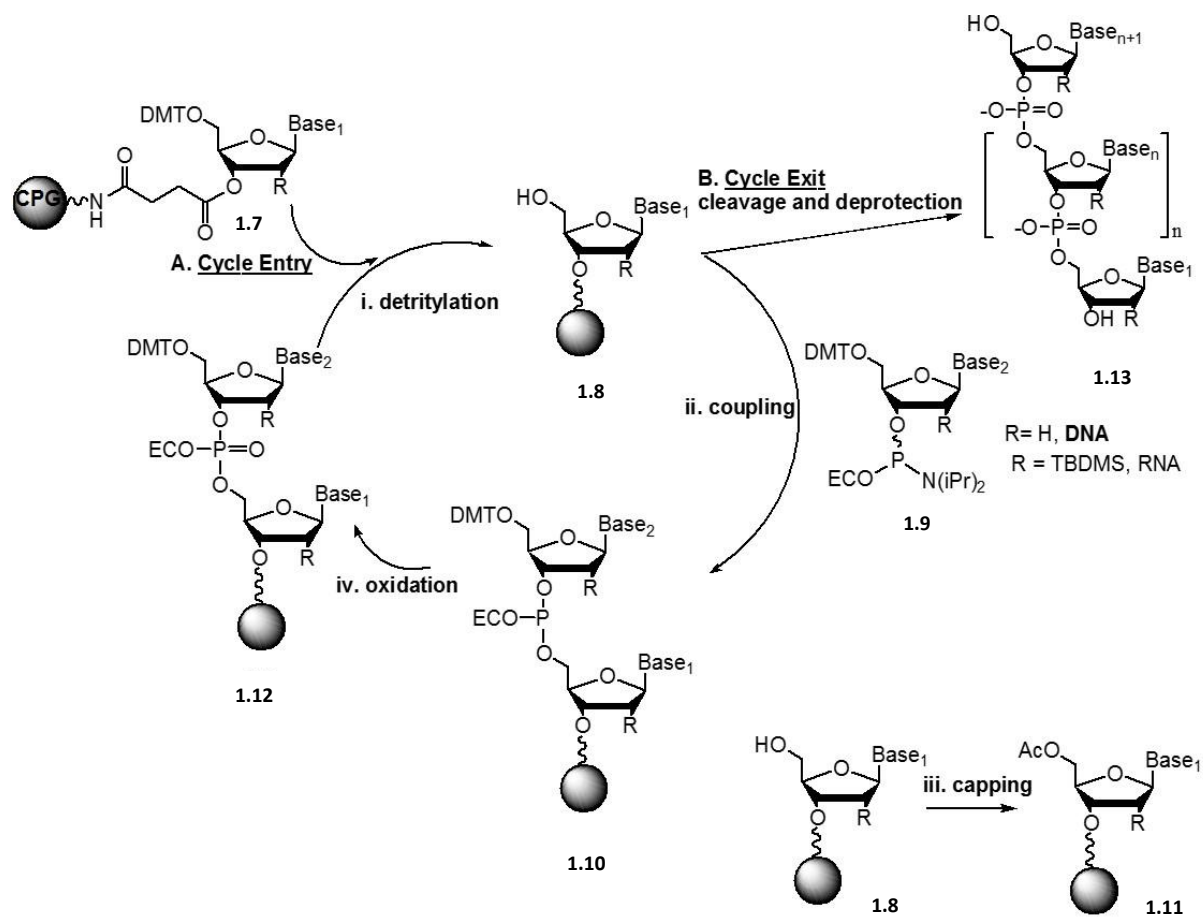
**Figure 1.5.** Rational design of an oligonucleotide bioconjugate

### 1.3.1 SYNTHESIS OF OLIGONUCLEOTIDES

Solid phase synthesis methods have been developed to allow for the small scale synthesis ( $\mu\text{g}$ - $\text{mg}$  quantities) and preparative scale production ( $\text{g}$ - $\text{kg}$  quantities) of oligonucleotides for applications in chemical biology, gene therapy and biotechnology [23]. For all these purposes, oligonucleotides are manufactured almost exclusively using automated solid phase synthesis methods [24,25]. The automated solid phase oligonucleotide synthesis cycle (**Scheme 1.1**) begins with a detritylation step, for the removal of the 5'-DMT group from the building block DNA or RNA monomer linked to the controlled pore glass (CPG) solid support, **1.7**. The detritylation step is performed to completion with 3% dichloroacetic acid in dichloromethane, 3% DCA : DCM, followed by a DCM wash cycle to remove any residual acid prior to the coupling step. The DNA or RNA phosphoramidites (**Scheme 1.1**) are the monomers that lengthen the oligonucleotide strand during the coupling step of the solid phase synthesis cycle. They are dissolved in anhydrous acetonitrile, MeCN, and coupled to the growing oligonucleotide with 0.25 M 5-ethylthiotetrazole, ETT, in MeCN. Typical coupling times for RNA synthesis are on the order of 10 - 15 minutes while DNA synthesis occurs in 2-5 minutes. This discrepancy is due to the bulky 2'-OTBDMS protecting groups used in the RNA synthesis cycle. Following coupling, the dinucleotide bound support, **1.10**, is washed with MeCN and capped to prevent

elongation of failure sequences during the synthesis cycle. This capping step is performed with a solution (Cap A: 1:1:8 v/v/v acetic anhydride:pyridine:tetrahydrofuran, Cap B: 16% *N*-methylimidazole in tetrahydrofuran) which acetylates any unreacted 5'-OH and prevents side reactions with the uncoupled nucleoside bound support, **1.11**. During the course of the synthesis procedure this step generates failure sequences; short oligonucleotide fragments that must be removed during purification. Fortunately, each automated synthesis cycle for RNA is optimized to about 97-98% efficiency, while that of DNA typically occurs on the order of >98% such that the accumulation of failure sequences is minimal. Following capping, an oxidation step with a 0.02 M oxidant (I<sub>2</sub> in 75/20/5 v/v/v tetrahydrofuran/ pyridine/ water) converts the reactive phosphite triester to the more stable phosphate triester backbone, **1.12**. The support is then washed and dried with MeCN and argon prior to 5'-deprotection and continuation of the synthesis cycle until the desired sequence has been completed. Following synthesis, the oligonucleotide is cleaved from the solid support, **1.13**, and the phosphate cyanoethyl in addition to the nucleobase protecting groups are removed using alkaline conditions, 1 : 1 v/v ammonium hydroxide: methylamine (1 : 1 AMA) for 10 minutes at 65 °C. Of note, oligonucleotides which contain the more resilient protecting groups (*i.e.* Gua *N*-*i*Bu) require lengthier deprotection times, typically accomplished with 3 : 1 v/v ammonium hydroxide in ethanol (3 : 1 NH<sub>4</sub>OH:EtOH) for 16 hours at 55 °C. The alkaline solution is volatile and evaporated on a Speedvac<sup>®</sup> concentrator. The crude oligonucleotide is then extracted from the CPG with autoclaved distilled water and quantitated by UV-Vis spectroscopy using the Beer-Lambert law. For RNA samples, the oligonucleotide is then concentrated and treated with a 1:1 v/v dimethylsulfoxide:triethylamine trihydrofluoride (1:1 DMSO:TEA:THF, 125 μL) to complete the 2'-desilylation reaction at 65 °C for 90 min. Following the 2'-desilylation reaction, RNA is precipitated using 3 M NaOAc (25 μL) in *n*-

BuOH (1 mL), isolated by centrifugation and re-dissolved in autoclaved water for analyses and purification using anion exchange, AE, [26] or reverse phase, RP, HPLC [27] and with polyacrylamide gel electrophoresis, PAGE [28].



**Scheme 1.1.** Automated solid phase oligonucleotide synthesis cycle. Figure adapted from Wincott, F.; DiRenzo, A.; Shaffer, C.; Grimm, S.; Tracz, D.; Workman, C.; Sweedler, D.; Gonzalez, C.; Scaringe, S.; Usman, N.. *Nucleic Acids Res.* **1995**, *23*, 2677-2684. [24, 25].

### 1.3.2 SYNTHESIS AND ANTI-CANCER APPLICATIONS OF ANTISENSE OLIGONUCLEOTIDE BIOCONJUGATES

The antisense method for silencing gene expression originally implicated a short tridecamer oligodeoxynucleotide d(A-A-T-G-G-T-A-A-A-A-T-G-G), which was complementary to the Rous sarcoma virus 35S mRNA and led to potent inhibition of viral protein expression in a cell-free system [29, 30]. The antisense mechanism of action (**Figure 1.6**) is based on a short (~18-21 nucleotide base length) oligonucleotide ‘antisense’ strand with a sequence that is complementary to the specific mRNA targeted for gene silencing. This antisense oligonucleotide must penetrate the cell membrane to form a hybrid structure with the complementary sense mRNA strand in the cytosol of the cell. Formation of the “antisense:sense” duplex inhibits ribosome assembly for protein translation and/or elicits the binding of an RNaseH enzyme that selectively hydrolyzes the RNA strand within the DNA:RNA duplex [31]. The antisense strategy is highly efficient, necessitating minimal (pmol) quantities of antisense oligonucleotides in a catalytic mechanism which recycles the antisense strand for potent and long-lasting gene silencing effects *in-vitro* [29-31]. However, for useful applications *in-vivo*, antisense oligonucleotides must exhibit efficient cellular delivery, nuclease resistance, regio-specific and stable targeting and binding with a complementary mRNA sequence. These effects enable the efficient recruitment of RNaseH activity with favorable pharmacokinetics properties and minimal toxicities in cell based and animal models [32].

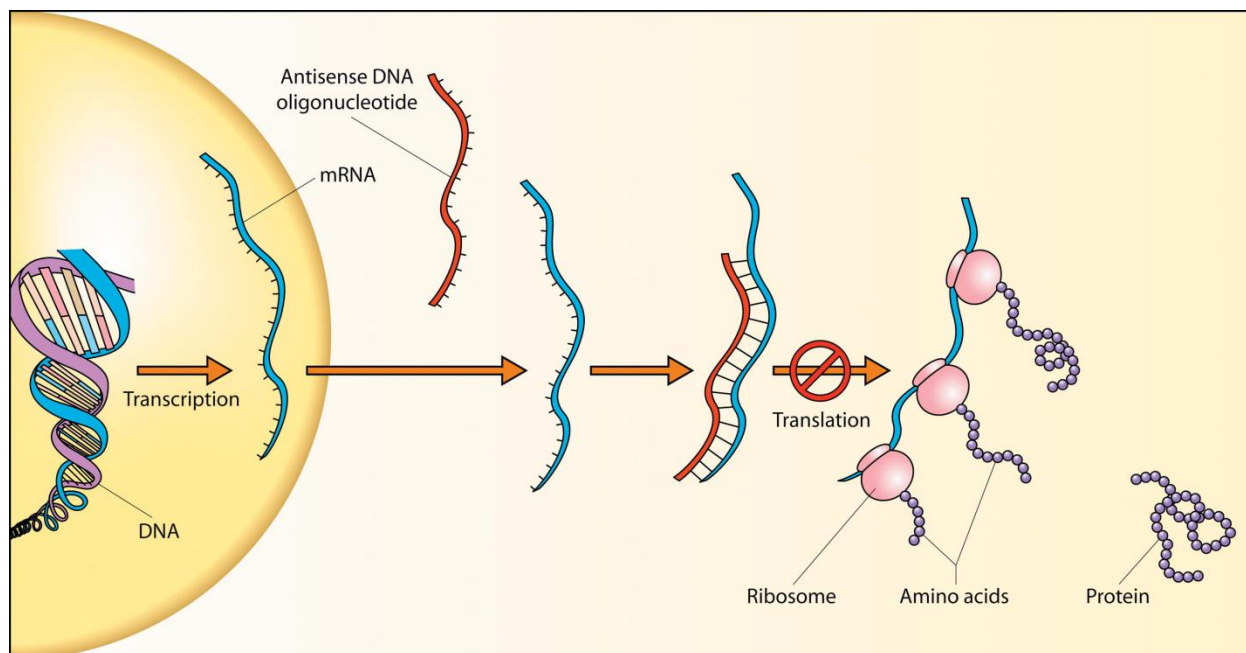


**Figure 1.6.** Antisense mechanism of inhibiting mRNA protein translation. Figure adapted from: Robinson R - RNAi Therapeutics: How Likely, How Soon? Robinson R PLoS Biology Vol. 2, No. 1, e28 doi:10.1371/journal.pbio.0020028

Synthetic methods are necessary to convert the native oligonucleotide into a modified oligonucleotide, MON, for potent antisense responses *in-vivo*. The MONs must possess comparable binding and structural properties to their native DNA/RNA hybrids, while improving nuclease resistance and cell penetration for efficient gene silencing responses within cells. Bioconjugation methods have been introduced to improve the ‘drug-like’ properties of the antisense oligonucleotides for various therapeutic applications [33,34], including those related to silencing oncogene expression in cancer [35].

For example, the 5'-cholesterol conjugate of an antisense phosphorothioate oligonucleotide, **1.14**, targeting the expression of the multidrug resistance (MDR) oncogene associated with P-glycoprotein (Pgp) enhanced the accumulation of a Pgp rhodamine-123

substrate as indicated by flow cytometry and laser scanning confocal microscopy [36]. This result is consistent with the rapid intracellular accumulation of the 5'-cholesterol antisense oligonucleotide conjugate, which favors MDR knockdown and efficacy of anti-cancer drugs in MDR mouse 3T3 fibroblasts. Moreover, replacement of the phosphodiester for a phosphorothioate bond increases metabolic stability, allowing for lengthier therapeutic indices during the MDR knockdown effect. In contrast, the unlabeled control triggered minimal Pgp knockdown in MDR cancer cells and uptake of Pgp substrates due to the drug efflux properties of the Pgp transporter. In this case, the non-polar cholesterol moiety enabled cellular uptake of the antisense oligonucleotide, while the phosphorothioate preserved oligonucleotide stability towards endonucleases, which enhanced the oncogene knockdown effect (**Figure 1.7**). The phosphorothioates are introduced during the course of the automated solid phase synthesis cycle, by replacing the oxidation step with a sulfurization reaction, **1.16**, with 3-amino-1,2,4-dithiazole-5-thione (ADTT) as efficient sulfur-transfer reagent [37]. The cholesterol moiety is coupled during the last step of the synthesis cycle with a commercially available cholesterol phosphoramidite, **1.15**.



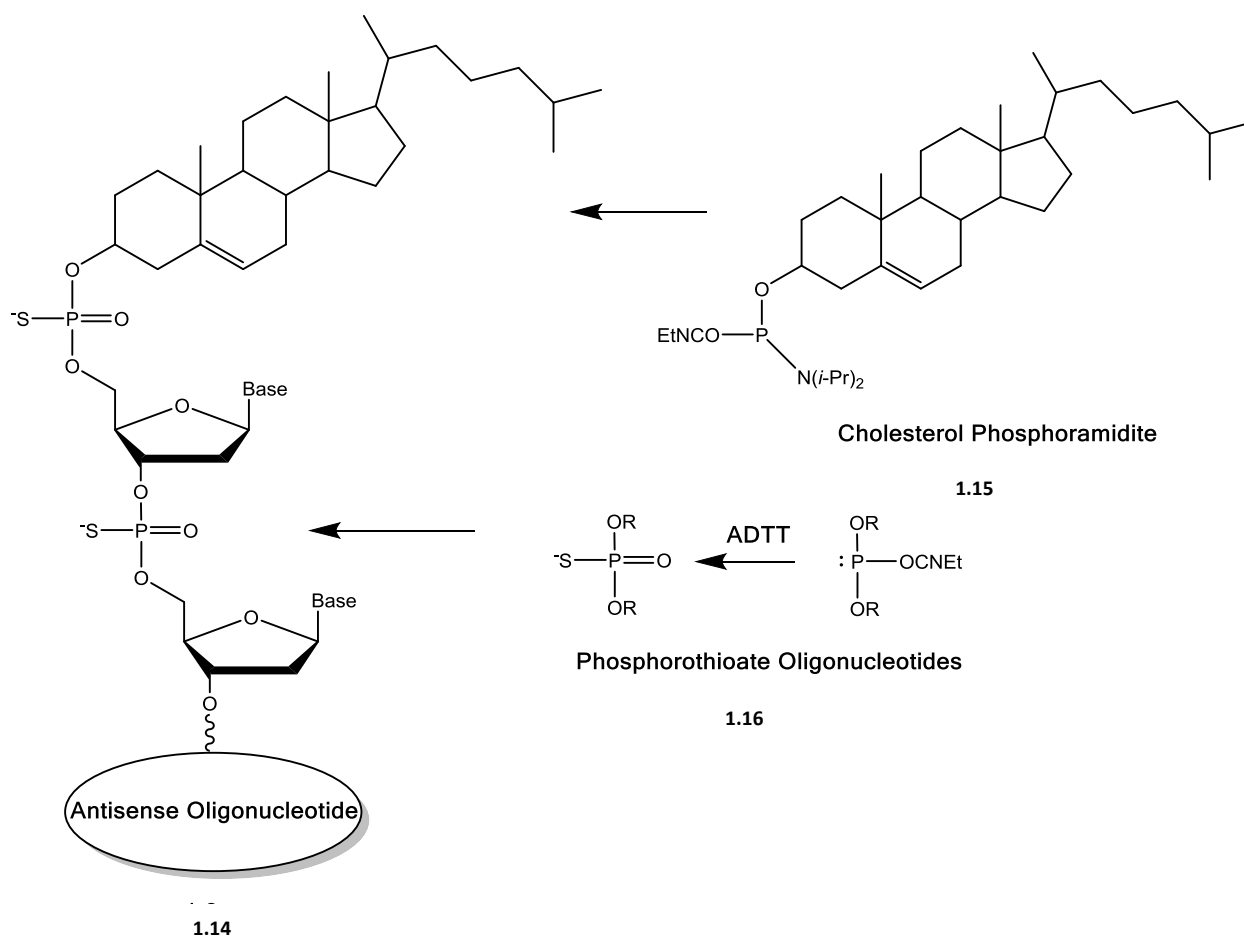


**Figure 1.7.** 5'-Cholesterol conjugate antisense phosphorothioate oligonucleotide, **1.14**.

Bioconjugation of antisense oligonucleotides is especially favorable in combination approaches, featuring specific silencing of oncogene expression by the antisense oligonucleotide, coupled with potent anti-cancer effects of the conjugated drug. For example, Bcl-2 antisense oligonucleotides sensitized radiation-induced fibrosarcoma 1 (RIF-1) cells to a silicon phthalocyanine photosensitizer, **1.17**, which triggered potent apoptotic events following antisense treatment and photodynamic therapy of the resistant tumor cells [38]. Similarly, combination approaches featuring the co-administration of an antisense oligonucleotide coupled with potent anti-tumor agents have had the most success in translating gene therapy from pre-

clinical to clinical applications. Combination of a Bcl-2 antisense oligonucleotide with potent anti-cancer drugs doxorubicin, **1.18**, and docetaxel, **1.19**, were administered to patients with locally advanced breast cancer in an extensive phase I/II clinical study [39]. Despite encouraging initial results, pharmacodynamics indicated the antisense oligonucleotide displayed modest oncogene knockdown effects, potentially related to the limited delivery at the localized tumor site. Thus, extensive research has been dedicated to improve the cellular delivery of the antisense oligonucleotides with an efficacy and selectivity that may trigger cell death exclusively in cancer.

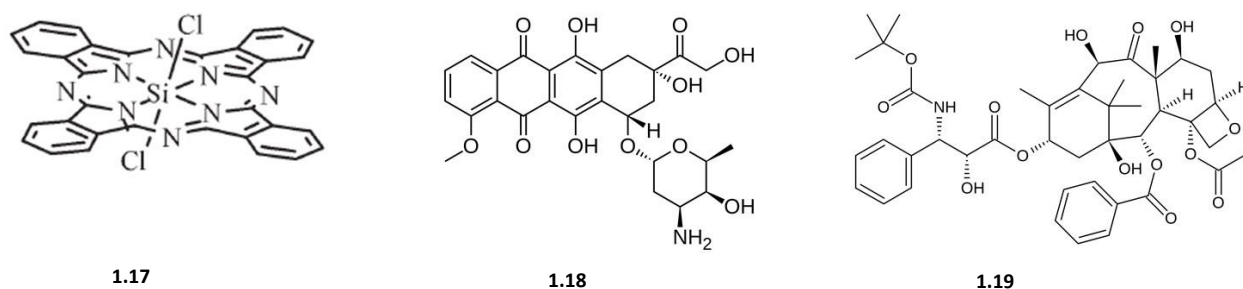


**Figure 1.8.** Potent anti-cancer drugs used in combination or conjugated to antisense oligonucleotides [38,39].

The arginine-glycine-aspartic acid (RGD) tripeptide is a selective and high affinity binding ligand for the  $\alpha\beta3$  integrin receptors that are overexpressed and cell surface localized on a variety of tumor cells types making them valid biomarkers for cancer-targeted delivery approaches [40]. RGD peptide conjugates of the splice switching antisense oligonucleotides were effectively administered in melanoma cells transplanted in mice xenografts [41]. Localized expression of the luciferase gene at the tumor site was apparent by optical imaging of the luciferin photon emission (**Figure 1.9**) following a 3 day incubation period with the RGD-

antisense oligonucleotide. This experiment underscores the significance of a cancer-targeting vector in ushering the selective delivery of oligonucleotides at the targeted tumor site for potential applications in cancer-targeting gene therapy. This was recently proven by combining the cancer-targeting properties of RGD, with the oncogene silencing effects of the antisense oligonucleotide down-regulating luteinizing hormone releasing hormone (LH-RH) overexpression in H1299 lung cancer cells and/or xenografts in athymic nude BALB/c mice [42].

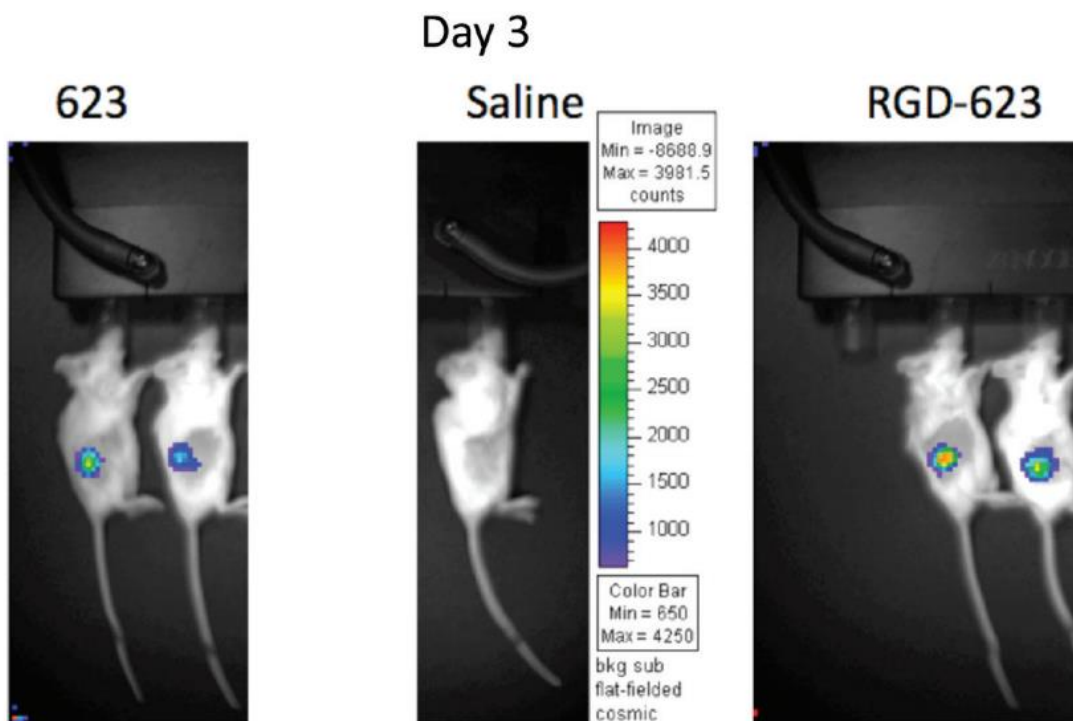
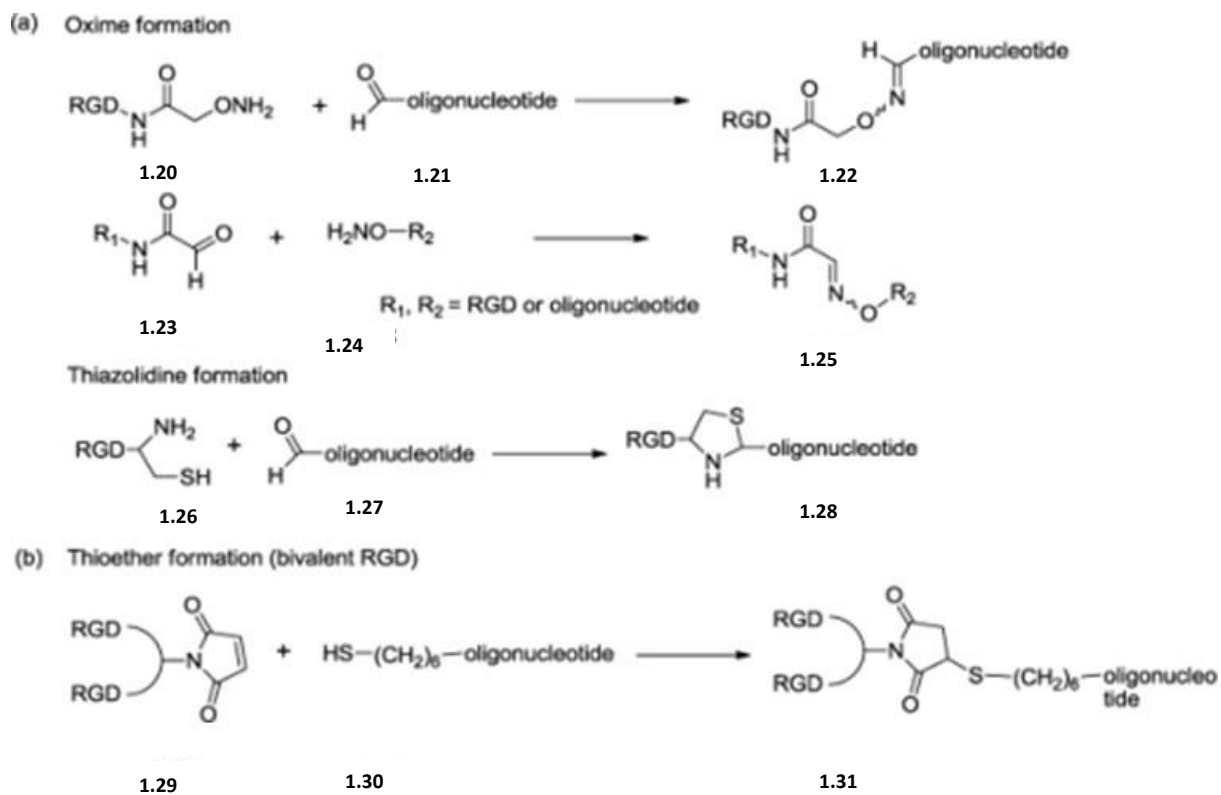


**Figure 1.9.** In vivo effects of RGD-antisense oligonucleotide (623). Localized site distribution of RGD-623 is apparent following a 3 day incubation treatment in nude mice xenografts bearing human A375 melanoma cells Figure adapted from reference Juliano, R.L.; Ming, X.; Nakagawa, O. *Acc. Chem. Res.* 2012, 45, 1067-1076. (41).

The preparation of RGD-oligonucleotide conjugates is based on a series of bio-orthogonal reactions which ligate the peptide and oligonucleotide by virtue of a reversible oxime

(Scheme 1.2, a), a cyclic thiazolidine (Scheme 1.2, a) and a thioether linkage (Scheme 1.2, b) [42].

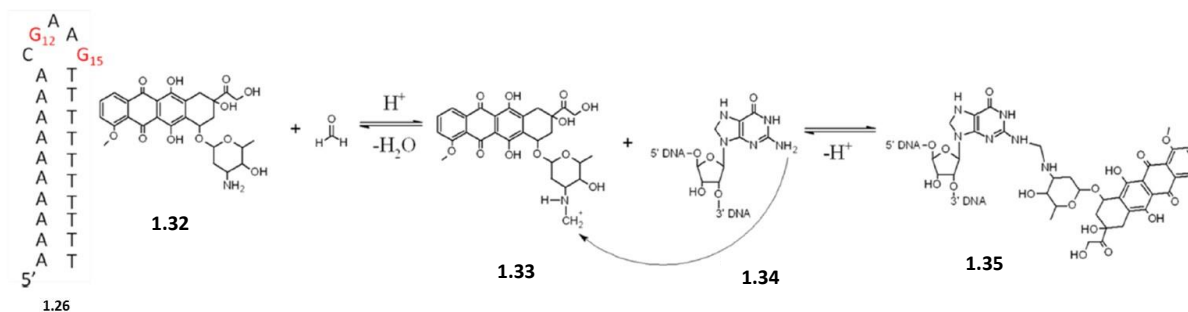


**Scheme 1.2.** Bioconjugation strategies for the preparation of RGD peptide-oligonucleotide conjugates. Figure adapted from Sundaram, S.; Trivedi, R.; Durairaj, C.; Ramesh, R.; Ambati, B.K.; Kompella, U.B. *Clin. Cancer Res.* **2009**, *15*, 7299-7308.

42.

### 1.3.3 SYNTHESIS AND ANTI-CANCER APPLICATIONS OF APTAMER OLIGONUCLEOTIDE BIOCONJUGATES

Drug resistance remains key obstacle for the successful treatment of metastatic cancers. Combinations approaches are at forefront of treating MDR tumors. In a recent case study, the selective conjugation of Doxorubicin (Dox) to a single site within a DNA hairpin results in a highly stable complex (*i.e.* aptamer) that enables Dox to be used more effectively in MDR tumor types [44]. Conjugation of Dox at a selective Gua 15 site within the loop domain of the DNA hairpin was accomplished by reductive amination (**Scheme 1.3**) and confirmed by site-specific labeling with [2-<sup>15</sup>N]-2'-deoxyguanosine followed by spectroscopic analyses using [<sup>1</sup>H-<sup>15</sup>N] 2D NMR.



**Scheme 1.3.** Reductive amination of Dox at localized Gua 12 and 15 on DNA hairpin, **1.26**, Sundaram, S.; Trivedi, R.; Durairaj, C.; Ramesh, R.; Ambati, B.K.; Kompella, U.B. *Clin. Cancer Res.* **2009**, *15*, 7299-7308.

[44].

Moreover, this conjugate was characterized as a 1:1 stoichiometric complex according to ESI-QTOF mass spectrometry, UV spectroscopy and computational analysis (**Figure 1.10**). This stable complex ultimately results in a DOX-conjugated hairpin (DCH) with a half-life >30 h.

This may translate into extended resident times of the drug at the localized tumor site leading to a prolonged therapeutic response. The DCH complex was subsequently conjugated with folic acid (FA) to increase internalization and activity within MDR breast cancer cells. Thus, this dual bio-conjugate, DCH-FA, can be used for a safer and more effective administration of Dox and additional anticancer drugs [44].

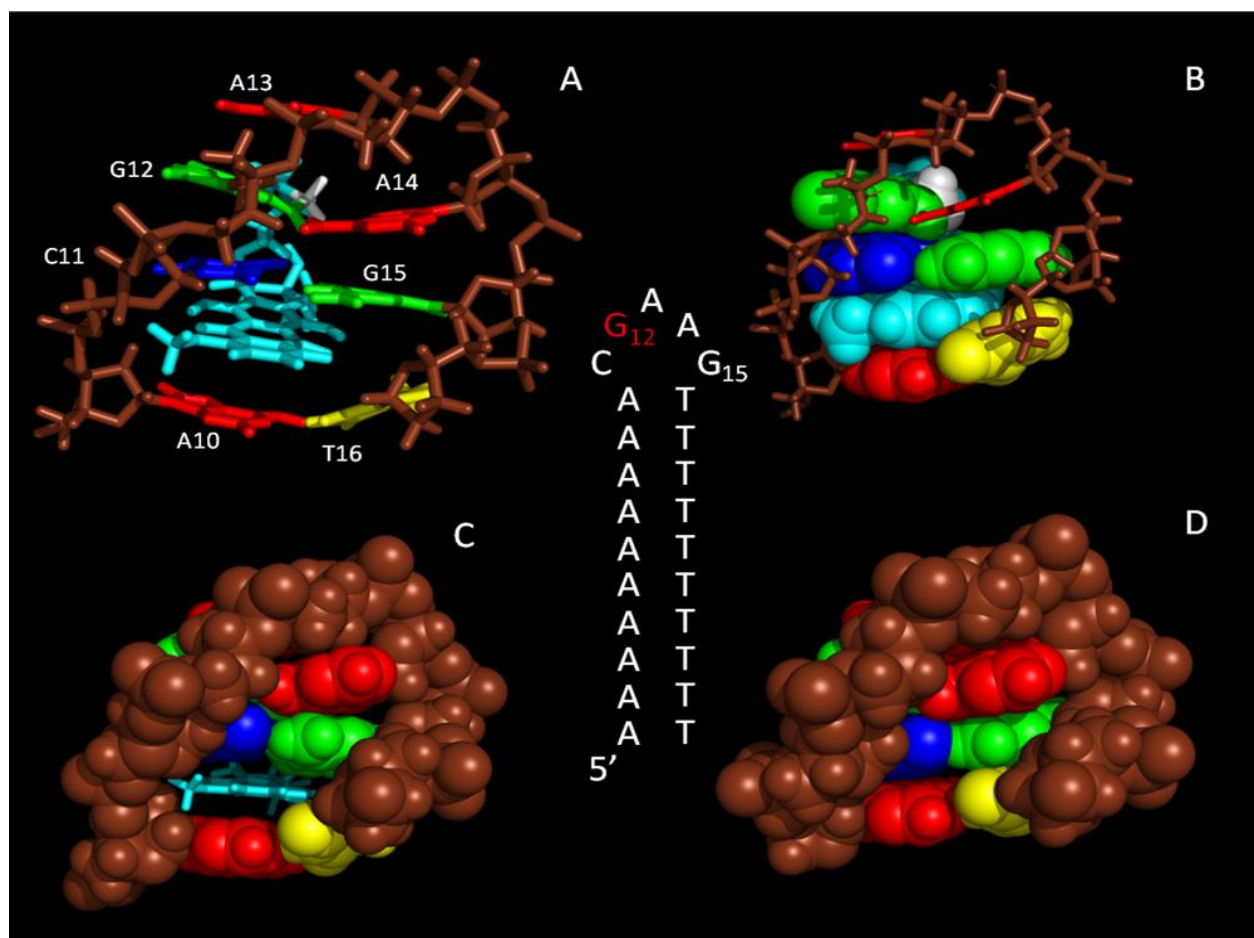


**Figure 1.10.** Structures and models of DCH. Dox is covalently bound to G12 and intercalated between the G15:C11 and the A10:T16 base pairs. Coloring scheme for structures are designated as follows: guanine, green; adenine, red; thymine, yellow; cytosine, blue; Dox, light blue; methylene linker, white; DNA backbone, brown. (A-C) 3D structure of DCH. (D) 3D structure of the unreacted hairpin. Figure adapted from reference 44.

### 1.3.4 SYNTHESIS AND ANTI-CANCER APPLICATIONS OF SHORT-INTERFERING RNA (siRNA) BIOCONJUGATES

The RNA interference (RNAi) mechanism for silencing oncogene expression in cancer has also received special attention since the seminal works of Fire and Mello, dating back to 1998, produced a full understanding of the RNAi pathway in *Caenorhabditis Elegans* [45]. For their contributions to the field, Fire and Mello were awarded the Nobel Prize in physiology or medicine in 2006. The RNAi mechanism for down-regulating gene expression is a naturally occurring process, that's triggered when short (18-21 base pairs) double-stranded RNA, aptly named short interfering RNA (siRNA), are delivered into cells causing sequence-specific gene silencing effects (**Figure 1.11**). The accepted RNAi mechanism of action initially involves long, double-stranded RNA (typically >200 nucleotides) that are cleaved by the RNA III protein Dicer into short RNA duplexes (siRNA) in an ATP-dependent reaction [46]. Typically the siRNAs are phosphorylated at their 5'-ends and have two unpaired nucleotides at the unphosphorylated 3'-ends for recognition, binding and activation of the RNA-Induced Silencing Complex (RISC). The siRNAs are assembled within RISC, a protein complex loaded with endoribonucleases such as the Argonaute 2 protein, which catalyzes sequence specific RNA hydrolysis [47]. The sense siRNA strand is hydrolyzed leaving behind the single-stranded antisense RNA (aRNA) which directs RISC to a target messenger RNA (mRNA) sequence forming the aRNA:mRNA hybrid. This ribonucleoprotein complex inhibits protein translation of the mRNA sequence. Moreover, the aRNA:mRNA hybrid is a substrate for the processing activity of the Argonaute 2 enzyme, which selectively hydrolyzes the mRNA strand and permanently silences mRNA expression. Since the aRNA strand is left intact, the RNAi mechanism for silencing mRNA expression is a catalytic process, resulting in potent effects with minimal quantities (pmol) of siRNA. Therefore,

the RNAi technology has been applied for treating many human diseases associated with the expression of malignant genes (*e.g.* metabolic disorders, cancer, gene mutations and deletions etc.) [48]. In spite of its unlimited potential in gene therapy applications, siRNAs are limited by poor pharmacokinetic properties which has hindered their translation from pre-clinical to clinical use [49]. Therefore, synthetic siRNAs have been created and conjugated with functionality which improves their ‘drug-like’ potential in treating genetic disorders *in vivo* [50].

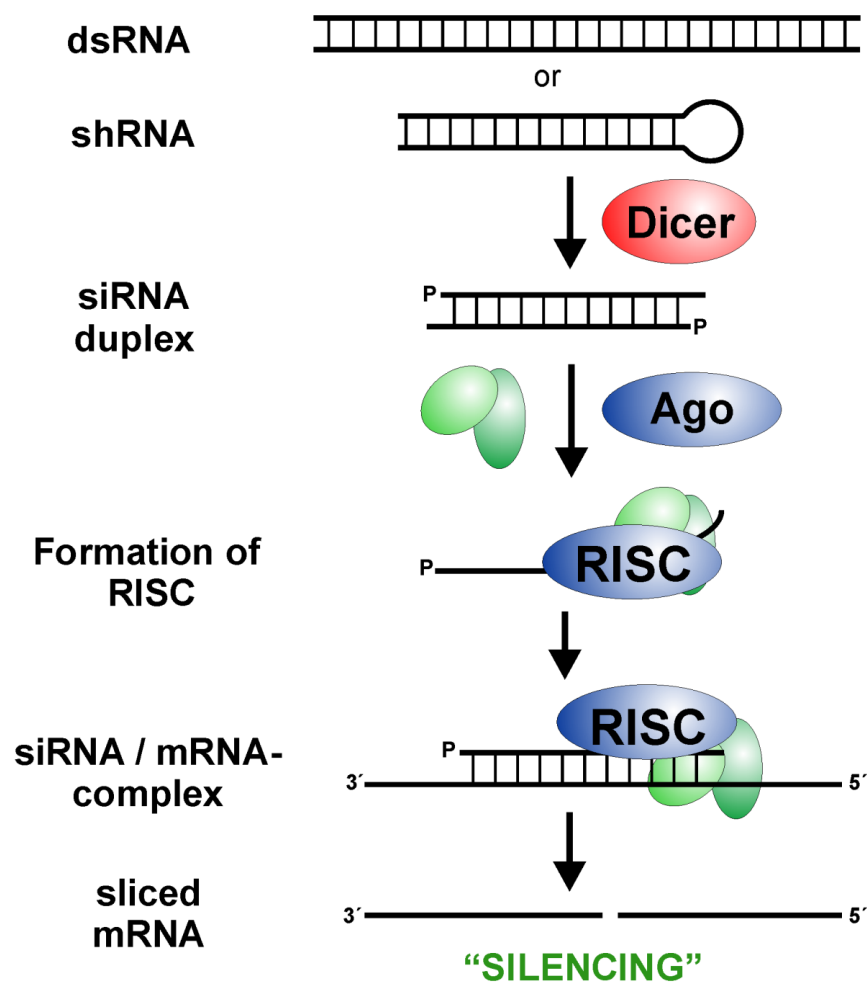
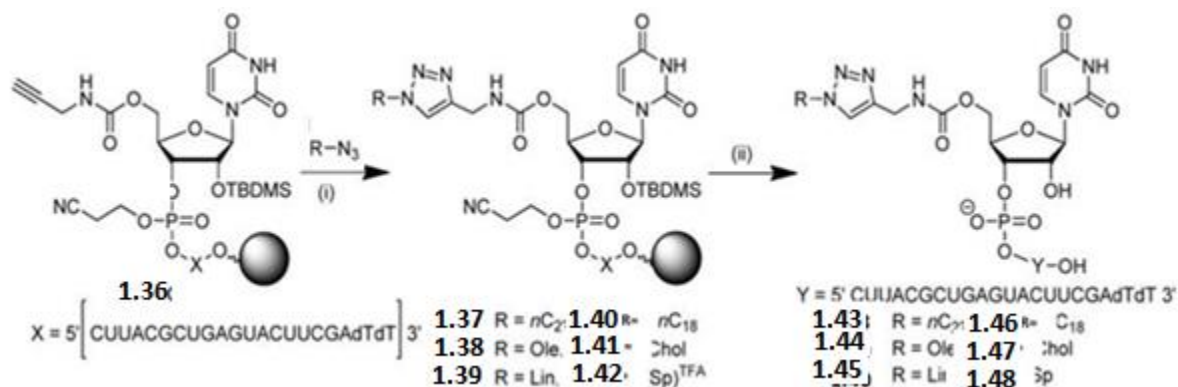


**Figure 1.11.** The RNAi mechanism of action. Dicer cleaves double-stranded RNA producing short siRNA duplexes. The RNA-induced silencing complex (RISC) binds to the siRNA



substrates and the Argonaute 2 endoribonuclease cleaves the sense siRNA strand. The siRNA is unwound and the antisense siRNA strand directs the RISC to a target messenger RNA (mRNA), resulting in the formation of the siRNA:mRNA hybrid. This hybrid inhibits mRNA translation and triggers endonucleolytic cleavage of the mRNA strand. The mRNA is degraded, and the gene silenced (Figure adapted from <http://www.uni-konstanz.de/FuF/chemie/jhartig/>).

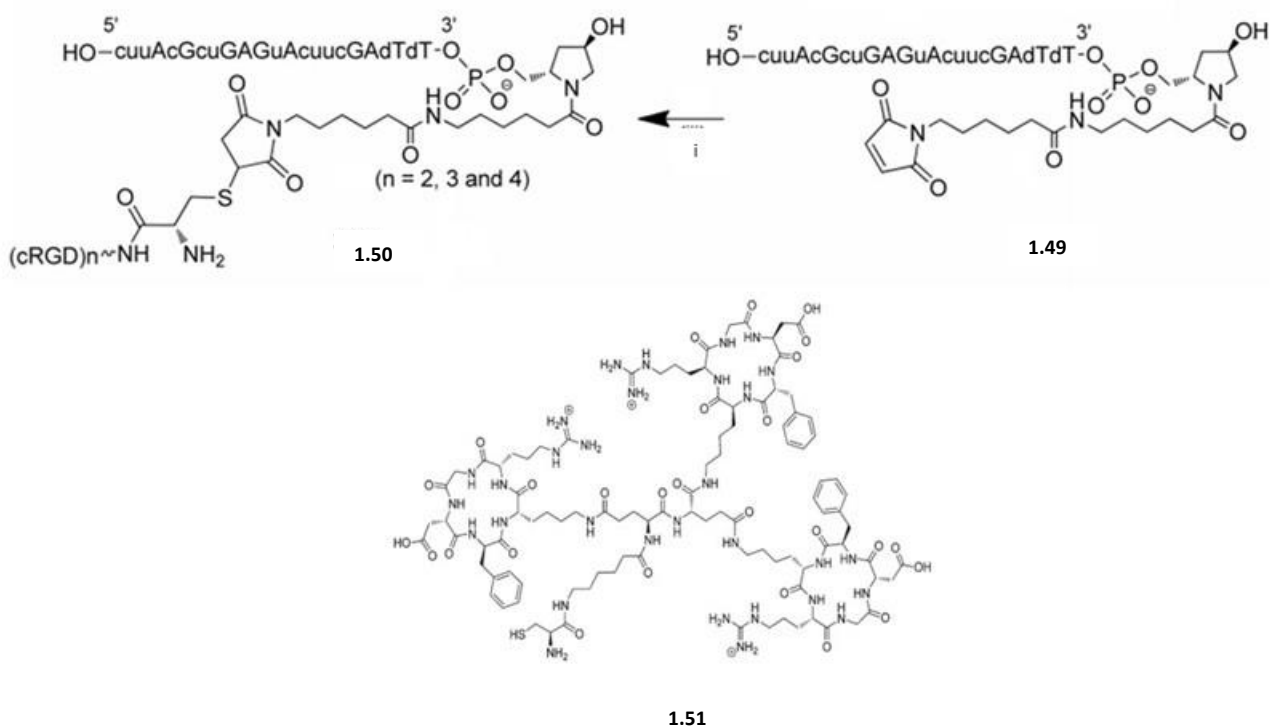
siRNA-ligand conjugates have been effectively produced using the copper-catalyzed azide-alkyne cycloaddition (CuAAC) or click reaction [51]. Nucleosides bearing 2', 3' or 5'-alkyne groups were effectively conjugated with ligands bearing azido groups such as lipophilic long chain alkyls, cholesterol, oligoamines and carbohydrates (**Scheme 1.4**). The conjugated siRNAs effectively silenced luciferase gene activity in a transformed HeLa cell line, illustrating their potential in RNAi applications.



**Scheme 1.4.** Click reaction of oligonucleotide alkynes with azido ligands to produce bioconjugates, **1.43-1.48**. Reaction and conditions: i. alkyne/azide/CuSO<sub>4</sub> 5H<sub>2</sub>O/TBTA/ sodium ascorbate (1:3:0.4:3:3 mol ratio), H<sub>2</sub>O/MeOH/THF (1 mL, 2:2:1, v/v), 60 °C, microwave radiation, 45 min, yields (89-99%). ii. 40% methylamine/H<sub>2</sub>O. Reaction scheme adapted from reference 51.

Cell targeting ligands have also been conjugated to siRNA for cell specific gene silencing effects. For example, di-, tri- and tetra-valent cyclic RGD peptides have been conjugated to

siRNA targeting the firefly luciferase gene in  $\alpha V\beta 3$  positive M21<sup>+</sup> human melanoma cells [52]. In this bioconjugation reaction a reactive cysteinyl thiol was introduced within the peptide sequence for Michael addition with a maleimide group at the 3'-end of the siRNA (**Scheme 1.5**).



**Scheme 1.5.** Michael addition of a trivalent cyclic RGD, **1.51**, with a maleimide-derived siRNA, **1.49**, to produce the bioconjugate, **1.50**. Reaction and conditions: i. 0.4 M KCl, 40% MeCN:H<sub>2</sub>O, room temperature, overnight reaction.

Recent advances in bioorthogonal chemistry have enabled the development of the first in human clinical trials of an siRNA conjugate targeting the vascular endothelial growth factor (VEGF) and the kinesin spindle protein (KSP) in liver metastases associated with endometrial cancer [8]. The siRNA therapeutic is well tolerated and shows promising pharmacodynamics

paving the way for the first siRNA oncogene therapeutic to reach the open market. The key to its success is associated with the combination of siRNA and a lipid nanoparticle, (LNP), which enables effective tumor penetration for RNAi activity (**Figure 1.1**). Thus, bioconjugation methods are at the heart of developing effective nucleic acid therapeutics against tumors.

## **1.4 THESIS OBJECTIVES**

Nucleic acid bioconjugates have gained widespread use in medicinal chemistry research programs aimed at fighting human malignancies such as cancer, diabetes, genetic and infectious diseases. Their popularity stems from the ability to accelerate the drug development process by conjugating chemical functionality that may improve the pharmacology of the bioactive nucleoside. Moreover, this strategy has been proven to be effective with small molecule nucleoside analogs and those derived from lengthy oligonucleotide sequences. Considering these fruitful applications, my thesis shows the synthesis, characterization and therapeutic potential of novel classes of nucleic acid bioconjugates. These are based on (a) aminoacyl nucleolipids, from which a simple, versatile and efficient synthesis strategy has been developed for this new class of DNA binding molecules (Chapter 2). This nucleoside based bio-conjugate exhibited GRP78 oncogene binding affinity ( $K_D$ : 0.25 mM) and selective anti-leukemic activity in a single dose (10  $\mu$ M) screen against a panel of 60 cancer cell lines [53]. Additionally, the (b) diacylhydrazine-linked dinucleosides, encompass a novel class of nucleic acid bioconjugates proposed to improve the structural stability of turn conformations in DNA or RNA hairpin secondary structures. My most recent advances in the synthesis, structure elucidation and biological evaluation of these putative hairpin mimics will also be described in Chapter 3. Lastly, (c) the synthesis, biophysical properties and GRP78 DNA cleavage activity of a phthalocyanine-linked

oligonucleotide bioconjugate will be highlighted for photodynamic oncogene therapy applications in Chapter 4 [54]. Thus, this thesis will underscore my contributions to the flourishing field of nucleic acid bioconjugation for potential anti-cancer applications.

## 1.5 REFERENCES

1. Hanahan, D.; Weinberg, R.A. *Cell* **2000**, *100*, 57–70.
2. Miles, D.; von Minckwitz, G.; Seidman, A.D. *Oncologist* **2002**, *7*, 13–19.
3. Khalil, A.; Ishita, K.; Ali, T.; Tjarks, W. *Future Med. Chem.* **2013**, *5*, 677-692.
4. Izquierdo, M. *Cancer Gene Ther.* **2005**, *12*, 217–227.
5. Mercola, D.; Cohen, J.S. *Cancer Gene Ther.* **1995**, *2*, 47–59.
6. Cho, K.; Wang, X.; Nie, S.; Chen, Z.G.; Shin, D.M. *Clin Cancer Res*, **2008**, *14*, 1310-1316.
7. Li, J.; Wang, Y.; Zhu, Y.; Oupický, D. *J. Control. Rel.* **2013**, *172*, 589–600.
8. Taberero, J.; Shapiro, G.I.; LoRusso, P.M.; Cervantes, A.; Schwartz, G.K.; Weiss, G.J.; Paz-Ares, L.; Cho, D.C.; Infante, J.R.; Alsina, M.; Gounder, M.M.; Falzone, R.; Harrop, J.; White, A.C.; Toudjarska, I.; Bumcrot, D.; Meyers, R.E.; Hinkle, G.; Svrzikapa, N.; Hutabarat, R.M.; Clausen, V.A.; Cehelsky, J.; Nochur, S.V.; Gamba-Vitalo, C.; Vaishnav, A.K.; Sah, D.W.; Gollob, J.A.; Burris, H.A. *Cancer Discov.* **2013**, *3*, 406-417.
9. Zatsepin, T.S.; Stetsenko, D.A.; Gait, M.J.; Oretskaya, T.S. *Bioconj. Chem.* **2005**, *16*, 471-489.
10. Jacobsen, M.F.; Cló, E.; Mokhir, A.; Gothelf, K.V. *ChemMedChem.* **2007**, *2*, 793-799.
11. Lee, S.E.; Sidorov, A.; Goullain, T.; Mignet, N.; Thorpe, S.J.; Brazier, J.A.; Dickman, M.J.; Hornby, D.P.; Grasby, J.A.; Williams, D.M. *Nucleic Acids Res.* **2001**, *29*, 1565-1573.
12. Vasseur, J.J.; Rayner, B.; Imbach, J.L.; Verma, S.; McCloskey, J.A.; Lee, M.; Chang, D.K.; Lown, J.W. *J. Org. Chem.* **1987**, *52*, 4994-4998.
13. El-Sagheer, A.H.; Brown, T. *Chem. Soc. Rev.* **2010**, *39*, 1388-1405.
14. Jordheim, L.P.; Durantel, D.; Zoulim, F.; Dumontet, C. *Nature Reviews.* **2013**, *12*, 447-464.
15. Klopfer, A.; Hasenjager, A.; Belka, C.; Schulze-Osthoff, K.; Dorken, B.; Daniel, P.T. *Oncogene* **2004**, *23*, 9408-9418.
16. Kantarjian, H.; Faderl, S.; Garcia-Manero, G.; Luger, S.; Venugopal, P.; Maness, L.; Wetzler, M.; Coutre, S.; Stock, W.; Claxton, D.; Goldberg, S.L.; Arellano, M.; Strickland,

- S.A.; Seiter, K.; Schiller, G.; Jabbour, E.; Chiao, J.; Plunkett, W. *Lancet Oncol.* **2012**, *13*, 1096-1104.
17. Saif, M.W.; Lee, Y.; Kim, R. *Ther. Adv. Med. Oncol.* **2012**, *4*, 341-346.
18. McGuigan, C.; Habib, N.A.; Wasan, H.S.; Gabra, H.; Jiao, L.R.; Slusarczyk, M.; Chabot, J.A.; Saif, M.W. *J. Clin. Oncol.* **2011**, *29*, e13540.
19. Jagan, S.; Paganessi, L.A.; Frank, R.R.; Venugopal, P.; Larson, M.; Christopherson, K.W. *Adv. Hematol.* **2012**, *72*, 76- 83.
20. Plunkett, W.; Huang, P.; Searcy, C.E.; Gandhi, V. *Semin. Oncol.* **1996**, *23*, 3-15.
21. Andersson, R.; Aho, U.; Nilsson, B.I.; Peters, G.J.; Pastor-Anglada, M.; Rasch, W.; Sandvold, M.L. *Scand. J. Gastroenterol.* **2009**, *44*, 782-786.
22. Slusarczyk, M.; Lopez, M.H.; Balzarini, J.; Mason, M.; Jiang, W.G.; Blagden, S.; Thompson, E.; Ghazaly, E.; McGuigan, C. *J. Med. Chem.* **2014**, *57*, 1531-1542.
23. Davis, R.H. *Curr. Opin. Biotech.* **1995**, *6*, 213-217.
24. Caruthers, M.H.; Barone, A.D.; Beaucage, S.L.; Dodds, D.R.; Fisher, E.F.; McBride, L.J.; Matteucci, M.; Stabinsky, Z.; Tang, J.Y. *Methods Enzymol.* **1987**, *154*, 287-313.
25. Wincott, F.; DiRenzo, A.; Shaffer, C.; Grimm, S.; Tracz, D.; Workman, C.; Sweedler, D.; Gonzalez, C.; Scaringe, S.; Usman, N. *Nucleic Acids Res.* **1995**, *23*, 2677-2684.
26. Cook, K.; Thayer, J. *Bioanalysis* 2011, *3*, 1109-1120.
27. McCarthy, S.M.; Gilar, M.; Gebler, J. *Anal. Biochem.* **2009**, *390*, 181-188.
28. Rio, D.C.; Ares, M.; Hannon, G.J.; Nilsen, T.W. *Cold Spring Harb. Protoc.* **2010**, *6*, 1-6.
29. Zamecnik, P. C.; Stephenson, M. L. *Proc. Natl. Acad. Sci. USA.* **1978**, *75*, 280-284.
30. Zamecnik, P.C.; Stephenson, M.L. *Proc Natl Acad Sci USA*, **1978**, *75*, 285-288.
31. Crooke, S.T. *Biochim Biophys Acta.* **1999**, *1489*, 31-44.
32. Heidenreich, O.; Kang, S.H.; Xu, X.; Nerenberg, M. *Mol. Med. Today* **1995**, *1*, 128-133.
33. Goodchild, J. *Bioconj. Chem.* **1990**, *1*, 165-187.
34. Lonngberg, H. *Bioconj. Chem.* **2009**, *20*, 1065-1094.
35. Dias, N.; Stein, C.A. *Mol. Cancer Ther.* **2002**, *1*, 347-355.
36. Alahari, S.K.; Dean, N.M.; Fisher, M.H.; Delong, R.; Manoharan, M.; Tivel, K.L.; Juliano, R.L. *Mol. Pharmacol.* **1996**, *50*, 808-819.
37. Tang, J.Y.; Han, Y.; Tang, J.X.; Zhang, Z. *Org. Proc. Res. Dev.* **2000**, *4*, 194-198.
38. Srivastava, M.; Ahmad, N.; Gupta, S.; Mukhtar, H. *J. Biol. Chem.* **2001**, *276*, 15481-15488.

39. Moulder, S.L.; Symmans, W.F.; Booser, D.J.; Madden, T.L.; Lipsanen, C.; Yuan, L.; Brewster, A.M.; Cristofanilli, M.; Hunt, K.K.; Buchholz, T.A.; Zwiebel, J.; Valero, V.; Hortobagyi, G.N.; Esteva, F.J. *Clin. Cancer Res.* **2008**, *14*, 7909-7916.
40. Dahnier, F.; Le Breton, A.; Preat, V. *Mol. Pharm.* **2012**, *9*, 2961-2973.
41. Juliano, R.L.; Ming, X.; Nakagawa, O. *Acc. Chem. Res.* **2012**, *45*, 1067-1076.
42. Sundaram, S.; Trivedi, R.; Durairaj, C.; Ramesh, R.; Ambati, B.K.; Kompella, U.B. *Clin. Cancer Res.* **2009**, *15*, 7299-7308.
43. Juliano, R.L.; Ming, X.; Nakagawa, O.; Xu, R.; Yoo, H. *Theranostics* **2011**, *1*, 2111-2119.
44. Stuart, C.H.; Horita, D.A.; Thomas, M.J.; Salsbury, Jr. F.R.; Lively, M.O.; Gmeiner, W.H. *Bioconjugate Chem.* **2014**, *25*, 406-413.
45. Fire, A.; Xu, S.; Montgomery, M. K.; Kostas, S. A.; Driver, S. E.; Mello, C. C. *Nature* **1998**, *391*, 806-811.
46. Tijsterman, M.; Plasterk, R.H.A. *Cell* **2004**, *117*, 1-3.
47. Liu, J.; Carmell, M.A.; Rivas, F.V.; Marsden, C.G.; Thomson, J.M.; Song, J.J.; Hammond, S.M.; Joshua-Tor, L.; Hannon, G.J. *Science* **2004**, *305*, 1437-1441.
48. Rossi, J.J.; Kim, D.H. *Nature* **2007**, *8*, 173-184.
49. Bumcrot, D.; Manoharan, M.; Koteliansky, V.; Sah, D.W.Y. *Nature* **2006**, *2*, 711-719.
50. Tiemann, K.; Rossi, J.J. *Embo Mol Med.* **2009**, *1*, 142-151.
51. Yamada, T.; Peng, C.G.; Matsuda, S.; Addepalli, H.; Jayaprakash, K.N.; Alam, M.R.; Mills, K.; Maier, M.A.; Charisse, K.; Sekine, M.; Manoharan, M.; Rajeev, K.G. *J. Org. Chem.* **2011**, *76*, 1198-1211.
52. Alam, M.R.; Ming, X.; Fisher, M.; Lackey, J.G.; Rajeev, K.G.; Manoharan, M.; Juliano, R.L. *Bioconjug. Chem.* **2011**, *22*, 1673-1681.
53. Patel, P.; Hanawa, E.; Yadav, R.; Samuni, U.; Marzabadi, C.; Sabatino, D. *Bioorg. Med. Chem. Lett.* **2013**, *23*, 5086-5090.
54. Patel, P.; Patel, H.H.; Borland, E.; Gorun, S.M.; Sabatino, D. *Chem. Commun.* 50-48, **2014**, 6309.

## CHAPTER 2: SYNTHESIS, DNA BINDING AND ANTI-LEUKEMIC ACTIVITY OF AN AMINOACYL NUCLEOLIPID

### 2.1 GENERAL INTRODUCTION

Aminoacyl nucleolipids encompass an interesting class of synthetic amphiphilic bioconjugates, which own the ability to assemble into higher-ordered biomaterials for applications in gene therapy, medicinal chemistry and biotechnology [1,2]. The self-assembly properties of aminoacyl nucleolipids is partly related to its structure [3,4]. This includes a nucleoside which contains a purine or pyrimidine nucleobase that may participate in H-bonding interactions, an aminoacyl group that contains the potential for ionic bonding and lipids which enable the self-assembly of these amphiphiles through non-polar interactions (**Figure 2.2**). For example, the synthetic guanosine aminoacyl nucleolipids (**Figure 2.1, 2.1, 2.2**) displayed the ability to form stable G-tetraplexes (G-tetrads) in organic solvents [5], were also found to behave as organometallic chelators with  $\text{Li}^+$  and  $\text{K}^+$  ions and displayed the ability to transport  $\text{H}^+/\text{OH}^-$  ions in the presence of an externally applied pH gradient [3]. Moreover, aminoacyl nucleolipids, **2.1** and **2.2** showed moderate to weak activity ( $\text{IC}_{50}$ :  $17 - >10^3 \mu\text{M}$ ) in an anti-proliferative assay across a panel of 5 tumor cell lines underscoring their potential in biomedical applications [3]. In a related case study, a cationic aminoacyl surfactant (**Figure 2.1, 2.3**) demonstrated micelle forming capabilities in water according to DLS studies and modest cell toxicities ( $\text{IC}_{50}$ :  $19 - 98 \mu\text{M}$ ) relative to the cytotoxic cetyl triethylammonium bromide (CTAB) cationic amphiphile in a panel of human, rat and murine cell lines [4]. Interestingly, the biological activity of the aminoacyl nucleolipid, **2.3**, was found to occur at concentrations nearing its critical micelle concentration (cmc:  $40 \mu\text{M}$ ), highlighting its structure-activity relationship. In light of their abilities to form stable and relatively benign cationic assemblies, aminoacyl nucleolipids have

been applied to gene delivery applications in cell-based studies [6,7]. The rise of short interfering RNAs (siRNAs) has enabled the widespread application of silencing detrimental mRNA expression through the RNA interference (RNAi) pathway [8]. In spite of its unlimited potential in gene therapy applications, siRNAs are plagued by poor cell permeability which limits their therapeutic efficacy. In an effort to overcome this challenge, siRNA delivery agents (transfection agents) have been formulated to effectively condense and deliver siRNA across the amphiphilic cell membrane for RNAi activity. In this scope, a small library of synthetic polycationic nucleolipids have been formulated for siRNA packaging and transfection within a HeLa cell line for potent suppression of Vascular Endothelial Growth Factor (VEGF) expression [6]. The spermine derived aminoacyl nucleolipid (**Figure 2.1, 2.4**) exhibited comparable siRNA transfection efficiencies (>90% VEGF knockdown) and cell death (~20%) as the benchmark Lipofectamine-based siRNA transfections. Moreover, metabolically stable variants of aminoacyl nucleolipids have also been formulated for siRNA delivery applications in HeLa cells [7]. For example, an arginine-linked nucleolipid (**Figure 2.1, 2.5**) has been synthesized by virtue of a 1,3-dipolar cycloaddition to generate a stable triazole linkage in between the aminoacyl group and the nucleolipid, whereas the lipid groups were installed using carbamate linkages. This cationic nucleolipid formed stable complexes with anti-VEGF siRNA as discerned from gel shift binding assays and DLS experiments, while facilitating siRNA transfection for potent VEGF knockdown (>90%) which also paralleled the effects of the Lipofectamine-based siRNA transfections in HeLa cells [7]. These examples effectively demonstrate the fruitful implementation of aminoacyl nucleolipids in condensing oligonucleotides for medicinal chemistry applications.



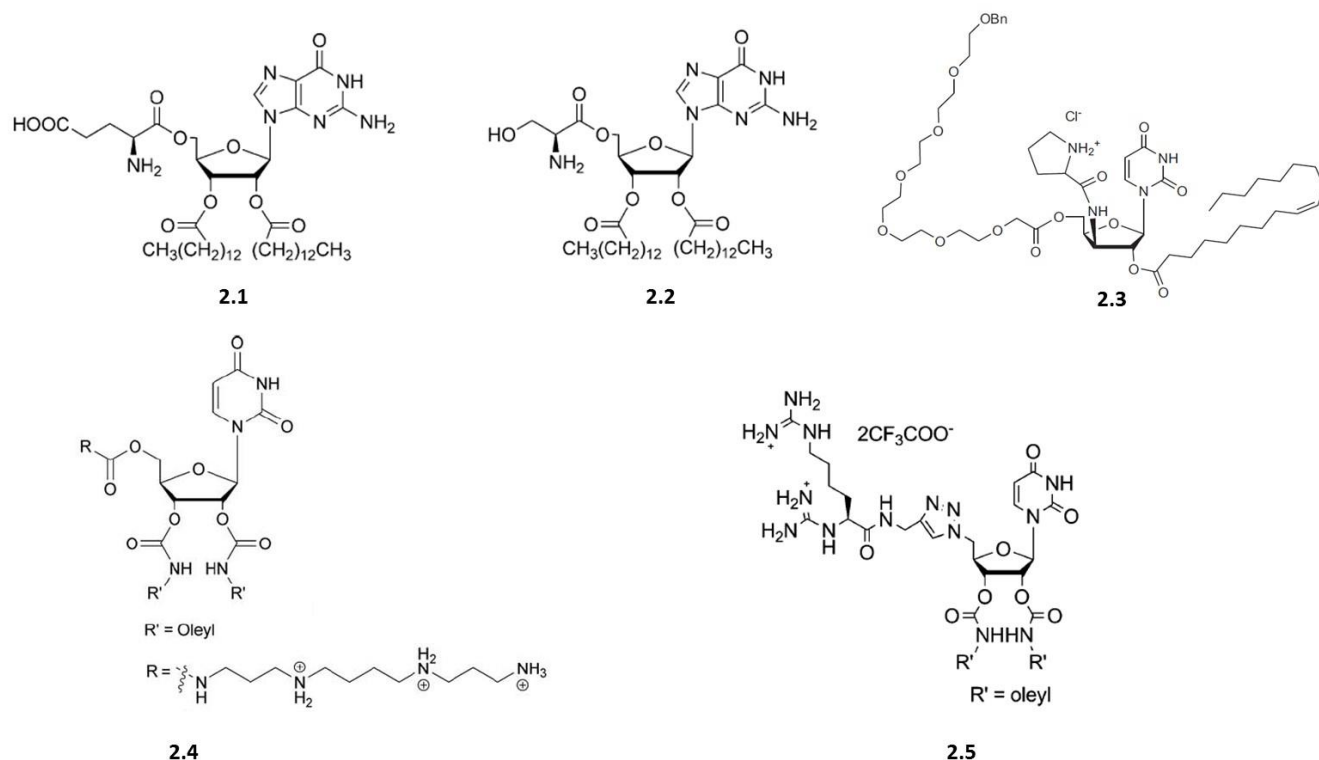


**Figure 2.1** Structures of synthetic aminoacyl nucleolipids [3-7].

## 2.2 CHAPTER OBJECTIVES

Inspired by their versatility and utility in bio-medical applications, this thesis chapter aims to design, develop and apply aminoacyl nucleolipids to anti-cancer therapy. In this study, an aminoacyl nucleolipid was designed to contain an ionizable ammonium group that can participate in ionic binding interactions (**Figure 2.2**) with the target promoter sequence of the GRP78 oncogene. Moreover, the nucleolipid scaffold was also rationalized to exhibit favorable amphiphilic properties (**Figure 2.2**) that may translate to effective anti-cancer activities in

tumors. The synthesis strategy developed in collaboration with Emi Hanawa (Ph.D. student) in the laboratory of Dr. Cecilia Marzabadi (Department of Chemistry, Seton Hall University) enabled the chemical modification of guanosine with a carboxylic acid group at the 5'-position in order to attach various bioactive modalities, one of which contained the desired aminoacyl functionality. Moreover, the 2' and 3'-hydroxyl groups of the nucleoside were used for the attachment of the fatty acids, in order to produce the amphiphilic aminoacyl nucleolipid. It was then characterized for its ability to bind to GRP78 DNA using Circular Dichroism (CD) Spectroscopy, UV-Vis thermal denaturation and gel shift assays. In collaboration with Reeta Yadav (Ph.D. student) in the laboratory of Dr. Uri Samuni (Department of Chemistry, Queen's College) the sizes of the complexes formed in between the aminoacyl nucleolipid and the oncogene sequence was also characterized by Dynamic Light Scattering (DLS). Following synthesis and characterization, the anti-cancer activity of the aminoacyl nucleolipid was evaluated by the National Cancer Institute's (NCI's) 60 Cancer Cell Line Screen. Taken together, this study highlights the rational design, synthesis, oncogene binding and anti-cancer activity of a new representative of the aminoacyl nucleolipids. They encompass a relatively new class of cationic amphiphilic conjugates whose structure, biophysical and biological properties remain largely un-explored. In this chapter, we describe the synthesis, characterization and medicinal chemistry applications of an aminoacyl nucleolipid (**Figure 2.2**). This study forms the basis for the development of new chemistries that may empower the combinatorial library synthesis of aminoacyl nucleolipids for exploring structure-activity relationships with biological targets in cancer.

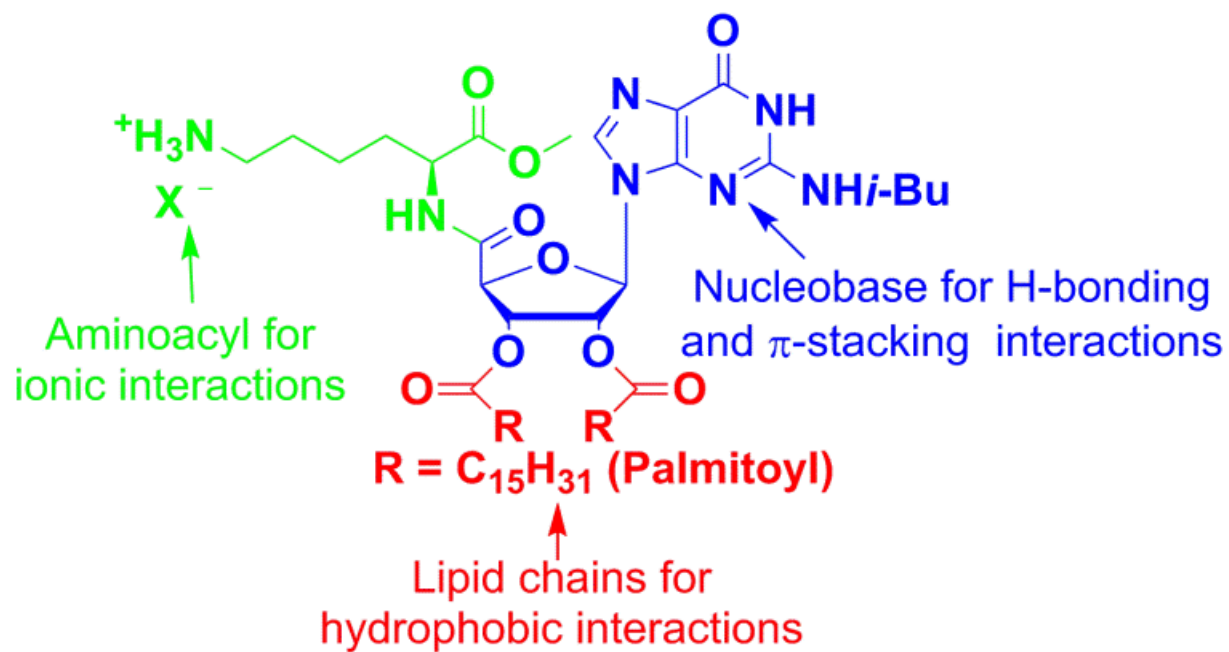


**Figure 2.2.** Chemical structure and DNA-binding interactions of aminoacyl nucleolipid, **2.6**.

## 2.3 SYNTHESIS, DNA BINDING AND ANTI-LEUKEMIC ACTIVITY OF AN AMINOACYL NUCLEOLIPID

Pradeepkumar Patel<sup>a</sup>, Emi Hanawa<sup>a</sup>, Reeta Yadav<sup>b</sup>, Uri Samuni<sup>b</sup>, Cecilia Marzabadi<sup>a</sup>, David Sabatino<sup>a,\*</sup>

<sup>a</sup>Department of Chemistry and Biochemistry, Seton Hall University, 400 South Orange Avenue, South Orange, New Jersey 07079, United States

<sup>b</sup>Department of Chemistry and Biochemistry, Queens College, City University of New York, 65-30 Kissena Blvd, Flushing, New York 11367,

United States

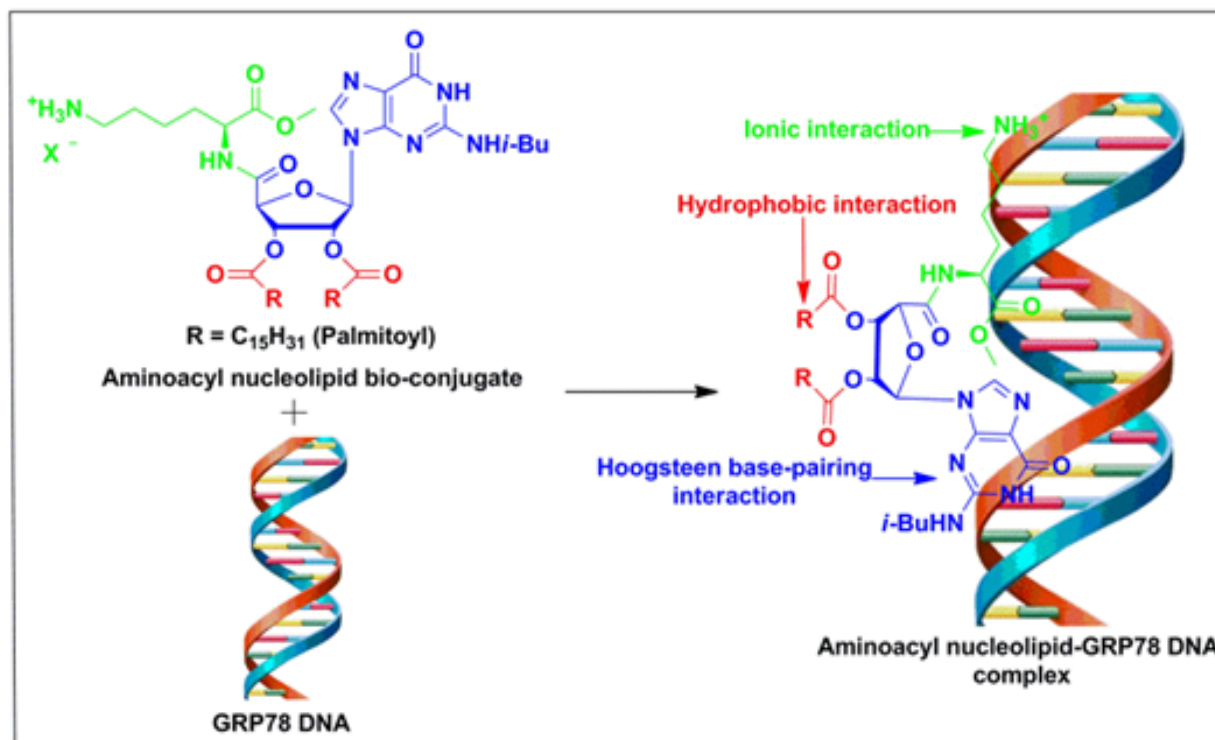


**Figure 2.3.** Graphical abstract describing the binding of an aminoacyl nucleolipid bioconjugate to the oncogene GRP78 DNA sequence. Figure adapted from Patel, P.; Hanawa, E.; Yadav, R.; Samuni, U.; Marzabadi, C.; Sabatino, D. *Bioorg. Med. Chem. Lett.* **2013**, *23*, 5086-5090 [9].

### 2.3.1 ABSTRACT

The synthesis and characterization of a new class of DNA binding molecules exhibiting potent and selective anti-leukemic activity is described. The synthesis of an aminoacyl nucleolipid was developed from an efficient EEDQ coupling strategy, in which a series of seven bioconjugates were synthesized in yields of 53-78%. Guanosine bioconjugate **2.13**, was used as building block for the synthesis of a target aminoacyl nucleolipid **2.6**. Its GRP78 DNA binding affinity was confirmed by gel shift assay, CD spectroscopy,  $T_m$  measurements and dynamic light scattering experiments. Moreover, in a single dose (10  $\mu$ M) screen against a panel of 60 cancer cell lines, aminoacyl nucleolipid **2.6** was found to selectively trigger greater than 90% cell death in a SR human leukemia cancer cell line. The reported aminoacyl nucleolipid represents a useful model for a new class of DNA binding molecules for the development of potent and selective anti-cancer agents.

### 2.3.2 INTRODUCTION

Aminoacyl nucleolipids represent an interesting class of bioconjugates owning the ability to form stable, higher-ordered structures for potential applications in medicinal chemistry [1-4,6,7,9]. For example, they form complexes with short-interfering RNA (siRNA), applicable in siRNA transfection leading to the down-regulation of mRNA and protein expression in cancer cells [6,7].

Aminoacyl nucleolipids may also own the ability to bind and stabilize double-stranded DNA by a series of non-covalent interactions. These include, H-bond base-pairing and  $\pi$ -stacking of the

nucleoside base as seen in the canonical Watson-Crick [10a] and Hoogsteen base-pairing interactions of ligand with duplex DNA [10b,10c]. The ionic interactions between the positively charged aminoacyl and the anionic phosphodiester DNA backbone as described in the condensation of DNA with poly-Arg and poly-Lys sequences [11]. Lastly, the van der Waals/hydrophobic interactions of the lipids create an amphiphilic microenvironment for DNA complex formation and cell permeability [12] (**Figure 2.2**). In the fight against cancer, stable DNA-bioconjugate interactions may form the basis for an effective gene therapy strategy [13].

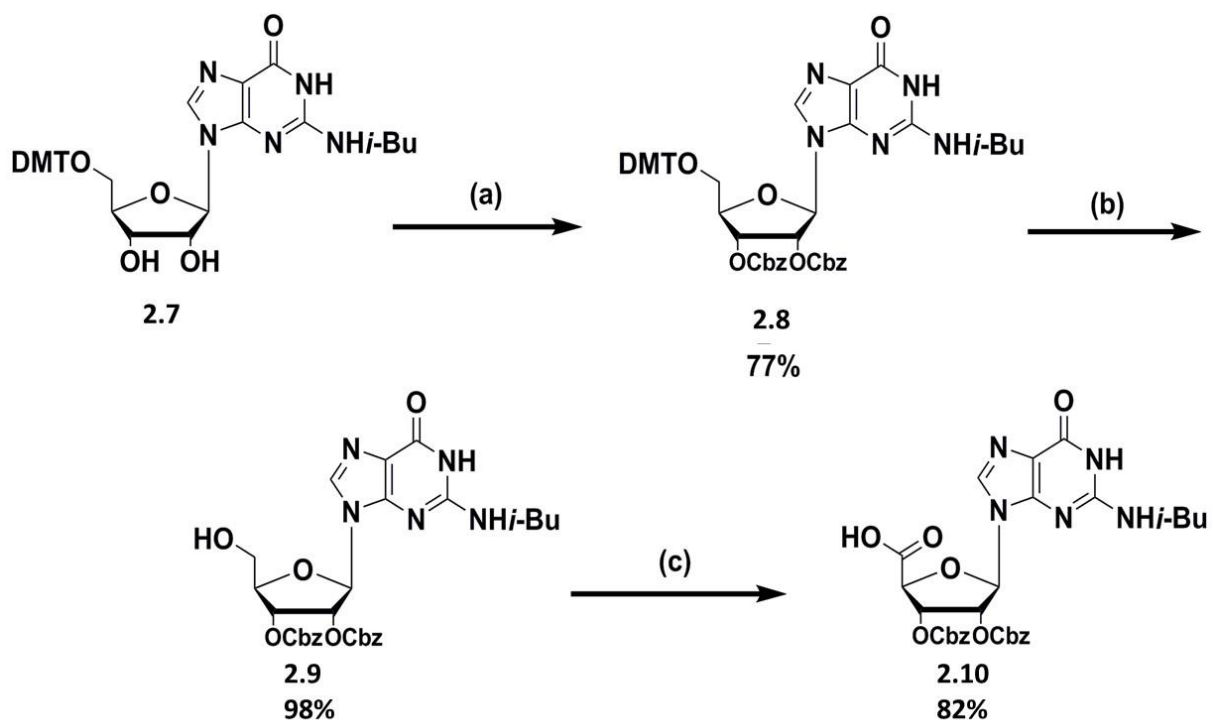
The Glucose-regulated protein 78 (GRP78) is a chaperone protein that functions to regulate protein folding events in the lumen of the endoplasmic reticulum (ER) of all cell types [14]. In cancer, GRP78 is overexpressed and exclusively localized on the cell surface where it exhibits a variety of signal transduction pathways associated with tumorigenesis and resistance towards apoptosis [15]. Thus, GRP78 functions as an ideal molecular marker for the selective detection and treatment of cancer cells [16]. In an effort to develop potent GRP78 DNA binders for anti-cancer applications, we describe the development of an aminoacyl nucleolipid, **2.6**. This aminoacyl nucleolipid has been validated by its ability to bind to the promoter region of GRP78 DNA, while soliciting potent and selective anti-leukemic activity.

### **2.3.3 RESULTS AND DISCUSSION**

#### **2.3.4 SYNTHESIS OF AN AMINOACYL NUCLEOLIPID**

The synthetic strategy begins with the generation of *N*-isobutyryl 5'-carboxy 2',3'-bis-*O*-(carbobenzyloxy) guanosine, **2.10**, (**Scheme 2.1**) as the building block component for furnishing bioconjugates (**Table 2.1**). In the preparation of **2.10**, *N*-isobutyryl 5'-dimethoxytrityl guanosine, **2.7**, was used as commercially available starting material to initiate the synthesis strategy. The

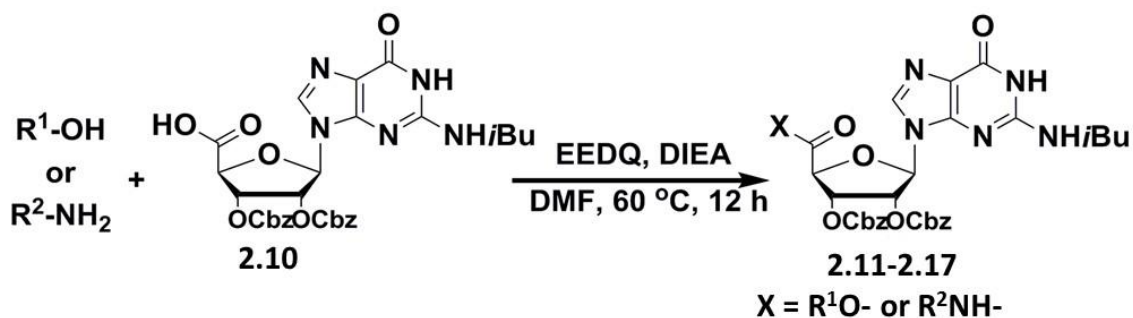
Cbz protecting groups were installed using an excess of benzylchloroformate and DMAP in DCM [17]. Following carbonylation, **2.8**, was detritylated in 98% yield using 3% trichloroacetic acid in DCM [18]. *N*-isobutyryl-2',3'-bis-*O*-(carbobenzyloxy)guanosine, **2.9**, was then oxidized in 82% yield to the corresponding carboxylic acid, **2.10**, using a TEMPO oxidation [19].



**Scheme 2.1.** Synthesis of *N*-isobutyryl 5'-carboxy 2',3'-bis-*O*-(carbobenzyloxy) guanosine, **2.10**. Conditions: (a) DMAP, benzyl chloroformate, DCM, 0 °C then r.t., 72 h, 77%, (b) 3% TCA:DCM, r.t., 15 min, 98%, (c) TEMPO, BAIB, MeCN:H<sub>2</sub>O (50:50 v/v), r.t., 15 h, 82%.

With building block **2.10** in hand, a small library of aminoacyl and lipid conjugates were prepared. Coupling conditions were optimized based on literature precedence [20], by using *N*-ethoxycarbonyl 1,2-ethoxy-1,2-dihydroquinoline, EEDQ, (2 equiv) as coupling reagent and *N,N*-

diisopropylethylamine, DIEA (2 equiv) as the base in DMF. Briefly, alkyl amines or alcohols (Table 2.1, entries 2.11, 2.12, 2.17) were coupled with 2.10 to their corresponding amides or esters, respectively, in yields of 55-73%. In similar fashion, amino esters (Table 2.1, entries 2.13- 2.16) were coupled to their corresponding amides with building block 2.10 in yields ranging from 53-78%. The pure bioconjugates were characterized by NMR, IR, MS and polarimetry.

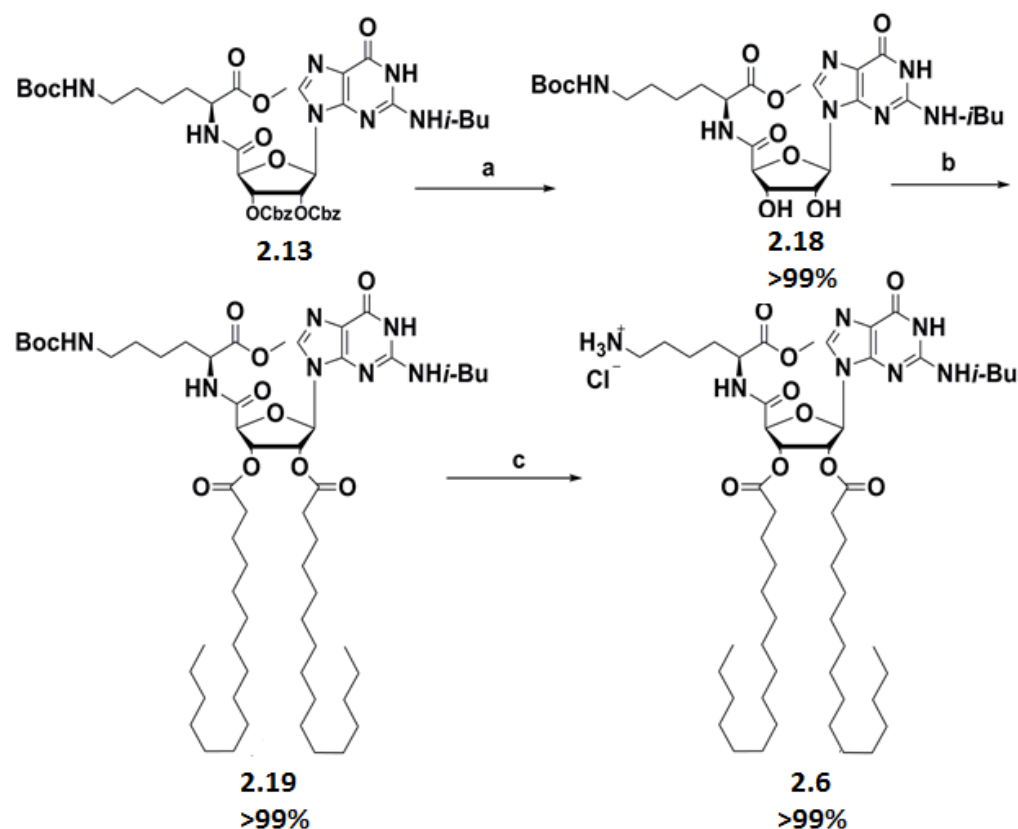


Entry	R <sup>1</sup> -OH or R <sup>2</sup> -NH <sub>2</sub>	X	Yield (%)
2.11			73
2.12			55
2.13			53
2.14			78
2.15			67
2.16			70
2.17			70

**Table 2.1.** Bioconjugation of aminoacyl and lipid nucleosides.



Bioconjugate **2.13**, was selected for the preparation of aminoacyl nucleolipid, **2.6**, following a simple three-step procedure. Firstly, the Cbz protecting groups were removed using conventional hydrogenation conditions [17], generating diol **2.18** in quantitative yields. The product was then dissolved in pyridine and acylated with an excess of palmitoyl chloride [21] to afford the protected aminoacyl nucleolipid **2.19** in >99% yield. Following purification, the Boc-protecting group of **2.19** was removed using 50% TFA:DCM, followed by salt exchange with aqueous HCl. The desired product, **2.6**, obtained in quantitative yield was lyophilized to dryness and characterized (Scheme 2.2).



**Scheme 2.2.** Synthesis of aminoacyl nucleolipid, **2.6**. Conditions: (a) H<sub>2</sub>, 10% Pd/C, EtOH, r.t., 1.5 h, >99% (b) palmitoyl chloride, DMAP, pyr., 2 h, >99% (c) 50% TFA:DCM, 2 h, r.t., then 1 M HCl, 3 h, >99%.

Attempts to selectively deprotect the guanine NH-*i*-Bu using mildly basic conditions [22] resulted in concomitant ester cleavage of the palmitoyls and methyl ester groups. Thus, we rationalized that partial protection of aminoacyl nucleolipid, **2.6** may confer greater resistance towards degradation, while inhibiting formation of higher-order self-assemblies (*i.e.* guanine-tetraplexes) that may influence DNA binding and biological activity [3]. CD spectroscopy of aminoacyl nucleolipid **2.6** (0.2-3.9 mM) did not exhibit a guanine-tetraplex structure at higher concentrations (0.9-3.9 mM) (**Figure 2.4**). They are usually characterized by an intense positive band near 264 nm and a negative one near 245 nm (for parallel tetraplex structures), and a positive band near 290 nm and negative ones near 260 and 245 nm (for anti-parallel tetraplex structures) [23].

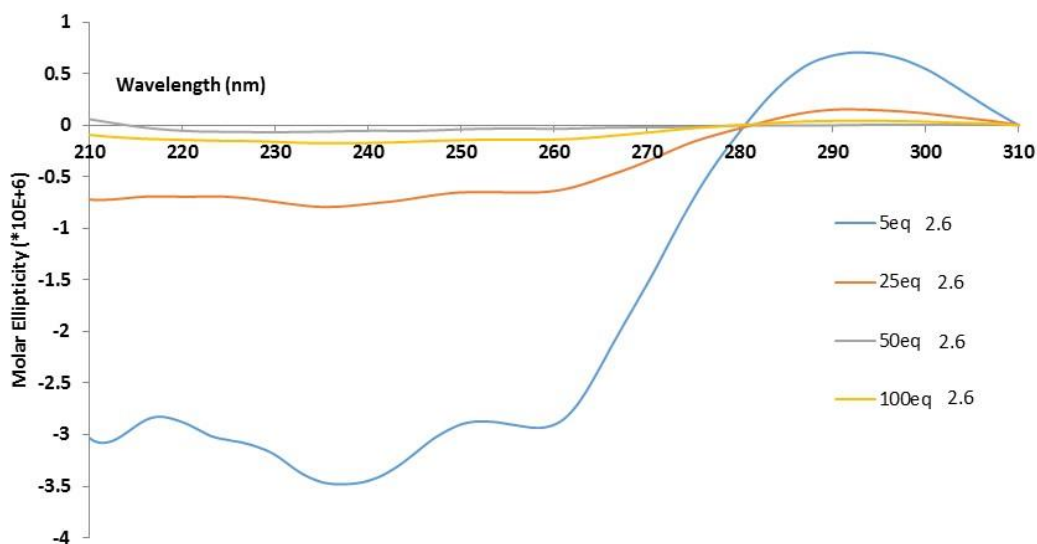


**Figure 2.4.** CD spectrum of **2.6** (0.2-3.9 mM) in phosphate buffer at 25 °C.

### 2.3.5 DNA BINDING STUDIES OF AMINOACYL NUCLEOLPID **2.6**

The promoter region of GRP78 DNA encompassing nucleotides 252-269 [24] was synthesized by conventional automated solid-phase oligonucleotide synthesis [25]. The oligonucleotides

were purified by reverse-phase ion-pairing HPLC (RP-IP HPLC) [26] and characterized by mass spectrometry (**Figure 2.5**).

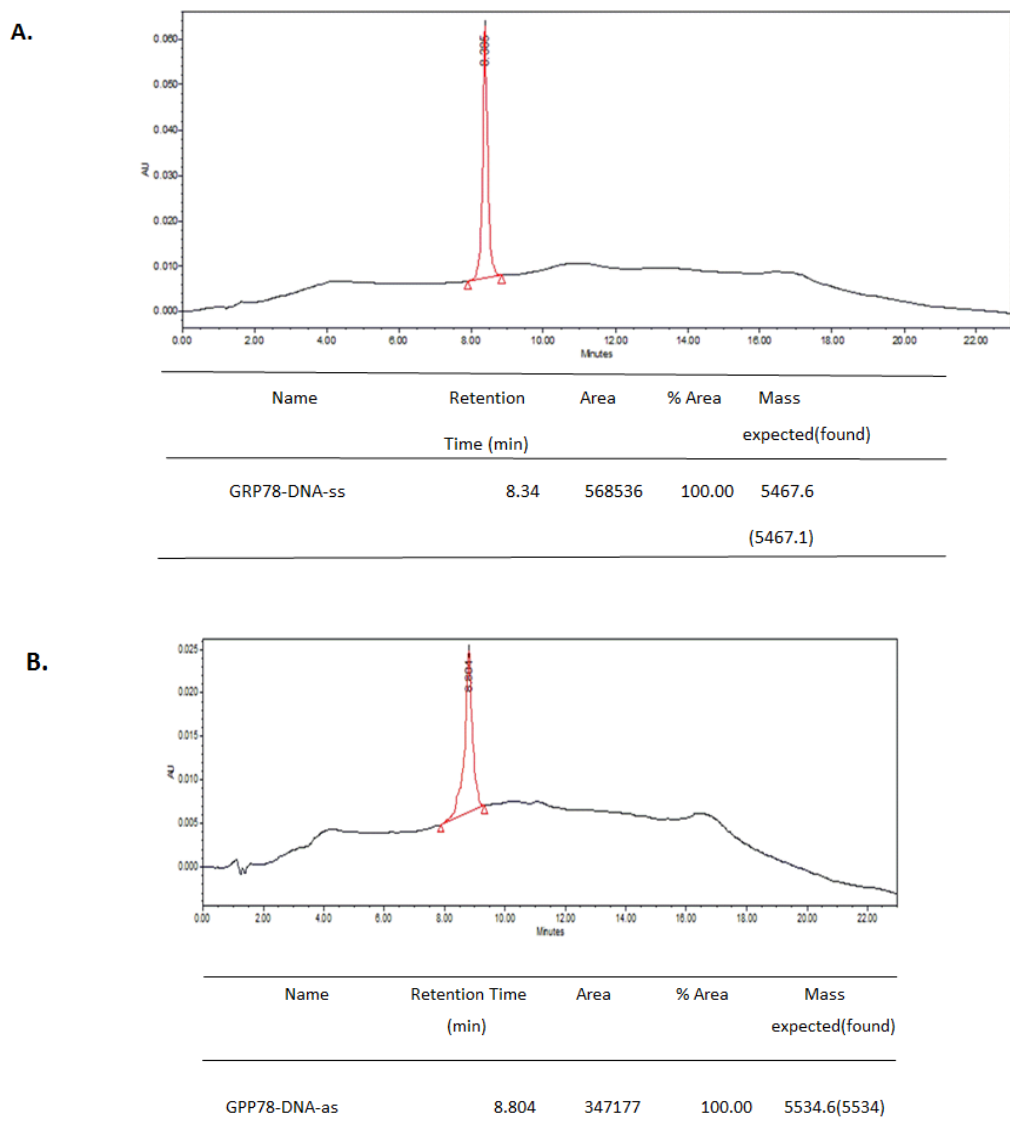


**Figure 2.5.** HPLC chromatograms (260 nm) and corresponding mass spectra data of GRP78 DNA (A) sense (ss) and (B) antisense (as) strands

Complementary sequences (0.57  $\mu\text{M}$ ) were annealed in 15  $\mu\text{L}$  of 30% sucrose in 5x TAE buffer (89 mM Tris/acetate, 2.5 mM EDTA, pH = 4.2) and incubated at 37  $^{\circ}\text{C}$  for 36 h with and without ligand **2.6**, at 0, 5, 25, 50, and 100 equiv, based on the ratio of **2.6**/DNA phosphate

groups, which corresponds to the following concentrations: 0, 0.2, 0.9, 1.9, 3.9 mM, respectively. A 24% native PAGE gel shift binding assay was performed to evaluate ligand binding to GRP78 DNA (**Figure 2.6**). Following electrophoresis, gradual disappearance of the DNA bands was visualized by UV-shadowing at 260 nm. The observed trend is typical of higher-order complex structures, which results in the diminished intensity of the UV-bands corresponding to duplex DNA [27]. Quantitative analysis of the ratio between duplex DNA with and without **2.6** demonstrated 50% duplex binding affinity ( $K_D$ ) at 0.7 mM.

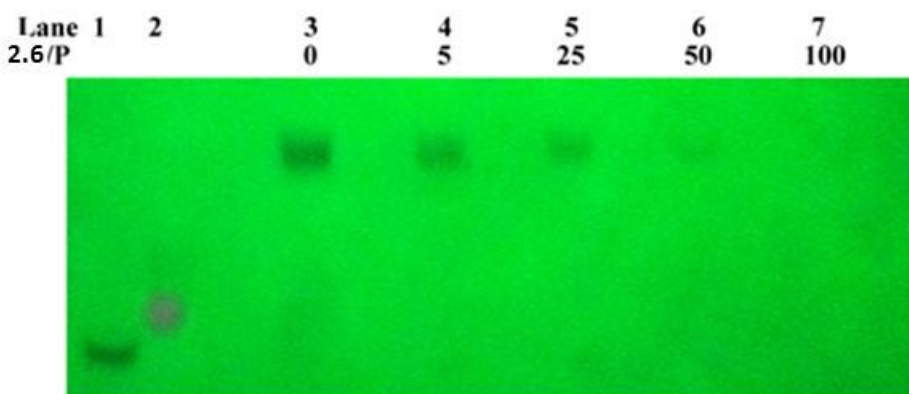


**Figure 2.6.** Gel shift assay for GRP78 DNA with **2.6**: From lane 3 to 7, increasing amount of ligand **2.6** from 0 to 100 equiv. **2.6**/P (0-3.9 mM). Lane 1 and 2 are single stranded GRP78 DNA

The GRP78 DNA binding stability with and without **2.6** was evaluated by thermal denaturation (**Figure 2.7**). Changes in duplex DNA UV-absorption at 260 nm was monitored with increasing temperatures (5-90 °C). DNA samples (1.1  $\mu$ M) were prepared by annealing complementary single strands in physiological phosphate binding buffer (140 mM KCl, 1 mM  $MgCl_2$ , 5 mM  $Na_2PHO_4$  adjusted to pH 7.2). The melting temperature ( $T_m$ ) of native GRP78 DNA was evaluated at 66 °C, whereas the addition of ligand (0.2-3.9 mM) produced drastic

changes in the DNA melting curves. For example, at 0.2 mM, **2.6** exhibited a stabilizing effect on GRP78 DNA duplex ( $\Delta T_m = +4$  °C), whereas at higher concentrations (0.9-3.9 mM) changes in duplex DNA hyperchromicities with increasing temperatures were indicative of higher-order structure transitions [28].

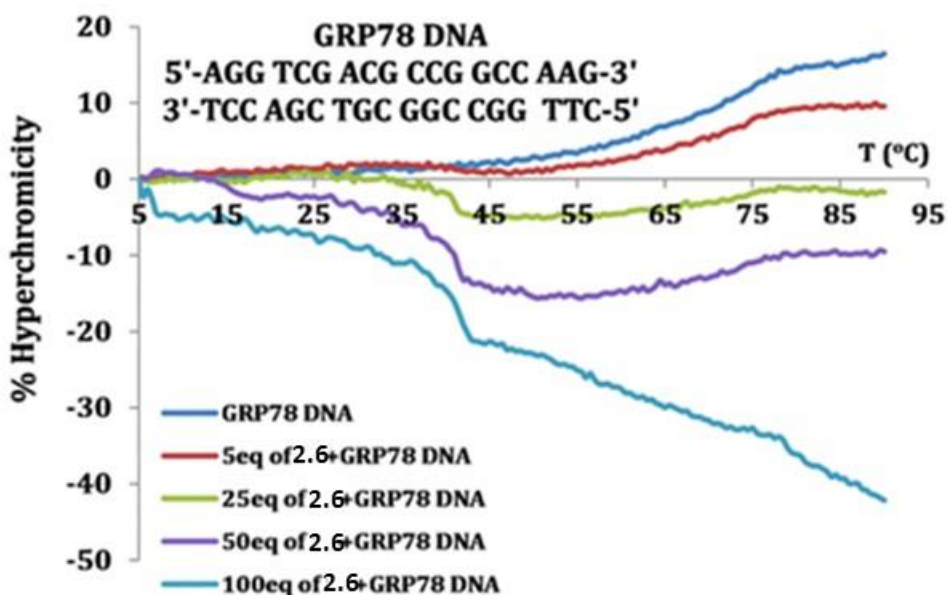


**Figure 2.7.** Thermal denaturation curves. Changes in % hyperchromicity at 260 nm versus temperature of GRP78 DNA (1.1  $\mu$ M) in the presence of ligand **2.6** (0.2-3.9 mM).

In order to gain greater insight into the structural changes of native GRP78 DNA with the addition of ligand **2.6**, the Circular Dichroism (CD) spectrum was collected (**Figure 2.8**). The samples were prepared as previously described for the thermal denaturation studies. The native GRP78 DNA duplex exhibited a CD structure consistent with a B-type helix, with characteristic broad maximum band between 260 - 280 nm and a minimum at 248 nm [29]. The amplitudes of the molar ellipticities at these characteristic wavelengths were found to diminish upon titration with **2.6** (0.2-3.9 mM) suggesting that the ligand-bound structure compromises DNA duplex

helicity until the formation of a higher-order complex persists at higher ligand concentrations (i.e. 100 equiv **2.6**/P, 3.9 mM).

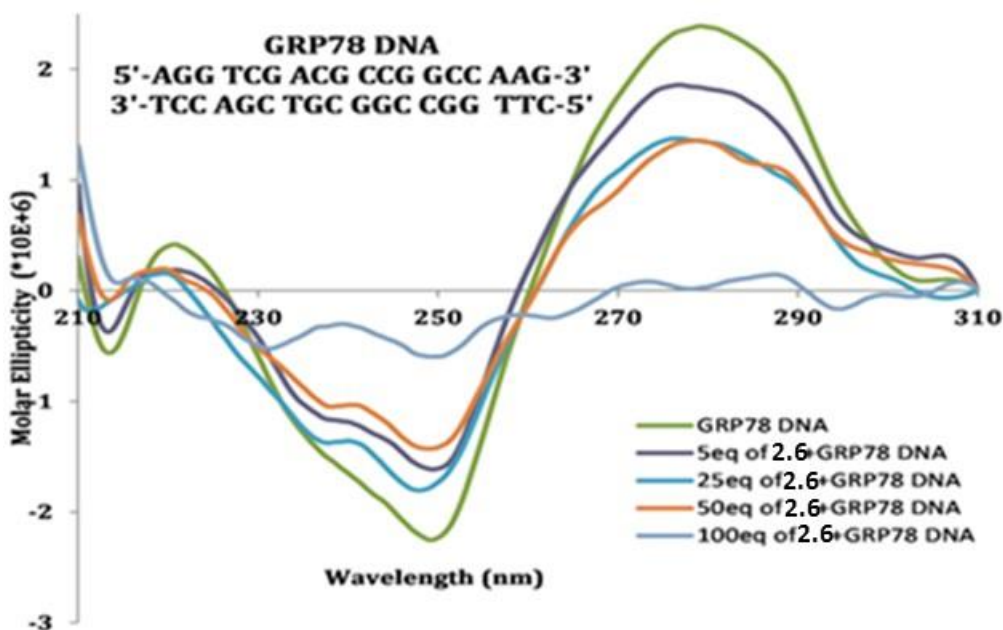


**Figure 2.8** Circular Dichroism (CD) spectrum of GRP78 DNA (1.1  $\mu\text{M}$ ) with complexing ligand **2.6** (0-3.9 mM) in phosphate buffer.

To further characterize the size of the complex formed between GRP78 DNA and **2.6**, dynamic light scattering (DLS) studies were performed relative to native DNA and aminoacyl nucleolipid, **2.6**. DNA (1.1  $\mu\text{M}$ ) was prepared with and without aminoacyl nucleolipid **2.6** (3.9 mM) and incubated in phosphate buffer for 36 hours prior to DLS measurements (**Table 2.2**). The observed hydrodynamic radii ( $R_h$ ) for the particles shows fixed values for DNA (0.9 nm) and aminoacyl nucleolipid **2.6** (~460 nm). Alternatively, the complex formed in between DNA and **2.6** illustrates a 3.4 fold increase in particle size, suggesting the formation of a higher-order complex structure.

**Table 2.2** Hydrodynamic Radii (Rh, nm) of aminoacyl nucleolipid, **2.6**, and DNA+**2.6** at 25 °C.

<b>Compound</b>	<b>Time</b>	<b>Rh</b>
	<b>(h)</b>	<b>(nm)</b>
<b>2.6</b>	0	468±1.9
	36	460±1.2
DNA+ <b>2.6</b>	0	2707±11
	36	9294±53

### **2.3.6 ANTI-CANCER ACTIVITY OF AMINOACYL NUCLEOLIPID 2.6**

In order to assess the anti-cancer activity of aminoacyl nucleolipid **2.6**, a cancer cell line screening assay was conducted against a panel of 60 cell lines selected at the National Cancer Institute (NCI) [30]. A single dose (10 µM) screen was performed with **2.6**, and cell viability was determined following 48 h incubation with cancer cells at 37 °C. A sulforhodamine B (SRB cell viability assay [31] was performed to determine cell death in the presence of **2.6**. Aminoacyl nucleolipid **2.6** was found to exhibit potent and selective anti-cancer activity (see Supporting Information, **Figure 2.10**), with greater than 90% cell death against a SR human lymphoblastic leukemia cancer cell line (**Figure 2.9**). Interestingly, GRP78 expression levels are elevated in leukemic blasts of adult patients and in early relapse childhood leukemia [32] suggesting a

correlation between the GRP78 DNA binding affinity and anti-leukemic activity of aminoacyl nucleolipid **2.6**. We are currently investigating the bio-molecular basis for the potent and selective activity of **2.6** in leukemia cells.

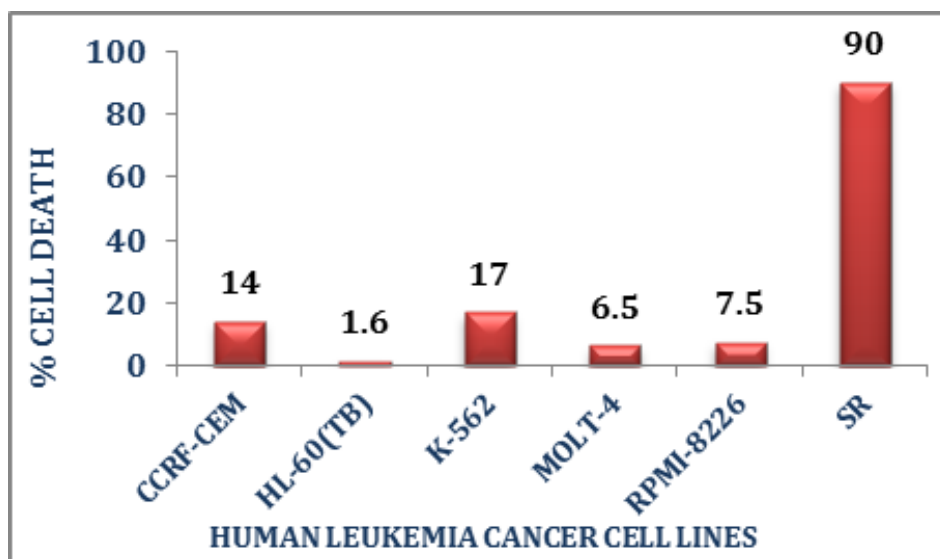


**Figure 2.9.** Cell death of human leukemia cell lines following treatment with **2.6** (10  $\mu$ M) for 48 h.

### 2.3.7 CONCLUSIONS

In conclusion, with the synthesis of derivative **2.6**, we have demonstrated the utility of a new class of aminoacyl nucleolipid, which can have great relevance due to their tight binding with GRP78 DNA and marked ability to trigger potent and selective anti-leukemic activity. This work paves the way for additional studies into the mechanism of aminoacyl nucleolipid anti-cancer activity. Moreover, **2.6** may form the basis for novel ligand design and development for anti-cancer applications.



### 2.3.8 EXPERIMENTAL SECTION

**General Methods.** All non-aqueous reactions were performed under inert atmosphere (nitrogen) unless specified. All glassware was dried and stored in a pre-heated oven (160 °C) and cooled under inert atmosphere prior to use. Anhydrous solvents and reagents were purchased from Aldrich (St. Louis, MO) and used as received. Analytical thin-layer chromatography (TLC) was performed on aluminum-backed silica gel plates (Merck 60 F254). TLCs were visualized under UV shadowing (260 nm) or staining (10% H<sub>2</sub>SO<sub>4</sub>/MeOH). Compound purification using silica gel chromatography was performed on a 230-400 mesh silica (Sorbent Technologies). Melting points were obtained on a Thermo Melt apparatus. Specific rotations measurements were recorded on a DigiPol 781 Automatic Polarimeter (Rudolph Instruments, Fairfield, NJ, USA) and collected as averages of five measurements per compound. Data are reported as follows:  $[\alpha]_{\lambda}$  temp, concentration (c in g/100 mL), in Ace, MeOH, DCM or CHCl<sub>3</sub>. Molecular weights were measured as direct injections on a Hewlett Packard series 1100 MSD equipped with ESI as ion-source in positive mode using 50/50 v/v MeOH/H<sub>2</sub>O at a flow-rate of 1 mL/min. Infrared (IR) spectra were obtained on a Nicolet 4700 FT-IR (ThermoElectron Co.) coupled with OMNIC software (driver version: 7.1). The compounds were deposited on a KBr plate with cast film technique and the data was collected as an average of 3 scans in wavenumbers (cm<sup>-1</sup>). Nuclear magnetic resonance spectra (<sup>1</sup>H, <sup>13</sup>C, COSY NMR) were recorded on an OXFORD NMR AS500 spectrophotometer. The NMR spectra were obtained at ambient temperature using an indirect pulse-field gradient (ID-PFG) probe. The obtained data was processed using VNMRJ software (version 2.2). The <sup>1</sup>H and <sup>13</sup>C assignments were based on gCOSY and gHMQC NMR correlation experiments.

## Synthesis.

***N*-Isobutyryl-5'-*O*-(4-dimethoxytrityl)-2',3'-di-*O*-(carbobenzyloxy) guanosine (2.8):** *N*-Isobutyryl-5'-*O*-(4-dimethoxytrityl) guanosine (3.0 g, 4.5 mmol) was suspended in dichloromethane (90 mL) and DMAP (8.2 g, 67 mmol) was added. After cooling to 0 °C, benzyl chloroformate (5.4 mL, 38 mmol) was added dropwise and the suspension was stirred at room temperature. After 3 days, the solution was diluted with dichloromethane and evaporated to a viscous oil. The product was purified by silica gel chromatography (Ace/DCM 9:1) giving nucleoside **2.8** (3.2 g, 3.9 mmol) as a white solid. Yield : 78%. m.p. 131 °C. TLC (Ace/DCM 9:1) R<sub>f</sub>: 0.8.  $[\alpha]_{589}^{23}$  -29 (c 0.005, DCM). IR (KBr)  $\nu_{\max}$  (cm<sup>-1</sup>) = 3160, 3009, 2917, 2837, 1759, 1674, 1608, 1564, 1508, 1463, 1408, 1381, 1275, 1252, 1177, 1155, 1094, 1033, 904, 829, 755. <sup>1</sup>H NMR (500 MHz, DMSO-d<sub>6</sub>):  $\delta$  8.09 (s, 1H, H8), 6.79-7.36 (m, 23H, arom. DMT, Cbz), 6.13 (d, *J* = 7 Hz, 1H, 1H'), 5.94 (t, *J* = 6 Hz, 1H, 2H'), 5.46 (dd, *J* = 3, 6 Hz, 1H, H3'), 5.13 (d, *J* = 5 Hz, 2H, CH<sub>2</sub>), 5.10 (d, *J* = 2 Hz, 2H, CH<sub>2</sub>), 4.33 (m, 1H, H4'), 3.71 (s, 6H, 2xOCH<sub>3</sub>), 3.49 (dd, *J* = 6, 10 Hz, 1H, 5H'), 3.28 (dd, *J* = 5, 10 Hz, 1H, H5''), 2.68 (m, 1H, *i*-BuH), 1.1 (d, *J* = 1 Hz, 3H, *i*-BuCH<sub>3</sub>), 1.09 (d, *J* = 1 Hz, 3H, *i*-BuCH<sub>3</sub>). <sup>13</sup>C NMR (126 MHz, DMSO-d<sub>6</sub>)  $\delta$ : 178.3, 158.8, 155.4, 154.2, 153.7, 148.1, 147.2, 144.6, 139.2, 135.9, 135.4, 134.5, 130.0, 130.02, 129.1, 128.8, 128.7, 128.6, 128.5, 128.5, 128.4, 128.1, 128.0, 127.8, 127.8, 127.2, 122.5, 113.3, 113.2, 113.1, 86.43, 85.03, 81.40, 77.31, 77.05, 76.80, 74.60, 74.13, 70.56, 70.34, 62.64, 55.23, 35.99, 18.95, 18.44. ESI MS (m/z) calculated for C<sub>51</sub>H<sub>48</sub>N<sub>5</sub>O<sub>12</sub> [M-H], 922.3; found 922.6.

***N*-Isobutyryl-2',3'-di-*O*-(carbobenzyloxy) guanosine (2.9):** To compound **2.8** (3.0 g, 3.2 mmol), 3% trichloroacetic acid in dichloromethane (50 mL) was added at room temperature. The reaction reached completion in 15 minutes as detected by TLC. The product was extracted with DCM (10 mL) and washed with 5% NaHCO<sub>3</sub> (10 mL). The organic layer was dried over Na<sub>2</sub>SO<sub>4</sub>

and concentrated *in vacuo* to afford a dark yellow crude residue. The crude product was purified by a flash silica gel column chromatography (Ace/DCM 1:3) giving nucleoside **2.9** (2 g, 3.2 mmol) as a white solid. Yield : 98%, TLC (Ace/DCM 1:3)  $R_f$  : 0.23. m.p. 98 °C.  $[\alpha]_{589}^{23}$ : 42.6 (c 0.005, DCM). IR (KBr)  $\nu_{\max}$  ( $\text{cm}^{-1}$ ) = 3363, 3204, 2974, 1755, 1677, 1605, 1568, 1457, 1384, 1277, 1156, 1100, 1012, 949, 904, 831, 783, 754.  $^1\text{H}$  NMR (500 MHz, DMSO- $d_6$ ):  $\delta$  12.07 (s, 1H, NH), 11.61 (s, 1H, NH), 8.3 (s, 1H, H8), 7.2-7.4 (m, 10H, arom. Cbz), 6.06 (d,  $J$  = 7 Hz, 1H, 1H'), 5.72 (dd,  $J$  = 5, 7.5 Hz, 1H, 2H'), 5.47 (t,  $J$  = 5 Hz, 1H, 3H'), 5.42 (t,  $J$  = 5 Hz, 1H, 4H'), 5.14 (d,  $J$  = 11 Hz, 2H, CH<sub>2</sub>), 5.07 (d,  $J$  = 2 Hz, 2H, CH<sub>2</sub>), 4.3 (brs, 1H, OH), 3.7 (dd,  $J$  = 5, 10 Hz, 2H, H5', H5''), 2.69 (m, 1H, *i*-BuH), 1.09 (d,  $J$  = 6, 7 Hz, 6H, *i*-BuCH<sub>3</sub>).  $^{13}\text{C}$  NMR (126 MHz, DMSO- $d_6$ ):  $\delta$  155.1, 153.9, 153.4, 137.6, 135.4, 135.2, 129.1, 129.0, 128.9, 128.8, 128.7, 123.1, 120.3, 83.89, 83.49, 76.90, 75.72, 70.31, 70.10, 61.25, 35.27, 19.29, 19.23. ESI MS ( $m/z$ ), calculated for C<sub>30</sub>H<sub>30</sub>N<sub>5</sub>O<sub>10</sub>, [M-H], 620.2; found 620.7.

***N*-Isobutyryl-5'-carboxy -2',3'-di-*O*-(carbobenzyloxy) guanosine (2.10)**: *N*-Isobutyryl-2',3'-di-*O*-(carbobenzyloxy) guanosine, **2.9**, (0.25 g, 0.4 mmol), **2,2,6,6-tetramethyl-1-piperidinyloxy** free radical (TEMPO) (15.6 mg, 1 mmol) and bis(acetoxy)iodobenzene (BAIB) (258 mg, 8 mmol) were combined in a mixture of MeCN/H<sub>2</sub>O (1:1 v/v, 20 mL) and stirred overnight at 25 °C. Acetone (5 mL) was added followed by Et<sub>2</sub>O (25 mL) and the mixture was stirred for an additional 2 h for completion as detected by TLC. The crude product, **2.10**, was filtered and washed with Et<sub>2</sub>O (10 mL) resulting in a yellow solid (0.21 g, 0.33 mmol). Yield: 82%, TLC (MeOH/DCM 1:9)  $R_f$  :0.25. m.p. >240 °C.  $[\alpha]_{589}^{23}$ :-39 (c 0.005, DCM). IR (KBr)  $\nu_{\max}$  ( $\text{cm}^{-1}$ ) = 3499, 3411, 2996, 2914, 1660, 1438, 1403, 1311, 950, 928, 894, 666.  $^1\text{H}$  NMR (500 MHz, DMSO- $d_6$ ):  $\delta$  8.96 (s, 1H, H8 ), 7.2-7.4 (m, 10H arom. Cbz), 6.12 (d,  $J$  = 10 Hz, 1H, 1H'), 5.61 (t,  $J$  = 4 Hz, 1H, 2H'), 5.51 (d,  $J$  = 4, 1H, 3H'), 5.0-5.2 (m, 4H, CH<sub>2</sub>Cbz), 4.4 (s, 1H,

4H'), 2.68 (m, 1H, *i*-BuH), 1.07 (d,  $J = 7$  Hz, 6H, *i*-BuCH<sub>3</sub>). <sup>13</sup>C NMR (DMSO-d<sub>6</sub>, 126 MHz):  $\delta$  180.5, 171.1, 155.2, 154.0, 153.4, 149.4, 148.8, 139.3, 135.4, 135.2, 129.1, 129.0, 128.9, 128.9, 128.8, 128.7, 128.6, 128.6, 120.0, 84.03, 83.58, 79.63, 78.76, 70.30, 70.09, 69.81, 35.23, 19.51, 19.30, 19.20. ESI MS (m/z); Calculated for C<sub>30</sub>H<sub>30</sub>N<sub>5</sub>O<sub>11</sub>, [M+H], 636.19; found 636.4.

### General procedure for the preparation of bio-conjugates (2.11-2.17) :

To a solution of **2.10** (50 mg, 0.08 mmol, 1 equiv) in DMF (2 mL), *N*-ethoxycarbonyl-2-ethoxy-1,2-dihydroquinoline (EEDQ) (39.6 mg, 0.16 mmol, 2 equiv.) was added and the mixture was stirred for 10 minutes at room temperature. *N,N*-Diisopropylethylamine (DIEA) (20.7 mg, 0.16 mmol, 2 equiv) was added to the reaction at room temperature. In a separate flask, alkyl amine or alcohol (0.12 mmol, 1.5 equiv) was dissolved in DMF (2 mL) and added to the reaction mixture. The reaction was then heated to 60 °C and continued for 12 hours. The reaction progress was monitored by TLC until completion. The product was extracted in DCM (10 mL) and washed with H<sub>2</sub>O (3 x 10 mL) and brine (10 mL). The organic layer was dried with Na<sub>2</sub>SO<sub>4</sub>, filtered and concentrated *in vacuo* prior to purification by silica gel column chromatography.

***N*-Isobutyryl-5'-octanoyl-2',3'-di-*O*-(carbobenzyloxy) guanosine (2.11).** Yield: 73%; light brown powder; m.p.= 72-74 °C; TLC (DCM:MeOH 95: 5): R<sub>f</sub> = 0.62; [ $\alpha$ ]<sub>589</sub><sup>24</sup> -8.2 (*c* 1.0, acetone); IR (KBr)  $\nu_{\max}$  (cm<sup>-1</sup>) = 2923, 2852, 1759, 1679, 1635, 1611, 1564, 1465, 1386, 1275, 1154, 1097, 1027, 971, 783, 754; <sup>1</sup>H NMR (acetone-d<sub>6</sub>, 500 MHz):  $\delta$  12.04 (s, 1H), 10.43 (s, 1H), 8.27 (s, 1H), 7.47-7.34 (m, 10H), 6.21 (d,  $J = 5.9$  Hz, 1H), 5.84 (m, 2H), 5.62 (s, 2H), 5.26 (dd,  $J = 9.3, 20$  Hz, 2H), 5.11 (dd,  $J = 4.4, 17.5$  Hz, 2H), 4.94 (s, 1H), 4.27 (t,  $J = 6.3$  Hz, 2H), 2.89 (dt,  $J = 6.8, 13.7$  Hz, 1H), 2.09 (s, 3H), 1.71-1.68 (m, 2H), 1.24 (d,  $J = 7$  Hz, 6H), 0.88 (t,  $J = 6.3$  Hz, 8H); <sup>13</sup>C NMR (acetone-d<sub>6</sub>, 126 MHz):  $\delta$  216.3, 210, 172.2, 170.2, 164, 155.4, 155,

138.6, 136.8, 130.3, 130.2, 118.7, 110.6, 86.3, 82.1, 78.2, 77.9, 72.0, 67.8, 61.7, 37.4, 33.3, 27.3, 24.1, 20.1, 15.1, 10.9; ESI MS (m/z) calculated for C<sub>38</sub>H<sub>44</sub>N<sub>5</sub>O<sub>11</sub>, [M-H]<sup>+</sup>, 746.8; found 746.8.

***N*-Isobutyryl-5'-diethyleneglycol-monoethyl-ether-2',3'- di-*O*-(carbobenzyloxy) guanosine**

**(2.12).** Yield: 55%; brown viscous liquid; TLC (DCM:MeOH 95:5): R<sub>f</sub> = 0.62; [α]<sub>589</sub><sup>24</sup> -70.2 (c 0.2, acetone); IR (KBr) ν<sub>max</sub> (cm<sup>-1</sup>) = 3138, 2928, 1753, 1691, 1238, 1126, 947, 784, 755; <sup>1</sup>H NMR (acetone-d<sub>6</sub>, 500 MHz): δ 11.97 (s, 1H), 10.52 (s, 1H), 8.02 (s, 1H), 7.47-7.34 (m, 10H), 6.64 (d, *J* = 2.5 Hz, 1H), 6.42 (t, *J* = 2.6 Hz, 1H), 6.24 (d, *J* = 2.5 Hz, 1H), 5.85 (m, 1H), 5.26 (dd, *J* = 5, 9 Hz, 2H), 5.14 (dd, *J* = 1.5, 8.5 Hz, 2H), 4.96 (s, 1H), 4.47 (m, 1H), 3.79-3.41 (m, 8H), 2.90 (q, *J* = 5 Hz, 1H), 1.27 (d, *J* = 25 Hz, 6H), 1.18 (t, *J* = 6.8 Hz, 3H); <sup>13</sup>C NMR (acetone-d<sub>6</sub>, 126 MHz): δ 181.5, 169.7, 160.3, 156.2, 155.3, 153.4, 150.3, 149.9, 138.9, 138.6, 136.6, 130.1, 130.0, 129.9, 122.8, 109.1, 90.6, 85.9, 84.8, 82.0, 78.0, 71.9, 71.8, 71.4, 71.2, 66.7, 65.4, 53.5, 39.3, 37.1, 19.9, 19.8, 16.1; ESI MS (m/z) calculated for C<sub>36</sub>H<sub>41</sub>N<sub>5</sub>O<sub>13</sub>, [M<sup>+</sup>] 751.7; found 752.3.

***N*-Isobutyryl-5'-*N*-Boc-*L*-Lys(OMe)-2',3'-di-*O*-(carbobenzyloxy) guanosine (2.13).** Yield:

53%; yellowish brown powder; m.p.= 46-48 °C; TLC (DCM:MeOH 95:5): R<sub>f</sub> = 0.61; [α]<sub>589</sub><sup>24</sup> -41.8 (c 1.0, acetone); IR (KBr) ν<sub>max</sub> (cm<sup>-1</sup>) = 3205, 3036, 2975, 1758, 1678, 1273, 1090, 1026, 901, 783; <sup>1</sup>H NMR (acetone-d<sub>6</sub>, 500 MHz): δ 11.96 (s, 1H), 10.53 (s, 1H), 8.37 (s, 1H), 8.00-7.97 (m, 2H), 7.44-7.33 (m, 10H), 6.22 (d, *J* = 7.5 Hz, 1H), 5.96 (d, *J* = 2.5 Hz, 1H), 5.75 (dd, *J* = 1.9, 4.9 Hz, 1H), 5.26 (dd, *J* = 12.5, 24.5 Hz, 2H), 5.15 (dd, *J* = 12.2, 25.1 Hz, 2H), 4.91 (d, *J* = 2 Hz, 1H), 4.50-4.46 (m, 1H), 3.05-3.01 (m, 2H), 2.94 (s, 3H), 2.89 (q, *J* = 6.8 Hz, 1H), 1.89-1.74 (m, 2H), 1.49-1.45 (m, 2H), 1.40-1.39 (m, 2H), 1.38 (s, 9H), 1.24 (d, *J* = 6.9 Hz, 6H); <sup>13</sup>C NMR

(acetone-d<sub>6</sub>, 126 MHz):  $\delta$  180.9, 172.8, 169.0, 162.8, 156.8, 155.7, 154.8, 154.3, 149.9, 149.7, 138.6, 136.3, 136.1, 129.6, 129.5, 121.9, 85.6, 85.2, 82.2, 78.5, 77.5, 77.4, 71.2, 71.1, 53.7, 52.6, 52.2, 40.8, 36.7, 36.2, 31.8, 30.39, 23.76, 19.44, 19.32; ESI MS (m/z) calculated for C<sub>42</sub>H<sub>51</sub>N<sub>7</sub>O<sub>14</sub>, [M<sup>+</sup>] 877.9; found 878.3.

***N*-Isobutyryl-5'-L-Phe(OMe)-2',3'-di-*O*-(carbobenzyloxy) guanosine (2.14).** Yield: 78%; light brown powder; m.p.= 73 °C; TLC (DCM:MeOH 95:5): R<sub>f</sub> = 0.62; [ $\alpha$ ]<sub>589</sub><sup>24</sup> -4.94 (c 0.1, acetone); IR (KBr)  $\nu_{\max}$  (cm<sup>-1</sup>) = 3188, 2927, 1754, 1683, 1275, 1083, 783; <sup>1</sup>H NMR (acetone-d<sub>6</sub>, 500 MHz):  $\delta$  12.07 (s, 1H), 10.43 (s, 1H), 8.12 (s, 1H), 7.84 (d, *J* = 7.8 Hz, 1H), 7.45-7.30 (m, 10H), 7.25-7.16 (m, 5H), 6.19 (d, *J* = 7.3 Hz, 1H), 5.86 (dd, *J* = 4.9, 7.3 Hz, 1H), 5.72 (dd, *J* = 1.7, 4.6 Hz, 1H), 5.21 (dd, *J* = 11.1, 25 Hz, 2H), 5.12 (dd, *J* = 12, 25 Hz, 2H), 4.85 (d, *J* = 1.5 Hz, 1H), 4.82-4.76 (m, 1H), 3.70 (s, 3H), 3.20 (d, *J* = 6.3 Hz, 1H), 3.17 (d, *J* = 7.8 Hz, 1H), 2.89-2.83 (m, 1H), 1.23-1.18 (m, 6H); <sup>13</sup>C NMR (acetone-d<sub>6</sub>, 126 MHz):  $\delta$  179.9, 171.2, 167.6, 154.7, 153.8, 153.4, 158.9, 148.9, 148.7, 137.5, 136.7, 135.3, 135.1, 129.1, 128.6, 128.5, 126.9, 121.1 84.6, 81.0, 76.1, 76.0, 70.3, 70.1, 53.9, 53.8, 51.7, 36.8, 35.7, 18.4; ESI MS (m/z) calculated for C<sub>40</sub>H<sub>39</sub>N<sub>6</sub>O<sub>12</sub>, [M-H] 795.3; found 795.2.

***N*-Isobutyryl-5'-L-Ser(*O**t*-Bu) methyl ester-2',3'-di-*O*-(carbobenzyloxy) guanosine (2.15).** Yield: 67%; light brown powder; m.p.= 91 °C; TLC (DCM:MeOH 95:5): R<sub>f</sub> = 0.55; [ $\alpha$ ]<sub>589</sub><sup>24</sup> -8.01 (c 0.1, acetone); IR (KBr)  $\nu_{\max}$  (cm<sup>-1</sup>) = 3172, 2975, 1751, 1679, 1611, 1564, 1388, 1274, 1249, 1154, 1091, 1026, 901, 783, 757; <sup>1</sup>H NMR (acetone-d<sub>6</sub>, 500 MHz):  $\delta$  12.06 (s, 1H), 10.43 (s, 1H), 8.34 (s, 1H), 7.84 (d, *J* = 8.3 Hz, 1H), 7.45-7.32 (m, 10H), 6.25 (d, *J* = 7.3 Hz, 1H), 5.93 (dd, *J* = 7.3, 4.9 Hz, 1H), 5.75 (dd, *J* = 4.6, 1.2 Hz, 1H), 5.32 (dd, *J* = 10.8, 22.9 Hz, 2H), 5.21 (dd, *J* = 11.8, 24.7 Hz, 2H), 4.95 (d, *J* = 1.5 Hz, 1H), 4.78-4.76 (m, 1H), 3.74 (d, *J* =

3.4 Hz, 1H), 3.72 (s, 3H), 2.91-2.82 (m, 1H), 2.88-2.84 (m, 1H), 1.12 (s, 9H), 1.24 (d,  $J = 7$  Hz, 6H);  $^{13}\text{C}$  NMR (acetone- $d_6$ , 126 MHz):  $\delta$  180.0, 170.1, 167.5, 154.7, 153.9, 153.4, 148.9, 148.8, 137.6, 135.3, 135.1, 128.6, 128.5, 121.2, 84.6, 81.2, 76.4, 75.9, 73.4, 70.2, 61.3, 53.1, 51.8, 35.7, 26.6, 19.9, 18.4; ESI MS ( $m/z$ ) calculated for  $[\text{M}+\text{H}] \text{C}_{38}\text{H}_{45}\text{N}_6\text{O}_{13}$ , 793.3; found 794.2.

***N*-Isobutyryl-5'-*L*-Asp(*O**t*-Bu)-methyl ester-2',3'-di-*O*-(carbobenzyloxy) guanosine**

**(2.16)**. Yield: 70%; light brown powder; m.p.= 64 °C; TLC (DCM:MeOH 95:5):  $R_f = 0.67$ ;  $[\alpha]_{589}^{23} -8.46$  ( $c$  0.1, acetone); IR (KBr)  $\nu_{\text{max}}$  ( $\text{cm}^{-1}$ ) = 2977, 1759, 1717, 1684, 1275, 1155, 783;

$^1\text{H}$  NMR (acetone- $d_6$ , 500 MHz):  $\delta$  11.91 (s, 1H), 10.55 (s, 1H), 8.23 (s, 1H), 7.99 (d,  $J = 3$  Hz, 1H), 7.43-7.34 (m, 10H), 6.25 (d,  $J = 7.3$  Hz, 1H), 6.00 (dd,  $J = 5.1, 7.1$  Hz, 1H), 5.76 (dd,  $J = 2.4, 4.9$  Hz, 1H), 5.21 (dd,  $J = 7, 19$  Hz, 2H), 5.12 (dd,  $J = 13.8, 25.9$  Hz, 2H), 4.94-4.89 (m, 1H), 4.85 (d,  $J = 2$  Hz, 1H), 4.06 (q,  $J = 6.8$  Hz, 1H), 3.69 (s, 3H), 2.94-2.93 (m, 1H), 2.88-2.85 (m, 1H), 1.39 (s, 9H), 1.24 (d,  $J = 6.3$  Hz, 6H);  $^{13}\text{C}$  NMR (acetone- $d_6$ , 500 MHz):  $\delta$  180, 170.5, 170.1, 170.0, 167.3, 154.7, 153.8, 153, 148.8, 148.7, 138.2, 138.0, 135.3, 135.1, 131.2, 128.6, 128.5, 121.5, 85.2, 81.4, 80.9, 80.8, 76.0, 75.1, 70.3, 70.1, 60.0, 59.6, 52.0, 48.9, 37.0, 35.7, 19.9, 18.5, 18.4; ESI MS ( $m/z$ ) calculated for  $\text{C}_{39}\text{H}_{44}\text{N}_6\text{O}_{14}$   $[\text{M}^+]$ , 820.8; found 819.7.

***N*-Isobutyryl-5'-hexadecyl-2',3'-di-*O*-(carbobenzyloxy) guanosine (2.17)**. Yield: 70%; light

brown viscous liquid; TLC (DCM:MeOH 95:5):  $R_f = 0.9$ ;  $[\alpha]_{589}^{24} -2.68$  ( $c$  0.2, acetone); IR (KBr)

$\nu_{\text{max}}$  ( $\text{cm}^{-1}$ ) = 3321, 2924, 2853, 1722, 1710, 1692, 1679, 1513, 1462, 1451, 1384, 1257, 1176, 1101, 1034, 843, 805, 761, 742;  $^1\text{H}$  NMR (methanol- $d_4$ , 500 MHz):  $\delta$  8.70 (s, 1H), 7.36-7.21 (m, 10H), 6.27 (d,  $J = 6.7$  Hz, 1H), 5.14 (m, 2H), 5.07 (m, 1H), 4.99 (m, 2H), 4.59 (s, 1H), 2.90 (m, 2H), 2.65 (m, 1H), 1.64 (m, 2H), 1.42-1.13 (m, 34H), 0.91-0.88 (m, 3H);  $^{13}\text{C}$  NMR (methanol- $d_4$ , 126 MHz):  $\delta$  231.3, 191.5, 189.1, 187.9, 155.7, 155.2, 144.3, 136.8, 136.4, 129.8, 129.76, 129.4,

99.5, 94.3, 84.4, 71.6, 71.3, 42.7, 41.1, 37.2, 35.5, 33.2, 30.9, 30.8, 30.4, 29.1, 27.6, 23.8, 14.5;  
ESI MS (m/z) calculated for [M+] C<sub>46</sub>H<sub>62</sub>N<sub>6</sub>O<sub>10</sub>, 859.0; found 858.6.

***N*-Isobutyryl-5'-*N*-Boc-L-Lys(OMe) guanosine (2.18).** *N*-Isobutyryl-5'-*N*-Boc-L-Lys(OMe)-2',3'-di-*O*-(carbobenzyloxy) guanosine **2.13** (100 mg, 0.11 mmol) was dissolved in EtOH (2 mL) and 10% Pd/C (10 mg) was added. The mixture was stirred under an atmosphere of H<sub>2</sub> for 90 min at room temperature until TLC indicated complete reaction. The reaction mixture was filtered through a pad of Celite and washed with MeOH. The filtrate was concentrated using a rotary evaporator to afford the product **2.18** (68.8 mg, 0.11 mmol) as a solid. Yield: 99%; light yellow powder; m.p.= 132 °C; TLC (DCM:MeOH 95:5): R<sub>f</sub> = 0.36; [α]<sub>589</sub><sup>23</sup> -13.5 (c 2.0, acetone); IR (KBr) ν<sub>max</sub> (cm<sup>-1</sup>) = 3307, 2934, 1772, 1678, 1562, 1403, 1165, 948, 865, 757; <sup>1</sup>H NMR (acetone-d<sub>6</sub>, 500 MHz): δ 8.26 (s, 1H), 7.74 (d, *J* = 6.5, 1H) 6.00 (d, *J* = 6.5 Hz, 1H), 5.94 (s, 1H), 4.80 (s, 1H), 4.56 (s, 2H), 4.46 (d, *J* = 5.5 Hz, 1H), 3.69-3.66 (m, 2H), 3.04 (d, *J* = 6.5 Hz, 2H), 2.94-2.91 (m, 2H), 2.80 (s, 1H), 2.78 (s, 1H), 1.86-1.85 (m, 1H), 1.78-1.76 (m, 1H), 1.48 (d, *J* = 4.5 Hz, 2H), 1.39 (s, 13H), 1.29-1.24 (m, 6H). <sup>13</sup>C NMR (acetone-d<sub>6</sub>, 126 MHz): δ 179.9, 172.3, 169.7, 155.9, 155.0, 149.1, 148.5, 137.8, 121.0, 110, 87.7, 83.9, 77.5, 74.1, 73.8, 56.9, 52.2, 51.6, 39.9, 35.7, 31.0, 22.8, 18.5, 18.4, 18.0; ESI MS (m/z) calculated for C<sub>26</sub>H<sub>40</sub>N<sub>7</sub>O<sub>10</sub>, [M+H] 610.6; found 610.3.

***N*-Isobutyryl-5'-*N*-Boc-L-Lys(OMe)-2',3'-di-*O*-(palmitoyl) guanosine (2.19)** : Palmitoyl chloride (108 mg, 0.39 mmol) and DMAP (5 mg, 0.04 mmol) were added to a solution of guanosine **2.18** (0.8 g, 0.13 mmol) in dry pyridine (2.5 mL) at 0 °C. The reaction mixture was stirred at room temperature for 2 h. The solution was then concentrated *in vacuo*, partitioned between DCM (20 mL) and brine (10 mL) and dried over MgSO<sub>4</sub>. The crude product was



concentrated and purified by silica gel column chromatography using DCM/MeOH (90/10) yielding **2.19** (0.14 g, 0.13 mmol) as a white solid. Yield: 99 %; off white powder; m.p.= 51-53 °C; TLC (DCM:MeOH 90:10):  $R_f = 0.6$ ;  $[\alpha]_{589}^{23} -16$  (c 1.0, acetone); IR (KBr)  $\nu_{\max}$  (cm<sup>-1</sup>)= 2916, 2850, 1741, 1721, 1692, 1678, 1636, 1607, 1563, 1468, 1410, 1366, 1249, 1172, 945, 738, 721; <sup>1</sup>H NMR (DCM-d<sub>2</sub>, 500 MHz):  $\delta$  12.1 (s, 1H), 9.46 (s, 1H), 7.79 (s, 1H), 7.42 (d,  $J = 8$  Hz, 1H), 6.01 (d,  $J = 5.5$ , 1H) 5.97 (dd,  $J = 4, 5$  Hz, 1H) 5.77 (t,  $J = 5$  Hz, 1H), 4.76 (t,  $J = 5.75$  Hz, 1H), 4.66 (d,  $J = 4$  Hz, 1H) 4.49 (dt,  $J = 6, 10.5$  Hz, 1H) 3.74 (s, 3H), 3.00 (dd,  $J = 7, 13$  Hz, 2H), 2.69 (t,  $J = 7$  Hz, 1H), 2.41 (m, 2H), 2.30 (m, 4H), 1.52-1.70 (m, 6H), 1.37-1.41(m, 9H), 1.22-1.33 (m, 56H), 0.86-1.12 (m, 6H); <sup>13</sup>C NMR (DCM-d<sub>2</sub>, 126 MHz):  $\delta$  179.7, 172.9, 172.4, 172.1, 168.0, 155.0, 148.4, 147.9, 138.6, 122.0, 87.6, 81.3, 72.1, 72.0, 52.4, 52.3, 36.1, 33.8, 33.6, 31.9, 31.1, 29.7, 29.6, 29.6, 29.5, 29.4, 29.3, 29.3, 29.2, 29.1, 29.0, 28.1, 24.8, 24.7, 24.5, 22.7, 22.6, 18.8, 18.6, 13.8. ESI MS (m/z) calculated for C<sub>58</sub>H<sub>100</sub>N<sub>7</sub>O<sub>12</sub>, [M+H] 1086.7; found 1086.7

***N*-Isobutyryl-5'-L-Lys(OMe)-2',3'-di-*O*-(palmitoyl) guanosine hydrochloride (2.6)** : To a stirred solution of guanosine **2.19** (0.14 mg, 0.13 mmol) in CH<sub>2</sub>Cl<sub>2</sub> (3 mL) was added TFA (4 mL, 51 mmol). The reaction mixture was stirred at room temperature for 3 h until TLC indicated complete reaction. The solvent was evaporated and the crude residue was dissolved in CH<sub>2</sub>Cl<sub>2</sub> (3 mL) and 1M HCl (3 mL). The resulting biphasic mixture was stirred for 2 min, separated and washed again with 1M HCl (2 x 3 mL) before the organic phase was isolated, dried over MgSO<sub>4</sub> and evaporated to dryness giving the crude product **2.6** (0.13 g, 0.13 mmol) as off white powder. Yield: 99 %; off white powder; m.p.= 186-189 °C; TLC (DCM:MeOH 95:5):  $R_f = 0.2$ ;  $[\alpha]_{589}^{23} -3$  (c 1.0, MeOH); IR (KBr)  $\nu_{\max}$  (cm<sup>-1</sup>) = 3418, 2917, 2850, 1746, 1681, 1614, 1567, 1468, 1404, 1204, 1157, 1108, 1022, 800, 722; <sup>1</sup>H NMR (DCM-d<sub>2</sub>, 500 MHz):  $\delta$  8.48 (s, 1H), 6.15 (d,  $J = 5.5$ , 1H), 5.95 (t,  $J = 5$ , 1H), 5.80 (d,  $J = 2$ , 1H), 4.44 (dd,  $J = 5, 8.5$  Hz, 1H), 3.78 (s, 3H), 2.92

(t,  $J = 7.5$ , 2H), 2.73 (t,  $J = 3$ , 1H), 2.43 (m, 2H), 2.30 (t,  $J = 6$  Hz, 2H), 1.88 (t,  $J = 7.5$ Hz, 1H), 1.68 (m, 4H), 1.53 (s, 2H), 1.40 (m, 2H), 1.28 (m, 56H), 0.88 (d,  $J = 6.5$  Hz, 6H).  $^{13}\text{C}$  NMR (acetone- $d_6$ , 126 MHz):  $\delta$  180.3, 172.1, 171.9, 171.8, 169.4, 138.7, 119.7, 86.1, 86.0, 81.6, 81.5, 73.7, 72.8, 72.7, 52.3, 51.6, 51.4, 39.0, 35.6, 35.5, 35.4, 33.1, 31.7, 30.3, 29.4, 29.2, 29.1, 28.9, 28.7, 26.6, 24.5, 24.4, 22.5, 22.3, 18.1, 18.0, 17.9, 13.1, 13.0. ESI MS ( $m/z$ ) calculated for  $\text{C}_{53}\text{H}_{92}\text{N}_7\text{O}_{10}$ ,  $[\text{M}+\text{H}]$  986.3; found 986.7.

**Solid-Phase Oligonucleotide Synthesis and Characterization data.** Synthesis of oligonucleotides was performed on an ABI 3400 DNA synthesizer using a 1  $\mu\text{mol}$  scale automated synthesis cycle on a Unylinker controlled pore glass (CPG) support (Chemgenes Co.). DNA phosphoramidites (Chemgenes Co.) were dissolved in anhydrous MeCN as 0.1 M solutions. The coupling times were 20 sec using 0.25 M 5-ethylthiotetrazole (ETT) in MeCN as activator. The detritylation times were set to 2 min using a solution of 3% dichloroacetic acid in DCM. Capping and oxidation steps were performed using a mixture of acetic anhydride/*N*-methyl imidazole in MeCN and a solution of 0.01 M iodine in pyr/THF/ $\text{H}_2\text{O}$ , respectively. Following synthesis, oligonucleotides were cleaved from the CPG and deprotected with  $\text{NH}_4\text{OH}:\text{EtOH}$  (3:1) for 16 h at 55  $^\circ\text{C}$ . The crude oligonucleotides were evaporated to dryness, extracted from the CPG with autoclaved  $\text{H}_2\text{O}$  (1 mL) and quantitated by UV/VIS spectrophotometry. Crude oligonucleotides were purified by reverse-phase ion-pairing HPLC on a Waters 2695 Alliance system equipped with a Nova-pak C-18 reverse phase column (3.9 x 150 mm, 4  $\mu\text{m}$  particle size) and gradient elution method of 5-95% B over 23 min (B:20% MeCN in 0.1 M TEAA).

**Characterization of oligonucleotides by ESI MS.** All spectra were acquired on an oligo HTCS LCMS system courtesy of Dr. Mark Hail at Novatia LLC (Newtown, PA). Oligonucleotide samples (100 pmol) were dissolved in 1 mL H<sub>2</sub>O and directly injected into ESI-MS. The data were processed by ProMass software.

**Polyacrylamide Gel Electrophoresis (native gel shift mobility assays).** PAGE was conducted under native conditions (no urea or formamide) to allow complex formation. The running buffer was 1 X TAE (89 mM TRIS/Acetate, 2.5 mM EDTA, pH = 4.2). The loading buffer for sample preparation was 30% sucrose in 10 X TAE buffer, pH = 4.2. The dried oligonucleotide samples were dissolved in 15  $\mu$ L of loading buffer, denatured at 90 °C for 2 min, annealed at room temperature for 2.5 h and overnight at 5 °C and then incubated with ligand **2.6** (0-3.9 mM) at 37 °C for 36 h. The samples were then loaded on a gel that consisted of 24 % acrylamide. The gel was run at 250 V, 32 mA, 12 W for 3-5 h. The gel was visualized under UV shadowing at 260 nm.

**Thermal denaturation experiments,  $T_m$ .** Thermal denaturation studies were conducted on a Varian UV-VIS Cary 300 dual beam spectrophotometer equipped with a temperature controller. Complementary oligonucleotides were annealed in phosphate buffer that mimics physiological ionic strength: 140 mM KCl, 5 mM NaH<sub>2</sub>PO<sub>4</sub>, 1 mM MgCl<sub>2</sub>, pH = 7.2. The solutions were denatured at 90 °C for 2 min then cooled to room temperature over 2.5 h and kept at 5 °C overnight prior to the addition of ligand **2.6**. Ligand **2.6** was added in increasing concentrations

to duplex GRP78 DNA (0-3.9 mM) and incubated at 37 °C for 36 h prior to thermal denaturation experiments. The thermal melts were run from 5-90 °C with temperature gradient increments of 0.5 °C/min and data points collected every 0.5 °C/min at 260 nm. The  $T_m$  measurements were calculated according to the temperature at which 50% of the duplex denatured to single strands from a plot comparing the changes in hyperchromicity vs temperature.

**Circular Dichroism (CD) Spectroscopy.** Samples were prepared as described in the thermal denaturation experiments and analyzed using an Aviv Circular Dichroism (CD) Spectrophotometer (Model: 62A DS). CD spectra were collected on an average of three scans using 1 nm bandwidth and 0.5 min step size at 25 °C from 310-210 nm. Samples were blank corrected, smoothed and the data converted to molar ellipticity values from the equation  $[\theta] = \theta / cl$ , where  $\theta$  is the relative ellipticity (mdeg),  $c$  is the molar concentration of the DNA ( $\mu\text{M}$ ) and  $l$  is the path length of the cell (1 cm). The data was imported into Microsoft Excel and the CD spectra were plotted in terms of molar ellipticity vs wavelength.

**Dynamic Light Scattering (DLS).** Dynamic light scattering (DLS) measurements were performed on a 90plus particle size analyzer (Brookhaven Instruments Corporation) employing a 90° scattering angle and a 35 mW incident laser (658 nm). All samples were filtered through a 0.02  $\mu\text{m}$  pore size membrane (Whatman ANOTOP, alumina based membrane). Samples were measured at time = 0 and 36 hours, for **2.6** (3.9 mM) in the absence or presence of GRP78 DNA (1.1  $\mu\text{M}$ ) in pH = 7.2 phosphate buffer (5 mM  $\text{NaH}_2\text{PO}_4$ , 140 mM KCl, 1 mM  $\text{MgCl}_2$ ). The reported diameter was the average of 3 runs for each sample.

**Cell Viability.** Cancer cell viability studies were performed by the Developmental Therapeutics Program, Division of Cancer Treatment and Diagnosis, National Cancer Institute (<http://dtp.cancer.gov>). Briefly, a panel of 60 human tumor cell lines for screening was grown in RPMI 1640 medium containing 5% fetal bovine serum and 2 mM L-glutamine. For a typical screening experiment, cells were inoculated into 96 well microtiter plates in 100  $\mu$ L at plating densities ranging from 5,000 to 40,000 cells/well depending on the doubling time of individual cell lines. After cell inoculation, the microtiter plates were incubated at 37 °C, 5 % CO<sub>2</sub>, 95 % air and 100 % relative humidity for 24 h prior to addition of **2.6**. After 24 h, two plates of each cell line are fixed *in situ* with TCA, to represent a measurement of the cell population for each cell line at the time of addition of **2.6** (Tz). Aminoacyl nucleolipid **2.6**, was solubilized in dimethyl sulfoxide (10  $\mu$ M) and added to the appropriate microtiter wells. Following addition of **2.6**, the plates were incubated for an additional 48 h at 37 °C, 5 % CO<sub>2</sub>, 95 % air, and 100 % relative humidity. Cells were fixed *in situ* by the gentle addition of 50  $\mu$ l of cold 50 % (w/v) TCA (final concentration, 10 % TCA) and incubated for 60 minutes at 4°C. The supernatant was discarded, and the plates were washed five times with tap water and air dried. Sulforhodamine B (SRB) solution (100  $\mu$ L) at 0.4 % (w/v) in 1 % acetic acid was added to each well, and plates are incubated for 10 minutes at room temperature. After staining, unbound dye is removed by washing five times with 1 % acetic acid and the plates are air dried. Bound stain is subsequently solubilized with 10 mM trizma base, and the absorbance was read on an automated plate reader at a wavelength of 515 nm. Using seven absorbance measurements [time zero, (Tz), control growth, (C), and test growth in the presence of **2.6** (Ti)], the percentage growth inhibition was calculated as:

$[(Ti-Tz)/(C-Tz)] \times 100$  for concentrations for which  $Ti \geq Tz$

$[(Ti-Tz)/Tz] \times 100$  for concentrations for which  $Ti < Tz$ .

Growth inhibition of 50 % (GI50) was calculated from  $[(Ti-Tz)/(C-Tz)] \times 100 = 50$ . The drug concentration resulting in total growth inhibition (TGI) is calculated from  $Ti = Tz$ . A net loss of cells following treatment was calculated from  $[(Ti-Tz)/Tz] \times 100 = -50$ .

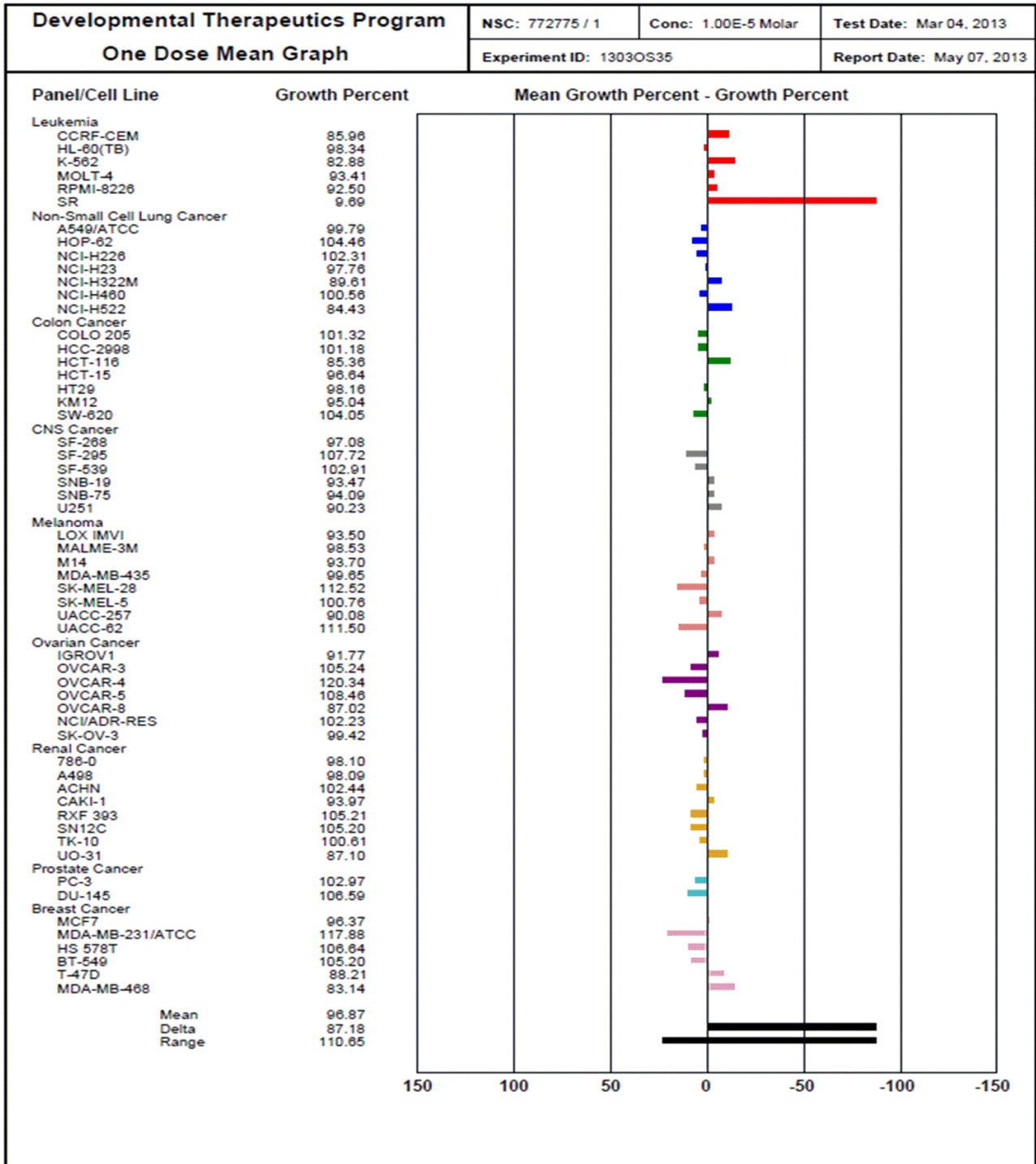


**Figure 2.10.** NCI 60 cancer cell line one-dose screen. Data is reported as a mean graph of the percent growth of cells treated with **2.6** (10  $\mu$ M) relative to no drug control and relative to time zero number of cells. Growth inhibition is detected as values between 0 and 100 whereas cell death is evaluated by values less than 0.

## 2.4 REFERENCES

1. Allain, V.; Bourgaux, C.; Couvreur, P. *Nucleic Acids Res.* **2012**, *40*, 1891-1903.
2. Gissot, A.; Camplo, M.; Grinstaff, M.W.; Barthélémy, P. *Org. Biomol. Chem.* **2008**, *6*, 1324-1333.
3. Simeone, L.; Milano, D.; De Napoli, L.; Irace, C.; Di Pascale, A.; Boccalon, M.; Tecilla, P.; Montesarchio, D. *Chemistry* **2011**, *17*, 13854-13865.
4. Simeone, L.; Irace, C.; Di Pascale, A.; Ciccarelli, D.; D'Errico, G.; Montesarchio, D. *Eur. J. Med. Chem.* **2012**, *57*, 429-440.
5. Doluca, O.; Withers, J.M.; Filichev, V.V. *Chem. Rev.* **2013**, *113*, 3044-3083.
6. Patil, S.P.; Yi, J.W.; Bang, E.K.; Jeon, E.M.; Kim, B.H. *Med. Chem. Commun.* **2011**, *2*, 505-508.
7. Yang, H.W.; Yi, J.W.; Bang, E.K.; Jeon, E. M.; Kim, B. H. *Org. Biomol. Chem.* **2011**, *9*, 291-296.
8. Agrawal, N.; Dasaradhi, P.V.; Mohmmmed, A.; Malhotra, P.; Bhatnagar, R.K.; Mukherjee, S.K. *Microbiol. Mol. Biol. Rev.* **2003**, *67*, 657-685.
9. Patel, P.; Hanawa, E.; Yadav, R.; Samuni, U.; Marzabadi, C.; Sabatino, D. *Bioorg. Med. Chem. Lett.* **2013**, *23*, 5086-5090.
10. (a) Watson, J.; Crick, H. *Nature* **1953**, *171*, 737-738. (b) Hoogsteen, K. *Acta Crystallogr.* **1963**, *16*, 907-916. (c) Hopton, S. R.; Thompson, A. S. *Biochemistry* **2011**, *50*, 4143-4154.
11. Mann, A.; Thakur, G.; Shukla, V.; Singh, A. K.; Khanduri, R.; Naik, R.; Jiang, Y.; Kalra, N.; Dwarakanath, B. S.; Langel, U.; Ganguli, M. *Mol. Pharmaceutics* **2011**, *8*, 1729-1741.
12. Safinya, C. R. *Curr. Opin. Struct. Biol.* **2001**, *11*, 440-448.
13. (a) Chien, P.Y.; Wang, J.; Carbonaro, D.; Lei, S.; Miller, B.; Sheikh, S.; Ali, S.M.; Ahmad, M.U.; Ahmad, I. *Cancer Gene Ther.* **2005**, *12*, 321-328. (b) Ward, C.M. *Curr. Opin. Mol. Ther.* **2000**, *2*, 182-187. (c) Yin, Z.; Liu, N.; Ma, M.; Wang, L.; Hao, Y.; Zhang, X. *Int. J. Nanomed.* **2012**, *7*, 4625-4635. (d) Wang, H.Y.; Yi, W.J.; Qin, S.Y.; Li, C.; Zhuo, R.X.; Zhang, X.Z. *Biomaterials* **2012**, *33*, 8685-8694.



14. (a) Ni, M.; Zhang, Y.; Lee, A.S. *Biochem J.* **2011**, *434*, 181-188; (b) Pfaffenbach, K.T.; Lee, A.S. *Curr. Opin. Cell Bio.* **2011**, *23*, 150-156; (c) Quinones, Q.J.; de Ridder, G.G.; Pizzo, S.V. *Histol. Histopathol.* **2008**, *23*, 1409-1416; (d) Ni, M.; Lee, A. S. *FEBS Lett.* **2007**, *581*, 3641-3651.
15. (a) Fu, Y.; Li, J.; Lee, A.S. *Cancer Res.* **2007**, *67*, 3734-3740; (b) Lee, A.S. *Cancer Res.* **2007**, *67*, 3496-3499; (c) Li, J.; Lee, A.S. *Curr. Mol. Med.* **2006**, *6*, 45-54; (d) Arap, M. A.; Lahdenranta, J.; Mintz, P. J.; Hajitou, A.; Sarkis, A. S.; Arap, W.; Pasqualini, R. *Cancer Cell* **2004**, *6*, 275-284; (e) Zhang, L.H.; Zhang, X.; *J. Cell. Biochem.* **2010**, *110*, 1299-1305; (f) Lee, A.S. *Nature Rev.* **2014**, *14*, 263-276.
16. (a) Kim, Y.; Lillio, A.M.; Steiniger, S.C.; Liu, Y.; Ballatore, C.; Anichini, A.; Mortarini, R.; Kaufmann, G.F.; Zhou, B.; Felding-Habermann, B.; Janda, K.D. *Biochemistry* **2006**, *45*, 9434-9444; (b) Liu, Y.; Steiniger, S. C. J.; Kim, Y.; Kaufmann, G. F.; Felding-Habermann, B.; Janda, K. D. *Mol. Pharmaceutics* **2007**, *4*, 435-447; (c) Yoneda, Y.; Steiniger, S.C.; Capková, K.; Mee, J.M.; Liu, Y.; Kaufmann, G.F.; Janda, K.D. *Bioorg. Med. Chem. Lett.* **2008**, *18*, 1632-1636.
17. Johnson, D. C.; Widlanski, T. S. *Org. Lett.* **2004**, *6*, 4643-4646.
18. Mourani, R.; Damha, M. *J. Nucleosides, Nucleotides Nucleic Acids* **2006**, *25*, 203-229.
19. Foitzik, R. C.; Devine, S. M.; Hausler, N. E.; Scammells, P. J. *Tetrahedron* **2009**, *65*, 8851-8857.
20. Matulic-Adamic, J.; Beigelman, L.; Dudycz, W. L.; Gonzalez, C.; Usman, N. *Bioorg. Med. Chem. Lett.* **1995**, *5*, 2721-2724.
21. Kaczmarek, O.; Brodersen, N.; Bunge, A.; Löser, L.; Huster, D.; Herrmann, A.; Arbuzova A.; Liebscher, J. *Eur. J. Org. Chem.* **2008**, *11*, 1917-1928.
22. Fan, Y.; Gaffney, B.L.; Jones, R.A. *Org. Lett.* **2004**, *6*, 2555-2557.
23. Karsisiotis, A.I.; Hessari, N.M.; Novellino, E.; Spada, G.P.; Randazzo, A.; Webba da Silva, M. *Angew Chem Int Ed Engl.* **2011**, *50*, 10645-10648.
24. Ting, J.; Lee, A. S. *DNA* **1988**, *7*, 275-286.
25. Caruthers, M.H.; Barone, A.D.; Beaucage, S. L.; Dodds, D. R.; Fisher, E. F.; McBride, L. J.; Matteucci, M.; Stabinsky, Z.; Tang, J. Y. *Methods Enzymol.* **1987**, *154*, 287-313.
26. Gilar, M.; Fountain, K. J.; Budman, Y.; Neue, U. D.; Yardley, K. R.; Rainville, P. D.; Russell, R. J.; Gebler, J. C. *J. Chrom. A.* **2002**, *958*, 167-182.

27. Kim, S. W.; Kim, N. Y.; Choi, Y. B.; Park, S. H.; Yang, M.; Shin, S. *J. Control. Release* **2010**, *143*, 335-343.
28. Arigon, J.; Prata, C. A. H.; Grinstaff, M. W.; Barthelemy, P. *Bioconjugate Chem.* **2005**, *16*, 864-872.
29. Kypr, J.; Kejnovska, I.; Renciuik, D.; Vorlickova, M. *Nucleic Acids Res.* **2009**, *37*, 1713-1725.
30. Showmaker, R.H. *Nat. Rev. Cancer* **2006**, *6*, 813-823.
31. Voigt, W. *Methods Mol Med.* **2005**, *110*, 39-48.
32. Wey, S.; Luo, B.; Tseng, C.C.; Ni, M.; Zhou, H.; Fu, Y.; Bhojwani, D.; Carroll, W.L.; Lee, A.S. *Blood* **2012**, *119*, 817-825.

## CHAPTER 3: PHTHALOCYANINE-NUCLEIC ACID BIOCONJUGATES AND THEIR APPLICATIONS IN CANCER

### 3.1 GENERAL INTRODUCTION

Metallo-phthalocyanines (MPcs) encompass an interesting class of photosensitizers owing the ability to absorb light in the near-IR region (650-900 nm) of the electromagnetic spectrum. Consequently, they exhibit fluorescence and/or the ability to convert ground state triplet oxygen ( $^3\text{O}_2$ ) to excited state singlet oxygen ( $^1\text{O}_2$ ) for applications in photodynamic therapy [1]. Their fruitful applications in photodynamic therapy have been linked to the production of  $^1\text{O}_2$ , a form of reactive oxygen species (ROS) that when produced in tumors leads to desirable anti-cancer effects [2,3]. In spite of their potential in cancer therapy, MPcs have exhibited poor water solubility due to their hydrophobic nature and tendency for aggregation which limits their photo-oxidation properties. Moreover, the hydrocarbon-based MPcs own limited chemical stability towards the ROS they produce and widespread dispersion in all tissue types leading to cytotoxicity which limits their therapeutic efficacy. In an effort to circumvent these limitations, bioconjugation approaches have been developed to effectively functionalize MPcs with bio-active moieties that may improve the ‘drug-like’ properties of the photosensitizers.

Nucleic acid conjugation has been especially applied to MPcs to improve their biological function (**Figure 3.1**). For example, uridine, 5-methyluridine, cytidine and 5-*N*-cytidine derivatives have been conjugated axially to silicon(IV) phthalocyanines in an attempt to improve their water solubility and minimize aggregation which limits ROS production [4]. This resulted in a uridine-based silicon phthalocyanine (**3.1**) which exhibited potent photocytotoxicity (IC<sub>50</sub>: 6 nM) in HepG2 hepatoblastoma cancer cells. In an attempt to improve the targeting abilities of

MPcs, oligonucleotide conjugation techniques, featuring reductive amination, amidation and Huisgen cycloaddition were successfully employed to generate MPcs-oligonucleotide bioconjugates, **3.2**, [5]. Dimerization of water soluble MPcs with a palindromic deoxyoligonucleotide sequence led to the hybridization of a 'quenched' hairpin. In the presence of a complementary sequence, the hairpin, **3.3**, unravels to form a duplex structure, **3.5**, with concomitant fluorescence release from the MPc [6]. These bioconjugates and related analogs, **3.6**, have been effectively employed as near-infrared fluorescent biosensors for detection of PCR gene amplification [7], DNA microarrays for gene mutation analyses [8] in addition to live cell and *in vivo* imaging [9]. In a related case study, short antisense oligonucleotides conjugated with MPcs, **3.7**, showed the ability to target and bind to complementary sequences for photo-oxidation and DNA cleavage activity following a hot piperidine or 8-oxoguanine DNA glycosylase (Fpg) treatment [10,11]. These conditions are known to cleave the phosphodiester bonds in oligonucleotides at oxidized sites, with the 8-oxoguanine modification being the most prevalent and susceptible for degradation [12]. Considering the relevance of oxidation in DNA damage and repair, MPcs conjugated oligonucleotides may serve as useful probes for elucidating the underlying mechanisms of gene expression at oxidized sites. Moreover, these findings may also have important contributions towards the development of targeted forms of photodynamic therapy. Combination approaches featuring Bcl-2 antisense oligonucleotides was shown to sensitize radiation-induced fibrosarcoma tumor cells to a silicon phthalocyanine, which triggered potent apoptosis [13]. Altogether, MPc-oligonucleotides form an interesting class of bioconjugates with widespread applications in diagnostics and therapy.

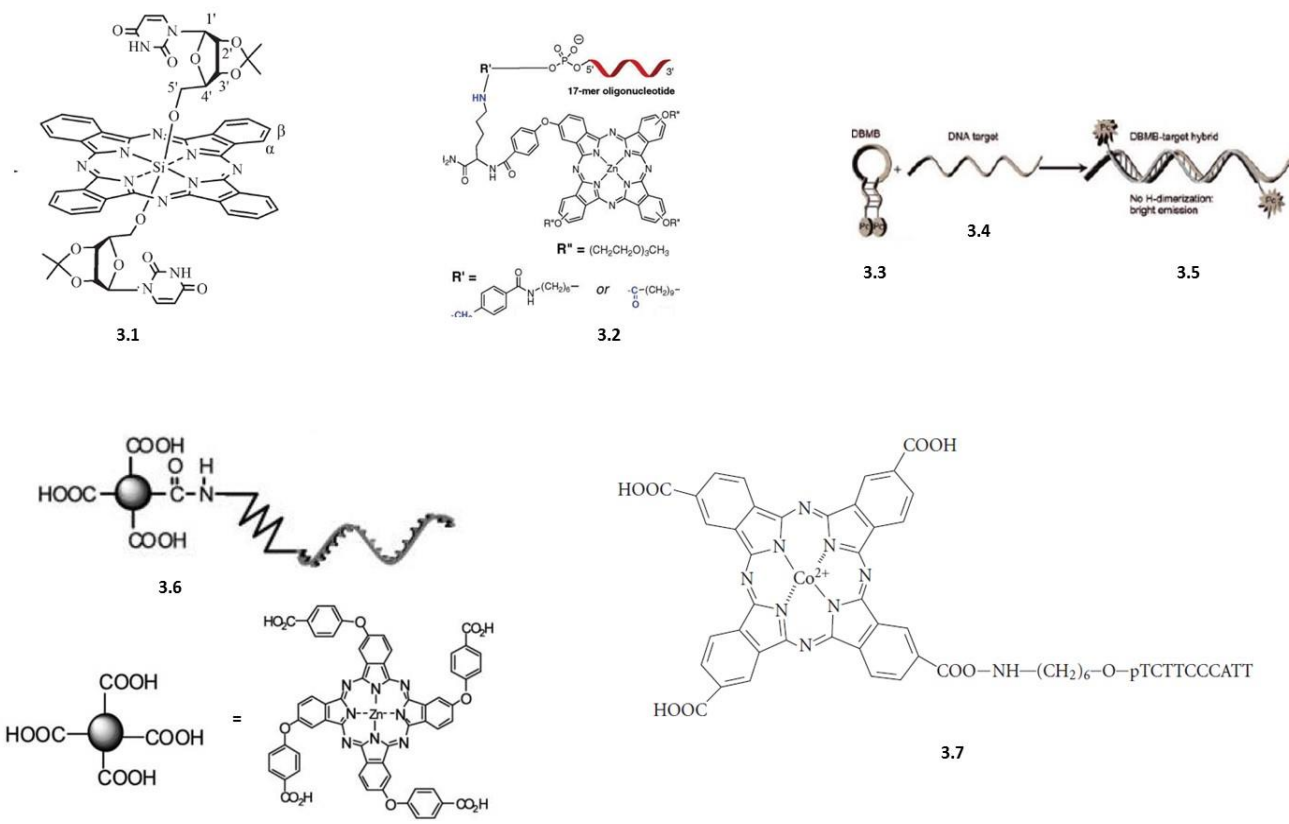


**Figure 3.1.** MPcs-nucleic acid conjugates for applications in detection and photodynamic therapy [4-11,13].

### 3.2 CHAPTER OBJECTIVES

Inspired by their important implications in biology and medicine, this thesis chapter delineates the discovery of a new perfluorophthalocyanine-cancer-targeting oligonucleotide (Pc-CTO) bioconjugate for potential anti-cancer therapy. In this study, the Pc-CTO was designed to contain a chemically robust fluoroalkyl phthalocyanine, which replaced most of the C-H with C-F bonds on the periphery of the macrocycle in order to withstand the production of ROS.

Moreover, the zinc(II) perfluorophthalocyanines have been characterized as efficient generators of reactive  $^1\text{O}_2$  for potent and long-lasting photodynamic effects [14]. In order to introduce an element of specificity in our photodynamic therapy approach, a cancer-targeting oligonucleotide (CTO), composed of an antisense sequence complementary to a portion of the Glucose Regulated Protein of 78 kilodalton (GRP78) oncogene was used to generate the putative Pc-CTO conjugate. In this manner, the CTO is proposed to target and bind to the GRP78 oncogene, while inhibiting its protein translation. Moreover, in the presence of aerobic illumination, the Pc activates reactive  $^1\text{O}_2$  for triggering potent apoptotic events in cancer (**Figure 3.2**). This combination approach has proven to be effective in chemo-resistant tumors in an effort to eradicate some of the more resilient forms of cancer [13]. Thus, the Pc-CTO forms the basis of our cancer-targeting photodynamic therapy approach. The synthesis strategy was developed in collaboration with Emily Borland (B.Sc. student) and Hemantbhai Patel (Ph.D. student) in the laboratory of Dr. Sergiu M. Gorun (Department of Chemistry, Seton Hall University). Their expertise in the material sciences encompass a broad range of phthalocyanine applications, such as their use as artificial enzymes [15], anti-cancer drugs [14], photosensitizers for degradation of azo dyes [16], and as redox catalysts [17]. In a collaborative effort with the Gorun group, this thesis chapter describes the synthesis, characterization and GRP78 oncogene photocleavage activity of a chemically robust Pc-CTO bioconjugate for potential cancer-targeted photodynamic therapy.

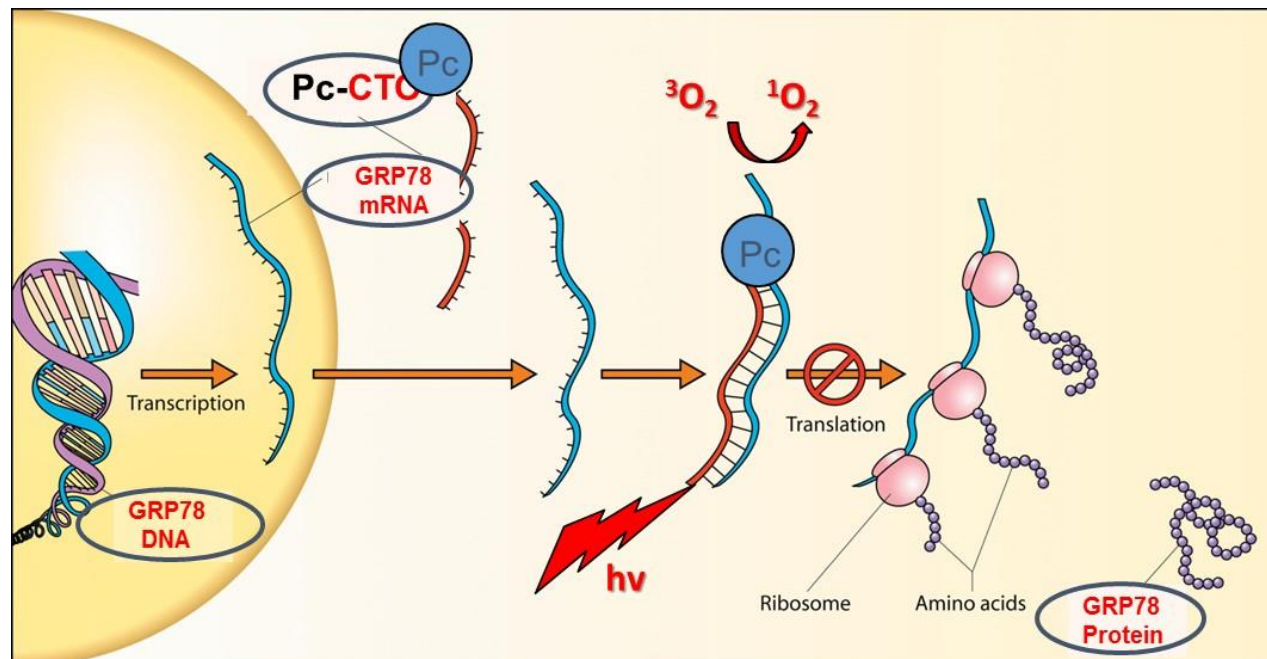


**Figure 3.2.** Mechanism of action of Pc-CTO bioconjugates.

### 3.3 CHEMICALLY ROBUST FLUOROALKYL PHTHALOCYANINE-OLIGONUCLEOTIDE BIOCONJUGATES AND THEIR GRP78 ONCOGENE PHOTOCLEAVAGE ACTIVITY

#### 3.3.1 ABSTRACT

The first representative of a functionalized fluoroalkyl phthalocyanine,  $F_{48}H_7(COOH)PcZn$ , is reported. The complex generates  $^1O_2$  affording long-lasting photo-oxidation of an external substrate without self-decomposition. The carboxylic group couples with an antisense oligonucleotide targeting GRP78 oncogenes, resulting in the  $F_{48}H_7PcZn$ -cancer

targeting oligonucleotide (CTO). The bioconjugated fluorophthalocyanine effectively hybridizes complementary GRP78 DNA and mRNA sequences. Piperidine cleavage assays reveal desired photochemical oligonucleotide oxidative degradation for both F<sub>48</sub>H<sub>7</sub>PcZn-CTO:DNA and F<sub>48</sub>H<sub>7</sub>PcZn-CTO:mRNA hybrids (**Figure 3.3**). This new materials strategy could be extended to other functional fluorinated phthalocyanines - antisense oligonucleotide combinations for long-lasting oncogene-targeting photodynamic therapy.

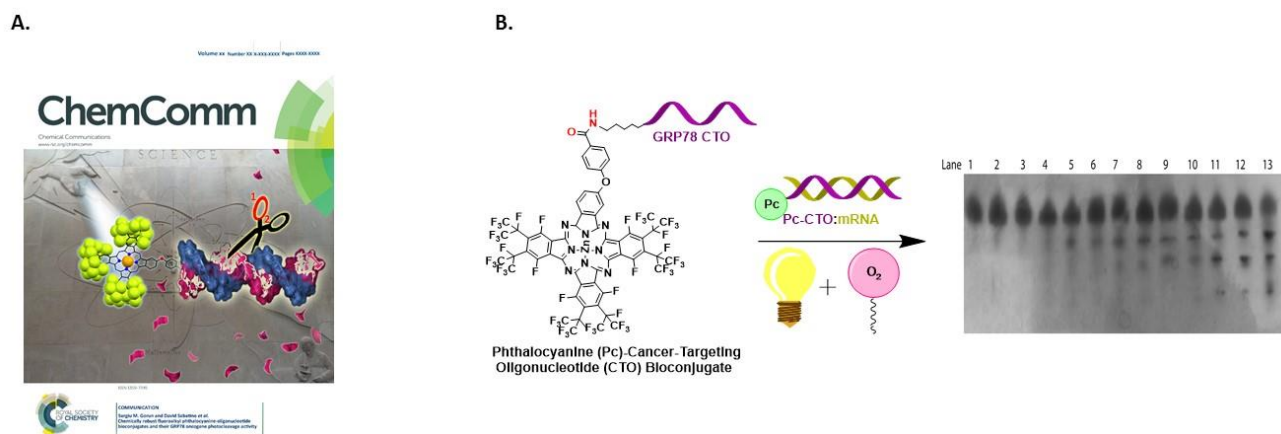


**Figure 3.3.** Graphical abstract representation of A. journal cover art image of perfluorophthalocyanine-GRP78 DNA photo-oxidation and cleavage activity, in addition to, B. perfluorophthalocyanine-GRP78 mRNA aerobic illumination and cleavage pattern at oxidized sites [18].

### 3.3.2. INTRODUCTION

Photodynamic therapy (PDT) uses photosensitizers to produce reactive oxygen species, ROS (e.g. singlet oxygen, <sup>1</sup>O<sub>2</sub>), that kill tumor cells [2,3,19]. Advantageously, PDT does not trigger immunosuppressive or myelosuppressive effects that accompany surgery, chemotherapy or radiation treatments. Historically, the first successful clinical application



of PDT in oncology was demonstrated over 100 years ago [20], with the first PDT drug approved for bladder cancer in 1993 [21]. However, unfavorable photosensitizer properties that lower therapeutic index, such as: poor water solubility, limited extinction coefficients in the maximum tissue penetration NIR region (600-900 nm), poor clearance from normal cells and photo-stability issues contributed to limited approval of PDT drugs for clinical use. Moreover, poor tumor-targeting results in dispersion in all tissue types, depressing efficiency and enhancing harmful side-effects. Most of the photosensitizers used in oncology are based on the tetrapyrrole scaffold, such as, the porphyrins, chlorins, corroles and phthalocyanines [19]. The phthalocyanines, in particular, are easily modified while exhibiting high thermal and chemical stability, in addition to intense light absorption toward the advantageous red spectral region [1].

In order to help mitigate current photosensitizers' limitations, this chapter describes the first example of a new class of *functionalized* fluoroalkyl phthalocyanine photosensitizers,  $F_{48}H_7(COOH)PcZn$ , **3.10**, in which most of the C-H bonds of the Pc macrocycle are replaced by aromatic and aliphatic C-F bonds. The fluorinated phthalocyanines,  $F_x(R_F)_yPcM$ , ( $F_x$  = fluorine,  $R_F$  = perfluoro alkyl group,  $x + y \leq 16$ , Pc = phthalocyanine and M = metal) constitute an important class of chemically robust photosensitizers [22]. The fluorinated alkyl substituents,  $R_F$ , in contrast to aromatic F groups are expected to enhance the stability of the Pc macrocycle towards nucleophilic attack by the ROS that the Pcs produce during the photodynamic events [23]. Thus, partial replacement of aromatic F in perfluorophthalocyanine,  $F_{16}PcM$  (M = Zn;  $x = 16$ ,  $y = 0$ ), with *iso*-perfluoroalkyl groups ( $R_F$ ) to give octakis-(perfluoro-*i*-C<sub>3</sub>F<sub>7</sub>)-(perfluoro)PcM,  $F_{64}PcM$  ( $x = y = 8$ ) was shown to improve the Pc's solubility in organic solvents, depress the

HOMO-LUMO gaps, thereby extending the Q-bands absorption in the 600-900 nm NIR region, while retaining high  $\sim 10^5$  molar extinction coefficients favouring efficient  $^1\text{O}_2$  production [24]. The  $\text{R}_\text{F}\text{Pc}$  macrocycle scaffold's resistance to degradation prompted their use as artificial enzymes [15], anti-cancer drugs [14], photosensitizers for degradation of azo dyes [16], and as redox catalysts [17]. However, the lack of the  $\text{R}_\text{F}\text{Pc}$ 's specific tissue distribution suggested the need for a targeting approach in our PDT applications. The enhanced tissue localization of photosensitizers is particularly useful for potentially increasing their therapeutic index. Strategies for specific tissue targeting include anchoring protio Pcs onto bio-probes, following their functionalization with  $-\text{COOH}$ ,  $-\text{NH}_2$ ,  $-\text{SO}_3\text{H}$ ,  $-\text{X}$  ( $\text{X} = \text{Cl}, \text{Br}, \text{I}$ ) groups [25,26] that thus facilitate Pc conjugation with carbohydrates [27], nucleosides [4], oligonucleotides [5,28], peptides [29] and proteins [30]. However, these approaches offer a limited therapeutic index for effective and long-lasting PDT due to the decomposition of the protio Pcs by the ROS they produce [10,11]. Moreover, chemically less stable hydrocarbon-based Pcs coupled to short, arbitrary oligonucleotide sequences have been reported in the literature [10,11]. However, to the best of our knowledge, coupling a chemically robust fluoro Pc with an oligonucleotide vector, **Figure 3.4**, targeting a DNA or mRNA oncogene, has not been reported.

The cancer-targeting oligonucleotide, CTO, was selected from the antisense DNA sequence exhibiting potent Glucose Regulating Protein 78, GRP78 knockdown in neonatal rat cardiomyocytes [31]. GRP78 functions as a chaperone that regulates protein folding events in the lumen of the endoplasmic reticulum (ER) of all cell types [32]. In cancer, GRP78 is overexpressed and localized on the cell surface where it exhibits a myriad of signaling activities related to cancer initiation, production and metastatic spread

[33]. The GRP78 oncogene is thus an excellent target for the development of potent and selective anti-cancer strategies [34].

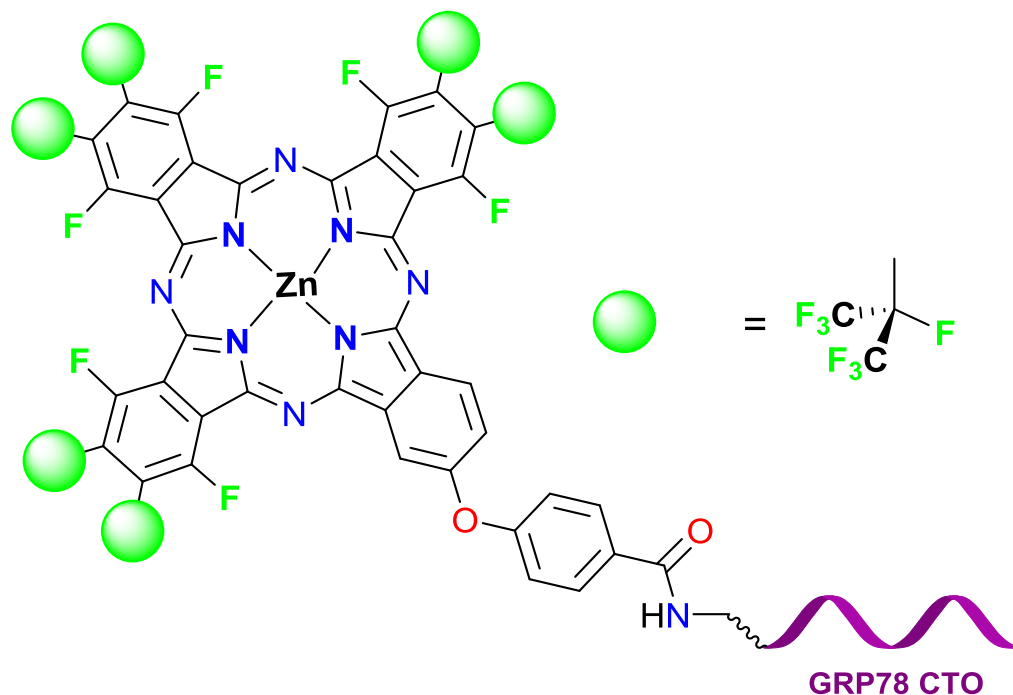


**Figure 3.4.**  $F_{48}H_7PcZn$ -GRP78 cancer-targeting oligonucleotide (CTO) bioconjugate, **3.14**.

### 3.3.3. RESULTS AND DISCUSSION

The  $F_{48}H_7(COOH)PcZn$ , **3.10**, was prepared in 21% isolated yield by reacting perfluoro phthalonitrile **3.8**, [35] with a carboxy phthalonitrile **3.9**, [5] in a microwave reactor, **Scheme 3.1**. Its composition and purity were confirmed by  $^1H$ ,  $^{19}F$  NMR and HRMS (see Experimental Section).



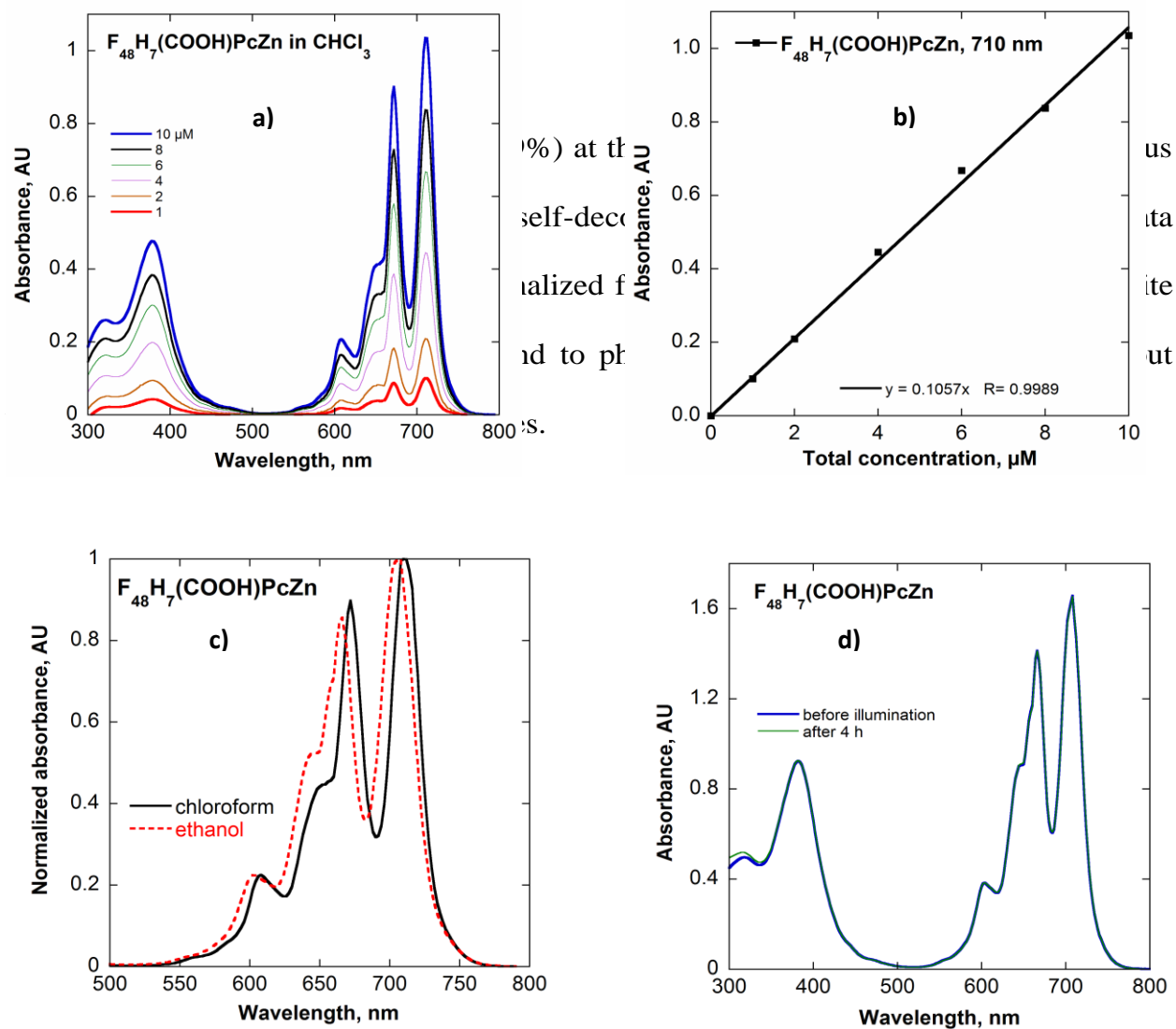


**Figure 3.5.** UV-Vis electronic absorption spectra of  $F_{48}H_7(COOH)PcZn$ , **3.10** a) **3.10** (1-10  $\mu M$ ) in chloroform; b) Lambert-Beer plot of the Q-band absorption maxima; c) normalized absorption spectra of **3.10** in chloroform and ethanol; d) Time-dependent UV-Vis of **3.10** during the photooxidation of  $\beta$ -citronellol in ethanol up to the time of complete consumption of  $O_2$ , ~14,400 sec. (4 hrs.). No catalyst decomposition is observed. The Q-band absorptions, shifted toward the red region of the spectrum are consistent with the expected effect of peripheral substitution by electron-withdrawing groups. The Q-bands split is due to the loss of the typical phthalocyanine

4-fold symmetry, as noticed previously, for example, for a related zinc-phthalocyanine, conjugated with deoxyribonucleosides. See B. Das, E. Tokunaga, M. Tanaka, T. Sasaki, and N. Shibata, *Eur. J. Org. Chem.* **2010**, 2010, 2878-2884.

Importantly, **3.10** generates  $^1\text{O}_2$  as demonstrated by the aerobic photo-hydroperoxidation of  $\beta$ -citronellol (**Figures 3.6a,b**). The reaction obeys pseudo-first order kinetics with an initial reaction rate of  $27.8 \mu\text{mol O}_2 \text{ min}^{-1}$  that corresponds to a turnover frequency  $460 \text{ mmol citronellol s}^{-1} \text{ mol Pc}^{-1}$ . This rate is consistent with the  $33.6 \mu\text{mol O}_2 \text{ min}^{-1}$  value reported for the homoleptic  $\text{F}_{64}\text{PcZn}$ , **3.11** [23,36]. In contrast, the hydrocarbon-based Pc-conjugates are not stable, as exemplified by the loss of Q-bands intensities in the case of a protio PcCo-oligonucleotide conjugate that is exposed to ROS [10]. The Pc complexes with Zn and Al are presumably active in generating singlet oxygen, but the stability of the Pc is not reported [11].

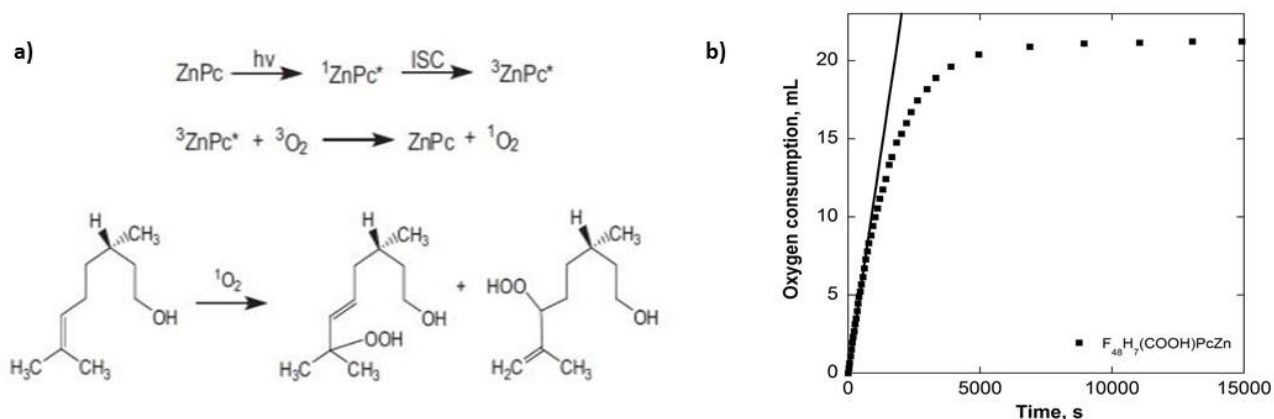
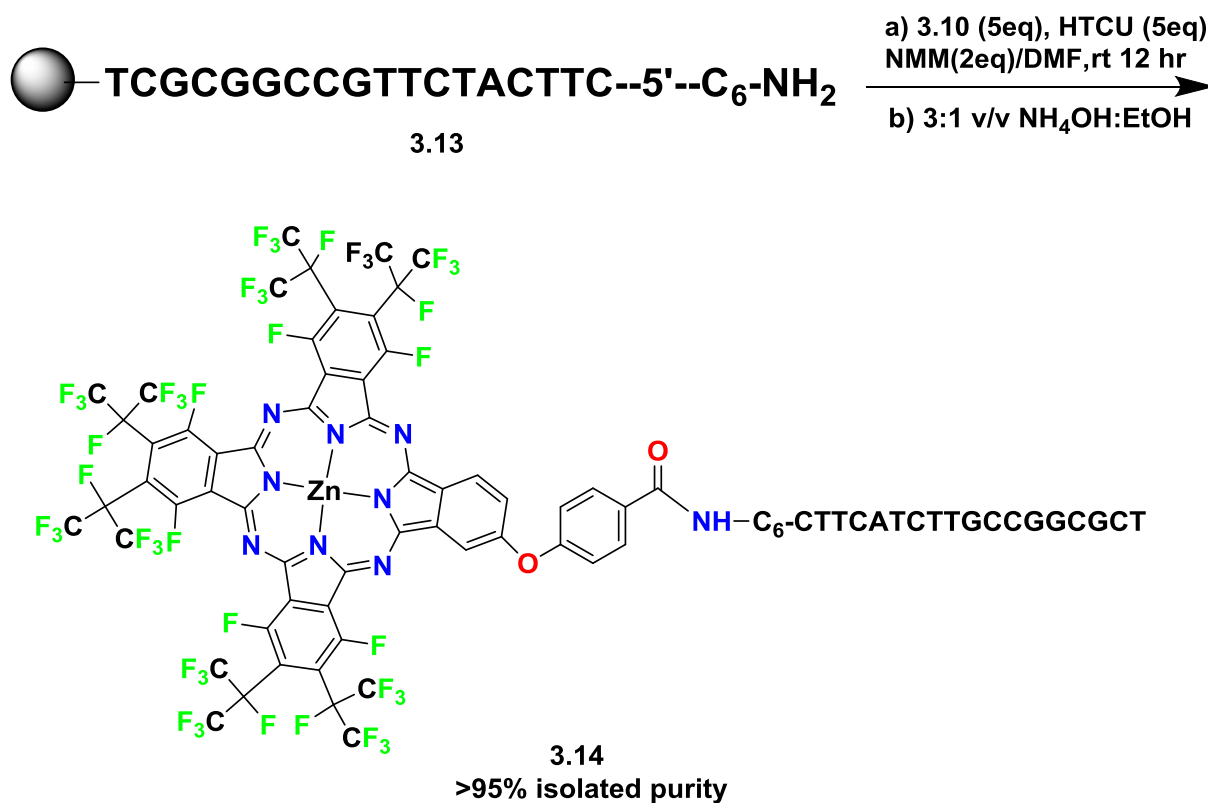


**Figure 3.6.** a) Photooxidation of  $\beta$ -citronellol in EtOH by **3.10**, ("ZnPc"). ISC = intersystem crossing; b) Time-dependent  $\text{O}_2$  titration at  $25^\circ\text{C}$ . No reaction occurs in the absence of either light or  $\text{O}_2$ . See also Figure 3.10. The  $\text{O}_2$  was consumed in the calculated stoichiometric amount.

The carboxy group of the Pc catalyst, **3.10**, was next coupled with the amino group of the solid-supported CTO, 3'-TCGCGGCCGTTCTACTC-5'-C<sub>6</sub>-NH<sub>2</sub>, **3.13**, using conventional amide coupling conditions [37] to yield after cleavage, deprotection and HPLC purification the bioconjugate F<sub>48</sub>H<sub>7</sub>PcZn-CTO, **3.14**, in isolated purity >95% (Scheme 3.2).



**Scheme 3.2.** Conjugation of **3.10** to an antisense GRP78 deoxyoligonucleotide bound to a solid support, **3.13**.

The hybridization of bioconjugate **3.14** with complementary GRP78 DNA, **3.15** and mRNA, **3.16** sense strands, afforded the duplexes F<sub>48</sub>H<sub>7</sub>PcZn-CTO:DNA, **3.14:3.15**, and F<sub>48</sub>H<sub>7</sub>PcZn-CTO:mRNA, **3.14:3.16**. These hybrids, soluble in phosphate buffers, exhibited stable ( $T_m = 75$  and  $72$  °C, respectively) temperature-dependent duplex to single-strand transitions (**Figure 3.7**). Taken together, these results unambiguously establish the ability of F<sub>48</sub>H<sub>7</sub>PcZn-CTO to target and bind to complementary GRP78 DNA and mRNA, affording thermally stable duplex structures, similar to the ones formed by the native controls (**Figure 3.7**).

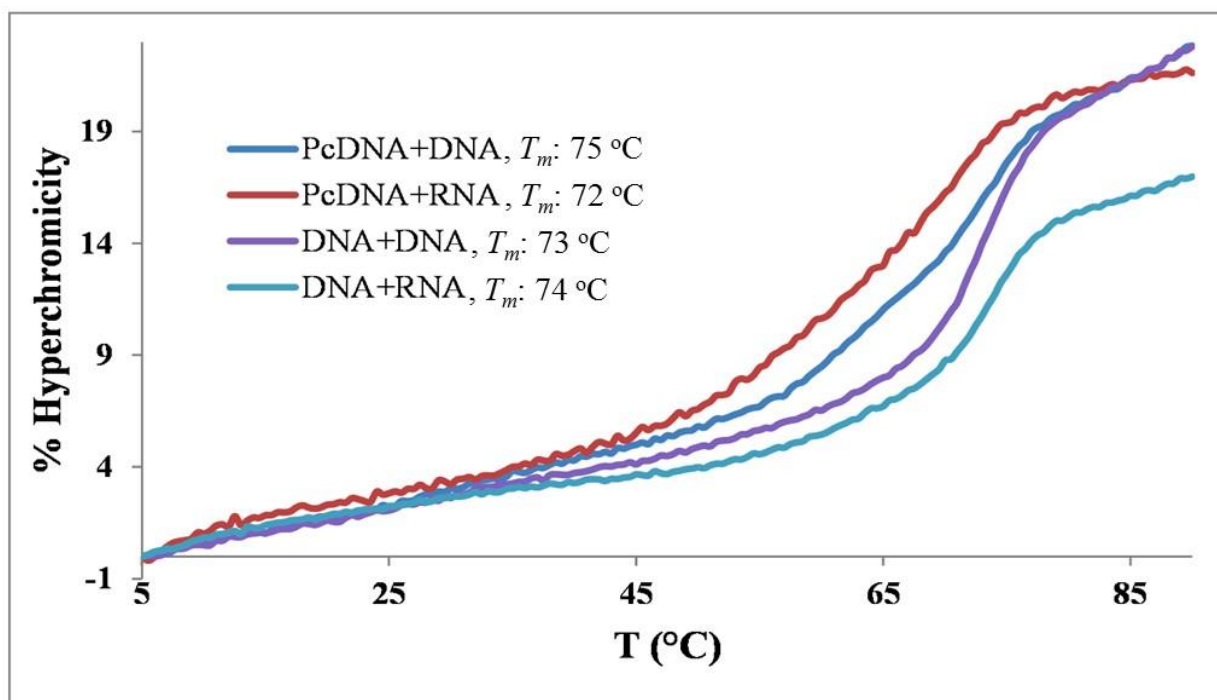


**Figure 3.7.** Thermal denaturation curves of PcDNA-DNA (**3.14:3.15**), PcDNA-RNA (**3.14:3.16**), DNA-DNA (**3.17:3.15**), RNA-DNA (**3.17:3.16**) hybrids



In order to examine the influence of Pc **3.10** on oligonucleotide hybrid structure, the circular dichroism (CD) spectrum was collected (**Figure 3.8**). The CD spectrum of the duplex formed with the native DNA hybrid showed a CD signature consistent with the canonical B-type helix structure, with a characteristic broad maximum band in between 260 - 280 nm and a minimum one at 248 nm [38]. Similarly, the control construct, formed with the DNA:RNA hybrid shows an AB-type helical structure, with characteristic maximum band at 265 nm and a broad minimum in between 250 – 230 nm [38]. In comparison, the CD spectra of the PcDNA:DNA and PcDNA:RNA hybrids exhibit structures similar to the ones formed from the native controls. Taken together, this data validates the capabilities of the PcDNA bioconjugate, **3.14**, to form stable duplex structures with complementary oligonucleotides for biological evaluation.

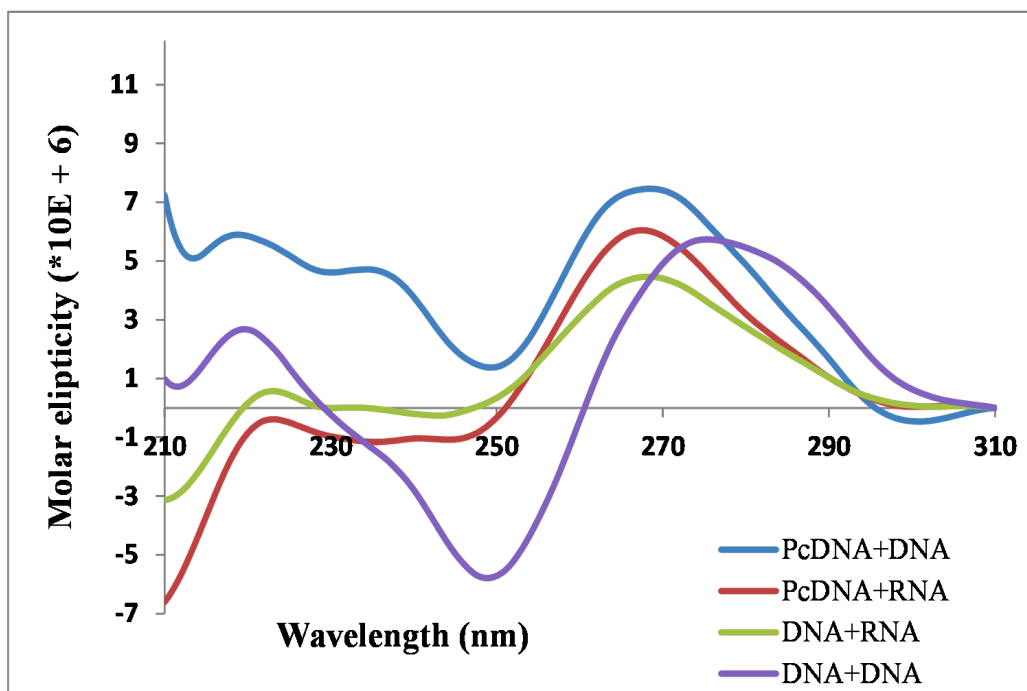


**Figure 3.8.** CD spectra of PcDNA-DNA (**3.14:3.15**), PcDNA-RNA (**3.14:3.16**), DNA-DNA (**3.17:3.15**), RNA-DNA (**3.17:3.16**) hybrid

Given the ability of  $F_{48}H_7(COOH)PcZn$ , **3.10**, to generate and survive  $^1O_2$  production, the photoreactivity of  $F_{48}H_7PcZn-CTO$ , **3.14**, hybridized with complementary GRP78 DNA and mRNA, i.e. **3.14:3.15** and **3.14:3.16**, respectively, was explored. This reactivity is critically important for establishing the ability of bioconjugates to generate singlet oxygen and the capacity of the latter to oxidatively cleave the thermally stable oligonucleotides. Thus, illumination with a 300 W halogen light for 12 hrs in the presence of  $O_2$  followed by hot piperidine treatment induced site-specific cleavage along the oligonucleotide backbone at oxidized sites [12], **Figure 3.9**. In contrast, no degradation occurred in the absence of light and/or  $O_2$ , or using unlabeled controls (see also **Figure 3.16**).

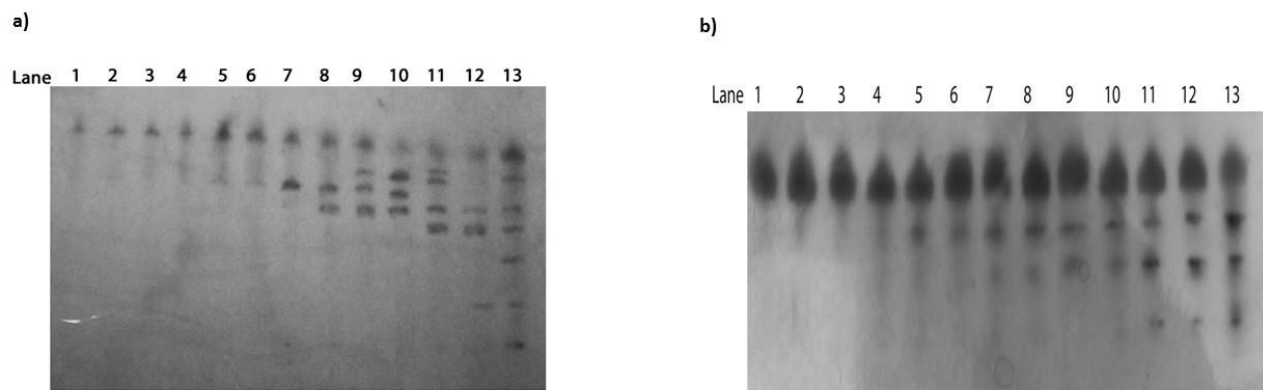


**Figure 3.9.** 24% PAGE for the photo-oxidation and piperidine cleavage pattern of a) **3.14:3.15** and b) **3.14:3.16**. Lane 1: light, but no  $O_2$ . Lane 2: no light, but with  $O_2$ . Lanes 3-13, time points from 0-12 hrs.

### 3.3.4. CONCLUSIONS

In conclusion, an entry point into a new family of highly fluorinated phthalocyanines was established. A highly fluorinated, functionalized molecule was synthesized and shown to generate  $^1\text{O}_2$  without self-decomposition, underscoring its potential in PDT [1-3] and other applications [39]. Its coupling with a cancer-targeting oligonucleotide vector proved useful in directing GRP78 DNA and mRNA oncogene stable binding, but also cleavage upon aerobic illumination. The photoactive and chemically robust fluorophthalocyanine-CTO bioconjugates encompass a new class of potential anticancer agents. Variations in the fluorinated phthalocyanine structure, coupled with variations in the types of vectors may facilitate the targeting of a broad range of oncogenes and cancer types.

### 3.3.5. EXPERIMENTAL SECTION

**Materials and Methods.** All commercial reagents and solvents (ACS grade) were used without further purification, unless stated otherwise. Cesium fluoride was dried *in vacuo* for 2 days over  $\text{P}_4\text{O}_{10}$  at 100 °C prior to use. Acetonitrile (MeCN) used for the synthesis of the perfluoro-(4,5-diisopropyl)phthalonitrile precursor was freshly distilled from calcium hydride before use. Perfluoro-(4,5-diisopropyl)phthalonitrile [35], **3.8** and 4-(3,4-dicyanophenoxy)benzoic acid [5], **3.9** were prepared according to a published literature procedure. Deuterated solvents were purchased from Cambridge Isotope Laboratories. Chromatographic separations were carried out on silica gel 60 (63–200  $\mu\text{m}$ ). Thin-layer chromatography was performed on pre-coated silica gel 60 F<sub>254</sub> plates.

$^1\text{H}$ ,  $^{13}\text{C}$  and  $^{19}\text{F}$  NMR spectra were obtained at ambient temperature on a Varian 500 MHz NMR spectrophotometer.  $^1\text{H}$  and  $^{13}\text{C}$  NMR spectra were referenced internally to residual solvent peaks and  $^{19}\text{F}$  chemical shifts were referenced to an internal  $\text{CFCl}_3$  ( $\delta = 0.00$ ) standard. NMR spectral data were processed using the ACD (version 12.01) software. Infrared spectra were obtained on a Nicolet FT-IR spectrophotometer. Electronic absorption spectra were collected using a Perkin Elmer UV-Vis spectrophotometer. High-resolution mass spectra (HRMS) were acquired at the University of Michigan (Ann Arbor, MI) by electron spray ionization in negative mode. A microwave CEM Discovery microwave reactor was used for Pc synthesis. Reactions were performed using a septum-sealed reaction vessel (10 mL) which included a thick-walled Pyrex glass reaction vessel sealed with Teflon septa caps. Melting points were taken using capillary tubes under air in a Mel-Temp apparatus and are uncorrected.

**Synthesis of  $\text{F}_{48}\text{H}_7(\text{COOH})\text{PcZn}$ , **3.10**.** 3,6-difluoro-4,5-bis(perfluoropropan-2-yl) benzene-1,2-dinitrile **3.8**, (100 mg, 0.199 mmol), 4-(3,4-dicyanophenoxy)benzoic acid, **3.9**, (53 mg, 0.199 mmol), zinc(II) acetate (18.3 mg, 0.999 mmol) and catalytic amounts of ammonium molybdate were mixed with few drops of nitrobenzene in a glass vial, sealed with a Teflon cap and heated in the microwave reactor at 190 °C for 20 minutes. The crude product was purified by column chromatography on silica gel using 4:6 v/v hexane/acetone.  $\text{F}_{64}\text{PcZn}$  was isolated as a green-blue solid (31% yield) while the desired product,  $\text{F}_{48}\text{H}_7(\text{COOH})\text{PcZn}$ , **3.10**, was isolated as a green solid. The latter was further purified by chromatography using 1:9 v/v of MeCN (contain 0.1 % TFA)/Hexane. Yield: 25.3 mg, 20.8%.  $^1\text{H}$  NMR (500 MHz, Acetone- $d_6$ ):  $\delta$  7.13 - 7.31 (m, 2 H), 7.46 - 7.59 (m, 1 H), 7.62 - 7.78 (m, 1 H), 7.80 - 8.20 (m, 3 H).  $^{19}\text{F}$  NMR (470 MHz, Acetone- $d_6$ ):  $\delta$  -164.57 (br. s., 6 F), -104.23 (br. s., 6 F), -72.87- -70.37 (m, 36F). IR (NaCl,  $\text{cm}^{-1}$ ): 2957,

2924, 2853, 1726, 1591, 1462, 1379, 1274, 1122, 1074, 951, 801. HRMS (-ve ESI)  $m/z$   $[M+Cl]^-$  calcd: 1862.8938; obsd: 1862.8964. UV-Vis ( $CHCl_3$ )  $\lambda_{max}$  ( $\log \epsilon$ ) 710 (5.02), 672 (4.96), 608 (4.32), 378 (4.68) nm ( $L mol^{-1} cm^{-1}$ ).

**Photo-oxidation of  $\beta$ -citronellol.** The catalyst  $F_{48}H_7(COOH)PcZn$ , **3.10**, was dried to constant weight at 150 °C prior to use. Photo-oxidation were performed at  $25 \pm 0.2$  °C under oxygen atmosphere (99.998% purity) in a closed, 100 mL double-walled jacketed glass vessel, while stirring at 180 rpm for 4 hrs. The temperature was kept constant with the use of a Lauda Brinkmann Ecoline RS-106 refrigerating water bath circulator. Oxygen was dosed with a Dosimat 665 dispenser (Metrohm, Switzerland) and its consumption was measured with a manometer in a closed system (see Figure 3.10). Catalyst stability measurements were performed by UV-Vis absorption measurements (300-800 nm) of aliquots (1 mL, 0-4 h) extracted periodically from the reaction mixture. The photooxidation reaction mixture consisted of Pc, **3.10** ( $20 \pm 2$   $\mu M$ ) catalyst dissolved in ethanol (50 mL) with (*S*)-(-)-citronellol (180  $\mu L$ , 1.0 mmol). Illumination was performed using the 300 W halogen lamp of a Kodak Ektagraphic III slide projector, creating a light intensity of  $2.5 \pm 0.1 \times 10^5$  lux, measured at the outer wall of the reaction vessel with an EA33 model light meter (Extech Instruments, Waltham, MA).

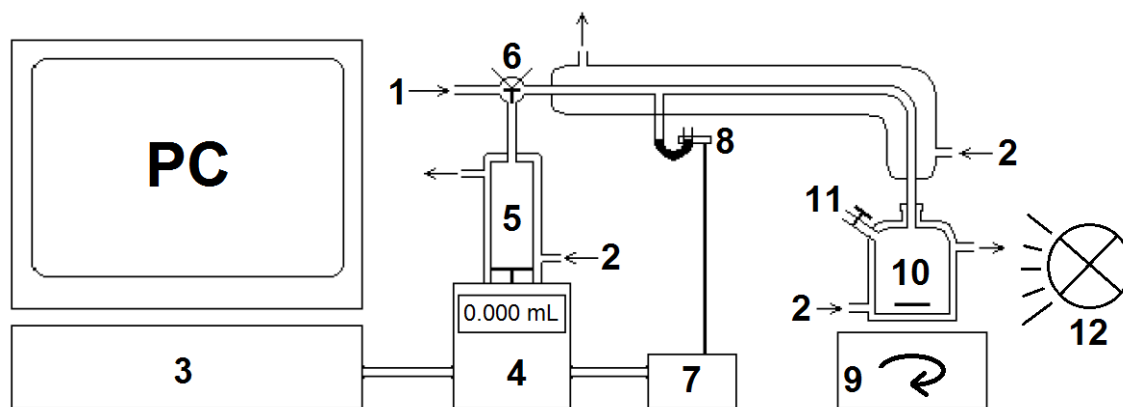


**Figure 3.10.** Schematic representation of the catalytic oxidation equipment. (1) Gas inlet; (2) thermostated water inlet; (3) computer-monitored oxygen consumption; (4) Dosimat; (5) oxygen reservoir; (6) three-way tap; (7) electrical couple for Dosimat dispenser control; (8) mercury switch; (9) magnetic stirrer; (10) 100 mL double-walled glass reaction vessel; (11) solution inlet; (12) light source.

**Solid-Phase Oligonucleotide Synthesis.** Synthesis of alkyl ( $C_6$ ) amino linker GRP78 antisense oligonucleotide, **3.17**, ( $5'$ -CTTCATCTTGCCGGCGCT- $3'$ ), sense oligonucleotide, **3.15**, ( $5'$ -AGCGCCGGCAAGATGAAG- $3'$ ) and sense RNA oligonucleotide, **3.16**, ( $5'$ -AGCGCCGGCAAGAUGAAG- $3'$ ) sequences were performed on an Unylinker controlled pore glass (CPG) support (Chemgenes Co.) using a  $1 \mu\text{mol}$  scale automated synthesis cycle on a ABI 3400 DNA synthesizer. All phosphoramidites were dissolved in anhydrous MeCN yielding 0.1 M solutions. The coupling times were 20 sec using 0.25 M 5-ethylthiotetrazole (ETT) in MeCN as activator. The detritylation times were set to 2 min using a solution of 3% dichloroacetic acid in  $\text{CH}_2\text{Cl}_2$  (DCM). Capping and oxidation steps were performed using a mixture of acetic anhydride/*N*-methyl imidazole in MeCN and a solution of 0.01 M iodine in pyr/THF/ $\text{H}_2\text{O}$ , respectively. Following synthesis, oligonucleotides were cleaved from the CPG and deprotected with  $\text{NH}_4\text{OH}:\text{EtOH}$  (3:1 v/v) for 16 hrs at  $55^\circ\text{C}$ . The crude oligonucleotides were evaporated to

dryness, extracted from the CPG with autoclaved H<sub>2</sub>O (1 mL) and quantitated by UV/Vis spectrophotometry. Crude oligonucleotides were purified by reverse-phase ion-pairing HPLC on a Waters 2695 Alliance system equipped with a Nova-pak C-18 reverse phase column (3.9 x 150 mm, 4 μm particle size) and gradient elution method of 5-95% A over 23 min (A: 20% MeCN in 0.1 M TEAA). The molecular masses of pure oligonucleotides were confirmed by ESI-MS. In the case of RNA, **3.16**, CPG-bound RNA was transferred into autoclaved eppendorf tubes and treated with a 1 mL solution of 1:1 v/v ammonium hydroxide/methylamine (AMA) and heated at 65 °C for 10 min. AMA was evaporated *in-vacuo* and the CPG was washed twice with autoclaved water (500 μL). Crude RNA oligonucleotides were re-suspended in a mixture of 1:1 v/v DMSO:triethylamine trihydrofluoride (125 μL) to complete the 2'-desilylation reaction at 65 °C for 90 min. The crude RNA was precipitated from the reaction mixture with 3 M NaOAc (25 μL) in n-BuOH (1 mL). Precipitation was completed on dry ice for 2 hrs prior to centrifugation (12,000 rpm) leaving the crude oligonucleotides as a solid white pellet. Crude oligonucleotides were re-suspended in autoclaved water (1 mL) and the yields were determined by UV absorbance measurements at 260 nm. Crude RNA was purified by reverse-phase ion-pairing HPLC and characterized by ESI-mass spectrometry as previously described.

**Preparation of the fluoro-Pc antisense oligonucleotide bioconjugate, 3.14.** The bioconjugate was produced on solid-phase, by combining the carboxy-derived perfluoro phthalocyanine, **3.10**, (3 eq, 5 mg) with the GRP78 antisense **3.13**, oligonucleotide-bound resin (1 μmol). A coupling reagent (HCTU, 1.2 mg, 3 eq) was added, the mixture was suspended in DMF (1 mL) and a base (NMM, 0.66 μL, 6 eq) was added to initiate the reaction. The reaction was performed overnight (16 hrs) at room temperature, in an overhead shaker. The mixture was filtered, and the resin was washed successively with DMF (3 x 10 mL), MeCN (3 x 10 mL), THF (3 x 10 mL) and DCM (3

x 10 mL) and dried *in vacuo*. The fluoro-Pc oligonucleotide-bound resin was cleaved and deprotected using  $\text{NH}_4\text{OH}:\text{EtOH}$  (1 mL, 3:1 v/v) for 24 hrs at 55 °C. The solution was centrifuged and concentrated to a solid pellet. The crude oligonucleotide was extracted in autoclaved water (1 mL), quantitated by UV-Vis spectrophotometry (Crude OD: 29, Absorption coefficient ( $\epsilon$ ): 159,100, Path-length: 1 cm, Concentration: 182  $\mu\text{M}$ )\* analyzed and purified by ion pairing reverse-phase HPLC as described above. The desired fluoro-Pc oligonucleotide bioconjugate, **3.14**, was isolated in purity >95% and 18% yield (1.35 mg) characterized by ESI mass spectrometry (See Table 3.1) and quantitated by UV-Vis spectrophotometry (Pure OD: 3, Absorption coefficient ( $\epsilon$ ): 159,100, Path-length: 1 cm, Concentration: 19  $\mu\text{M}$ )\*

\* Absorption coefficient ( $\epsilon$ ) was calculated using Intergrated DNA Technologies' OligoAnalyzer 3.1. Optical Density (OD) was converted to Concentration using converter.

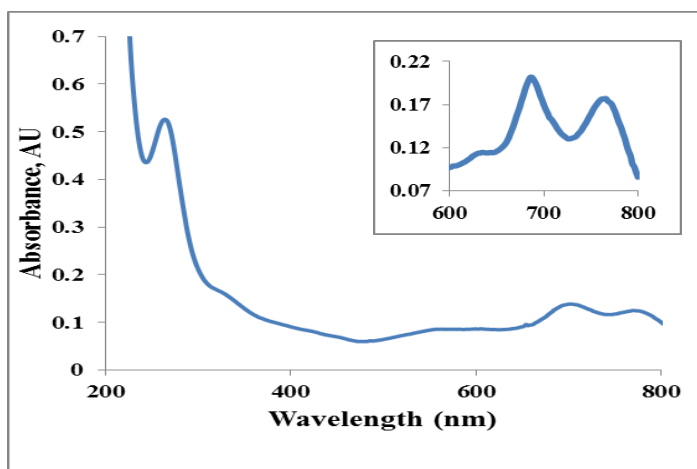


**Figure 3.11.** UV-Vis electronic absorption spectra of  $\text{F}_{48}\text{H}_7\text{PcZn-CTO}$  bioconjugate, **3.14**.



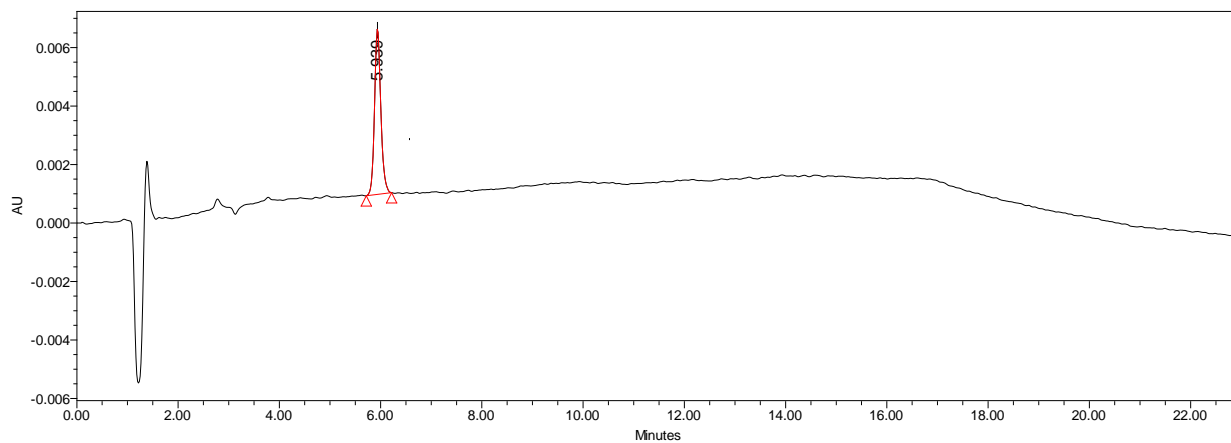


**Figure 3.12.** HPLC trace of GRP78 CTO, 3.13.

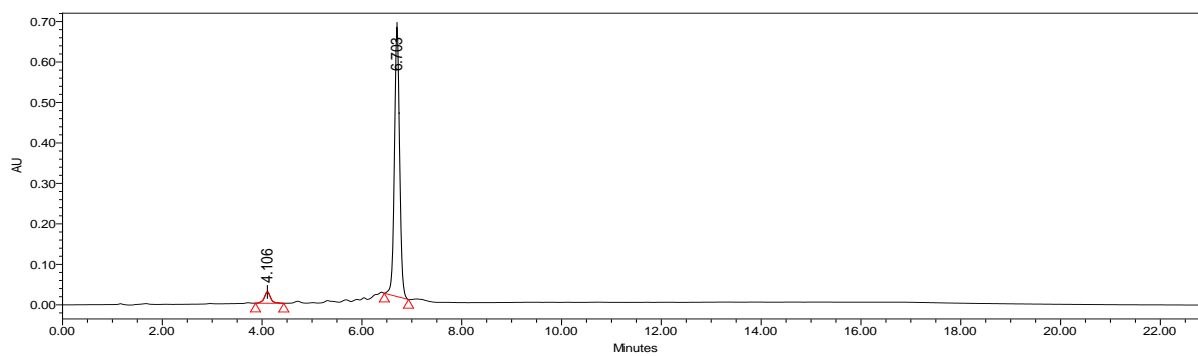


**Figure 3.13.** HPLC trace of GRP78 DNA, 3.15.

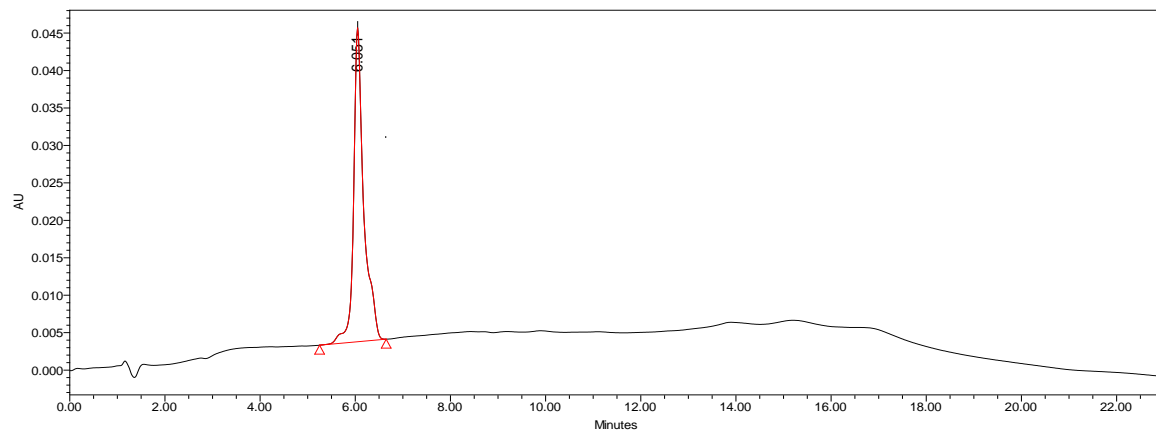


**Figure 3.14.** HPLC trace of GRP78 mRNA, **3.16.**

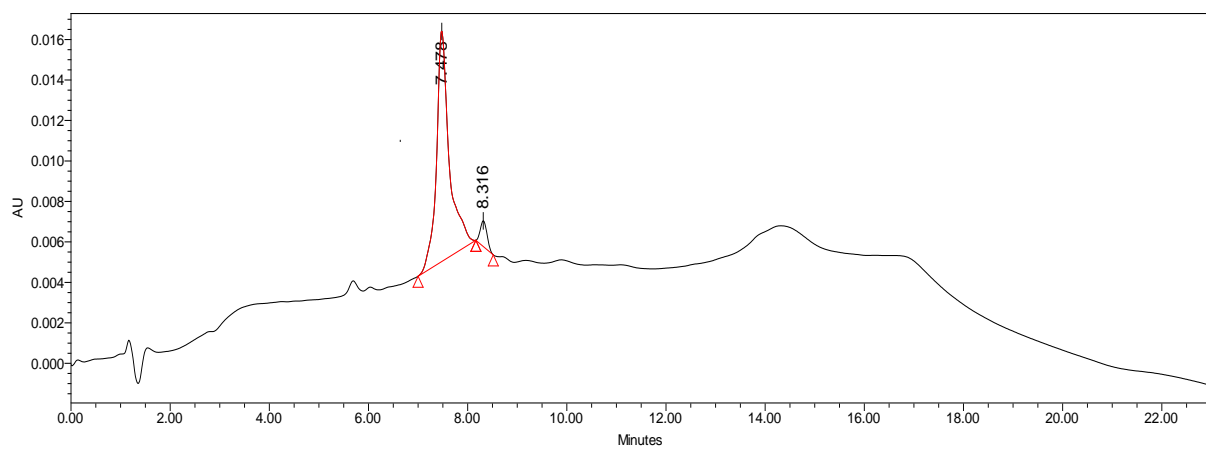


**Figure 3.15.** HPLC trace of F<sub>48</sub>H<sub>7</sub>PcZn-CTO bioconjugate, **3.14.**

**UV-Vis Spectroscopy.** Optical absorption spectra were acquired with a Perkin Elmer or a Varian Cary 300 dual beam UV-Vis spectrophotometer. Absorption values were obtained for **3.10** (10  $\mu\text{M}$ ) in chloroform/ethanol or for oligonucleotides **3.13-3.17** (0.67  $\mu\text{M}$ ) in a physiologically relevant phosphate buffer (140 mM KCl, 5 mM  $\text{NaH}_2\text{PO}_4$ , 1 mM  $\text{MgCl}_2$ , pH = 7.2). Absorption measurements were recorded at 300-800 nm for **3.10, 3.14** and 260 nm for oligonucleotides **3.13-3.17**, which were quantified according to the Beer-Lambert law. The data was averaged over a range of five different absorbance scans and reported as a mean value with a standard deviation no greater than 0.1 a.u.

**Electron spray ionization mass spectrometry.** All oligonucleotide mass spectra were acquired on an HTCS LCMS system at Novatia, LLC for 100 pmol of oligonucleotide sample dissolved in 1 mL  $\text{H}_2\text{O}$  and directly injected for ESI-MS. The data was processed by a ProMass software (Table 3.1). For high-resolution mass spectrometry of Pc, **3.10**, the sample was analyzed by direct injection on TOF/Q-TOF Mass Spectrometer at University of Michigan, Mass Spectrometry service laboratory.

**Table 3.1.** Electron spray mass spectrometry data for oligonucleotides **3.13-3.17**.

	Sequence	Calculated Mass	Observed Mass
<b>3.14</b>	$\text{F}_{48}\text{H}_7\text{PcZn}-\text{CONH-C6-5}'\text{-CTTCATCTTGCCGGCGCT-3}'$	7410.6	7411.4
<b>3.15</b>	$5}'\text{-AGCGCCGGCAAGATGAAG-3}'$	5582.7	5583.1
<b>3.16</b>	$5}'\text{-AGCGCCGGCAAGAUGAAG-3}'$	5856.1	5856.1
<b>3.17</b>	$5}'\text{-CTTCATCTTGCCGGCGCT-3}'$	5417.5	5417.1
<b>3.13</b>	$\text{NH}_2\text{-C6-5}'\text{-CTTCATCTTGCCGGCGCT-3}'$	5596.7	5596.8

**Thermal denaturation experiments,  $T_m$ .** Thermal denaturation studies were conducted on a Varian UV-Vis Cary 300 dual beam spectrophotometer equipped with a temperature controller. Complementary DNA and RNA oligonucleotides were annealed in a physiologically relevant phosphate buffer (140 mM KCl, 5 mM NaH<sub>2</sub>PO<sub>4</sub>, 1 mM MgCl<sub>2</sub>, pH = 7.2). The solutions were denatured at 95 °C for 1 min then cooled to room temperature over 2.5 h and kept at 4 °C overnight prior to conducting experimentation. The thermal melts were run from 5-90 °C with temperature gradient increments of 0.5 °C/min and data points collected every 0.5 °C/min at 260 nm. The  $T_m$  measurements were calculated according to the temperature at which 50% of the duplex denatured to single strands from a plot comparing the changes in hyperchromicity vs temperature.

**Circular Dichroism (CD) Spectroscopy.** Samples were prepared as described in the thermal denaturation experiments and analyzed using an Aviv Circular Dichroism (CD) Spectrophotometer (Model: 62A DS). CD spectra were collected on an average of three scans using 1 nm bandwidth and 0.5 min step size at 25 °C from 310-210 nm. Samples were blank corrected, smoothed and the data converted to molar ellipticity values from the equation  $[\theta] = \theta / cl$ , where  $\theta$  is the relative ellipticity (mdeg),  $c$  is the molar concentration of the DNA ( $\mu$ M) and  $l$  is the path length of the cell (1 cm). The data was imported into Microsoft Excel and the CD spectra were plotted in terms of molar ellipticity vs wavelength.

**Photo-oxidation and chemical cleavage assay.** The Pc labeled GRP78 antisense oligonucleotide, **3.14**, (6.7  $\mu$ M) was annealed with a complementary DNA or RNA sequences (**3.15-3.16**, 6.7  $\mu$ M) in a physiological phosphate binding buffer (140 mM KCl, 1 mM MgCl<sub>2</sub>, 5 mM Na<sub>2</sub>PHO<sub>4</sub> adjusted to pH 7.2). The unlabeled native GRP78 oligonucleotide sequences, **3.15-3.17**, were also hybridized and used as controls. Air was passed inside the microtube reactor

(1 mL) to saturate the solution with oxygen. The reaction was initiated by shining light (>250000 Lux) onto the samples at room temperature (22 °C). Aliquots (7 µL), collected at different time points (0-12 h), were transferred to separately sealed microtubes and stored in the absence of light at 4 °C until further use. Control experiments were also conducted as previously described in the absence of oxygen and/or light. Following the completion of the photooxidation reaction, the aliquots were dissolved in 1 M piperidine in water (150 µL, pH 12) and incubated for 45 min at 95 °C. The samples were centrifuged and concentrated to dryness on a Savant speedvac concentrator. Samples were then re-suspended in 80% formamide in autoclaved water (10 µL) and loaded on a 24% denaturing (7 M urea) PAGE. Following electrophoresis gels were visualized under short-UV shadowing (265 nm) and subsequently placed in a Stains-All® (Sigma) dye solution (25 mg Stains-All®, 50 mL isopropyl alcohol, 25 mL formamide, 125 mL water) for visualizing the resolved bands.



**Figure 3.16.** 24% PAGE for the photo-oxidation and piperidine cleavage reactions. a) **3.17:3.15** and b) **3.17:3.16**. Lane 1: light, but no O<sub>2</sub>. Lane 2: no light, but with O<sub>2</sub>. Lanes 3-12 or 13, time points from 0-12 hrs.

### 3.4. REFERENCES

- [1] Ishii, K. *Coord. Chem. Rev.* **2012**, *256*, 1556-1566.
- [2] Calin, M.; Parasca, S. *J. Optoelectr. Adv. Mat.* **2006**, *8*, 1173-1179.
- [3] Triesscheijn, M.; Baas, B.; Schellens, J.H.M.; Stewart, F.A. *Oncologist.* **2006**, *11*, 1034-1044.
- [4] Shen, X.M.; Zheng, B.Y.; Huang, X.R.; Wang, L.; Huang, J.D. *Dalton Trans.* **2013**, *42*, 10398-10403.
- [5] Erdem, S.S.; Nesterova, I.V.; Soper, S.A.; Hammer R.P. *J. Org. Chem.* **2009**, *74*, 9280-9286.
- [6] Nesterova, I.V.; Erdem, S.S.; Pakhomov, S.; Hammer, R.P.; Soper, S.A. *J. Am. Chem. Soc.* **2009**, *131*, 2432-2433.
- [7] Nesterova, I.V.; Verdree, V.T.; Pakhomov, S.; Strickler, K.L.; Allen, M.W.; Hammer, R.P.; Soper, S.A. *Bioconjug. Chem.* **2007**, *18*, 2159-2168.
- [8] Wabuyele, M.B.; Farquar, H.; Stryjewski, W.; Hammer, R.P.; Soper, S.A.; Cheng, Y.W.; Barany, F. *J. Am. Chem. Soc.* **2003**, *125*, 6937-6945.
- [9] Yuan, L.; Lin, W.; Zhao, S.; Gao, W.; Chen, B.; He, L.; Zhu, S. *J. Am. Chem. Soc.* **2012**, *134*, 13510-13523.
- [10] Kuznestova, A.A.; Chernonosov, A.A.; Kuznestov, N.A.; Koval, V.V.; Knorre D.G.; Federova, O.S. *Bioinorg. Chem. Appl.* **2006**, 1-10.
- [11] Koval, V.V.; Chernonosov, A.A.; Abramova, T.V.; Ivanova, T.M.; Federova, O.S.; Derkacheva V.M.; and Lukyantes, E.A. *Nucleosides, Nucleotides Nucleic Acids* **2001**, *4*, 1259-1262.
- [12] Burrows, C.J.; Muller, J.G. *Chem. Rev.* **1998**, *98*, 1109-1152.
- [13] Srivastava, M.; Ahmad, N.; Gupta, S.; Mukhtar, H. *J. Biol. Chem.* **2001**, *276*, 15481-15488.
- [14] Beveridge, A.C.; Bench, B.A.; Gorun, S.M.; Diebold, G.J. *J. Phys. Chem. A.* **2003**, *107*, 5138-5143.
- [15] Bench, B.A.; Brennessel, W.W.; Lee H.; Gorun, S.M. *Angew. Chem. Int. Ed.* **2002**, *114*, 776-780.
- [16] Drozd, D.; Szczubiałka, K.; Łapok, Ł.; Skiba, M.; Patel, H.; Gorun S.M.; Nowakowska, M. *App. Cat. B: Envir.* **2012**, *125*, 35-40.

- [17] Loas, A.; Gerdes, R.; Zhang Y.; Gorun, S.M. *Dalton Trans.* **2011**, *40*, 5162-5165.
- [18] Patel, P.; Patel, H.H.; Borland, E.; Gorun, S.M.; Sabatino, D. *Chem. Commun. (Camb)*. **2014**, [Epub ahead of print].
- [19] Ali, H.; van Lier, J.E. *Handbook of Porphyrin Science: Phototherapy, Radioimmunotherapy and Imaging*; **2010**, Kadish, K. M., Smith, K. M., Guillard, R., Eds.; World Scientific Publishing, NJ, *4*, 1.
- [20] Von Tappeiner, H.; Jesionek, A. *Münch. Med. Wochenschr.* **1903**, *47*, 2042-2044.
- [21] Dougherty, T.J.; Grindey, G.; Fiel, R.; Weishaupt K.R.; Boyle, D. *J. Natl. Cancer Inst.* **1975**, *55*, 115-121.
- [22] Bench, B.A.; Beveridge, A.; Sharman, W.M.; Diebold, G.J.; van Lier J.E.; Gorun, S.M. *Angew. Chem. Int. Ed.* **2002**, *41*, 747-750.
- [23] Gerdes, R.; Lapok, L.; Tsaryova, O.; Wöhrle D.; Gorun, S.M. *Dalton Trans.* **2009**, 1098-1100.
- [24] Keizer, S.P.; Mack, J.; Bench, B.A.; Gorun S.M.; Stillman, M.J. *J. Am. Chem. Soc.* **2003**, *125*, 7067-7085.
- [25] Dumoulin, F.; Durmuş, M.; Ahsen V.; Nyokong, T. *Coord. Chem. Rev.* **2010**, *254*, 2792-2847.
- [26] Kliesch, H.; Weitemeyer, A.; Müller S.; Wöhrle, D. *Liebigs Annalen.* **1995**, 1269-1273.
- [27] (a) Soares, A.R.; Tomé, J.P.; Neves, M.G.; Tomé, A.C.; Cavaleiro, J.A.; Torres, T.; *Carbohydr. Res.* **2009**, *344*, 507-510; (b) Koifman, O.I.; Hannack, M.; Syrbu, S.A.; Lyubimtsev, A.V. *Russ. Chem. Bull. Int. Ed.* **2013**, *62*, 896-917; (c) Iqbal, Z.; Lyubimtsev, A.; Hanack, M.; Ziegler, T. *Tetrahedron Lett.* **2009**, *50*, 5681-5685; (d) Zorlu, Y.; Dumoulin, F.; Bouchu, D.; Ahsen, V.; Lafont, D. *Tetrahedron Lett.* **2010**, *51*, 6615-6618.
- [28] Hammer, R.P.; Owens, C.V.; Hwang, S.H.; Sayes C.M.; Soper, S.A. *Bioconjug. Chem.* **2002**, *13*, 1244-1252.
- [29] Sibrian-Vazquez, M.; Ortiz, J.; Nesterova, I.V.; Fernandez-Lazaro, F.; Sastre-Santos, A.; Soper S.A.; Vicente, M.G. *Bioconjug. Chem.* **2007**, *18*, 410-420.
- [30] Ogunsipea A.; Nyokong, T. *Photochem. Photobiol. Sci.* **2005**, *4*, 510-516.
- [31] Pan, Y.X.; Ren, A.J.; Zheng, J.; Rong, W.F.; Chen, H.; Yan, X.H.; Wu, C.; Yuan W.J.; Lin, L. *Life Sci.* **2007**, *81*, 1042-1049.
- [32] Quinones, Q.J.; de Ridder G.G.; Pizzo, S.V. *Histol. Histopathol.* **2008**, *23*, 1409-1416.

- [33] Lee, A.S. *Cancer Res.* **2007**, *67*, 3496-3499.
- [34] (a) Patel, P.; Hanawa, E.; Yadav, R.; Samuni, U.; Marzabadi C.; Sabatino, D. *Bioorg. Med. Chem. Lett.* **2013**, *23*, 5086-5090; (b) Maina, A.; Blackman, B.A.; Parronchi, C.J.; Morozko, E. Bender, M.E.; Blake A.D.; Sabatino, D. *Bioorg. Med. Chem. Lett.* **2013**, *23*, 5270-5274.
- [35] Gorun, S.M.; Bench, B.A.; Carpenter, G.; Beggs, M.W.; Mague J.T.; Ensley, H.E. *J. Fluorine Chem.* **1998**, *91*, 37.
- [36] Meyer, S.; Tietze, D.; Rau, S.; Schäfer B.; Kreisel, G. *J. Photochem. Photobiol. A.* **2007**, *186*, 248-253.
- [37] Chantell, C.A.; Onaiyekan M.A.; Menakuru, M. *J. Pept. Sci.* **2012**, *18*, 88-91.
- [38] Kypr, J.; Kejnovska, I.; Renciuik, D.; Vorlickova, M. *Nucleic Acids Res.* **2009**, *37*, 1713-1725.
- [39] Nyokong T.; Ahsen, V. *Photosensitizers in Medicine, Environment, and Security*, **2012**, Springer, NY.



# CHAPTER 4: PROGRESS TOWARDS THE SYNTHESIS, STRUCTURAL ANALYSIS AND GRP78 BINDING OF A DIACYLHYDRAZINE LINKED DINUCLEOSIDE

## 4.1 GENERAL INTRODUCTION

A DNA hairpin is formed from a palindromic single stranded DNA (ssDNA) sequence which folds into a structure containing a base-pairing stem and a non-pairing loop (**Figure 4.1**). The DNA hairpin secondary structure is prevalent in naturally occurring DNA, such as those associated with the regulation of gene expression, modulating protein function and dictating the activity of mobile genetic elements [1]. These are likely to be ssDNA found within viruses, bacterial plasmids, transposons, and integrons.

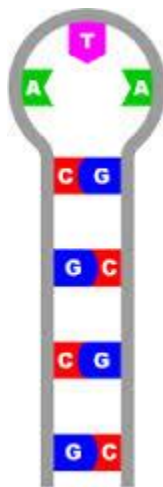


**Figure 4.1.** General structure of a DNA hairpin. Figure adapted from: <http://www.nfstc.org/>

The favorable formation of a stem-loop structure is dependent on the stability of the resulting base-pairing stem and non-pairing loop regions which is typically dictated by salts [2]. For example, hairpins with small loop sizes have been found to be stabilized by  $\text{Na}^+$  ions (100 mM NaCl), more so than the addition of  $\text{Mg}^{2+}$  ions (2.5 mM  $\text{MgCl}_2$ ) which were found to

destabilize intraloop interactions in short hairpin DNA (shDNA) motifs. Moreover, the sequence dependence on the thermal stability of shDNA has also been studied in depth by Bevilacqua and co-workers [3-7]. By temperature-gradient gel electrophoresis (TGGE) and in-vitro selection, DNA triloops, d(cGNAg) and tetraloops d(cGNNAg) (d = DNA; closing base pair in lower case; loop in upper case; N = A, C, G, or T) containing a closing C:G base-pair have shown exceptional thermal stabilities which paralleled those found within similar short hairpin RNA (shRNA) sequences [3,7]. This is partially due to the enhanced G:C base-pairing affinity, which shares three H-bonds compared to the two canonical A:T H-bonds or the non-pairing acyclic alkyl (C3) linkers that have destabilized shDNA structures [4,5]. These studies underscore the cooperative network of intraloop and loop-closing interactions which maintain the structural integrity and stability of shDNA sequences [6]. Interestingly, loops that are less than three bases are energetically unfavorable and have not been found in shDNA and related structures. Thus, modifications that can mimic and/or stabilize turn conformations may lead to the generation of stable shDNA analogs for structure-activity relationship studies in medicinal chemistry applications.

The development of modified nucleic acids through chemical synthesis has enabled the incorporation of synthetic modifications within naturally occurring sequences to improve their structure-function properties. For example, nonionic analogues of nucleic acids have been prepared to increase cellular permeability and nuclease resistance in biological media [8]. More specifically, a variety of phosphodiester backbone modifications have been explored in order to improve DNA structural stability without compromising biological activity (**Figure 4.2**). Historically, backbone modified oligonucleotides have been prepared for improving the therapeutic efficacy of DNA in antisense, antigene or aptamer methods of silencing malignant

gene expression [9]. Only a few examples have been reported of backbone modifications in DNA that may pre-organize biologically relevant secondary structures for enhanced therapeutic applications (**Figure 4.3**) [10-13].

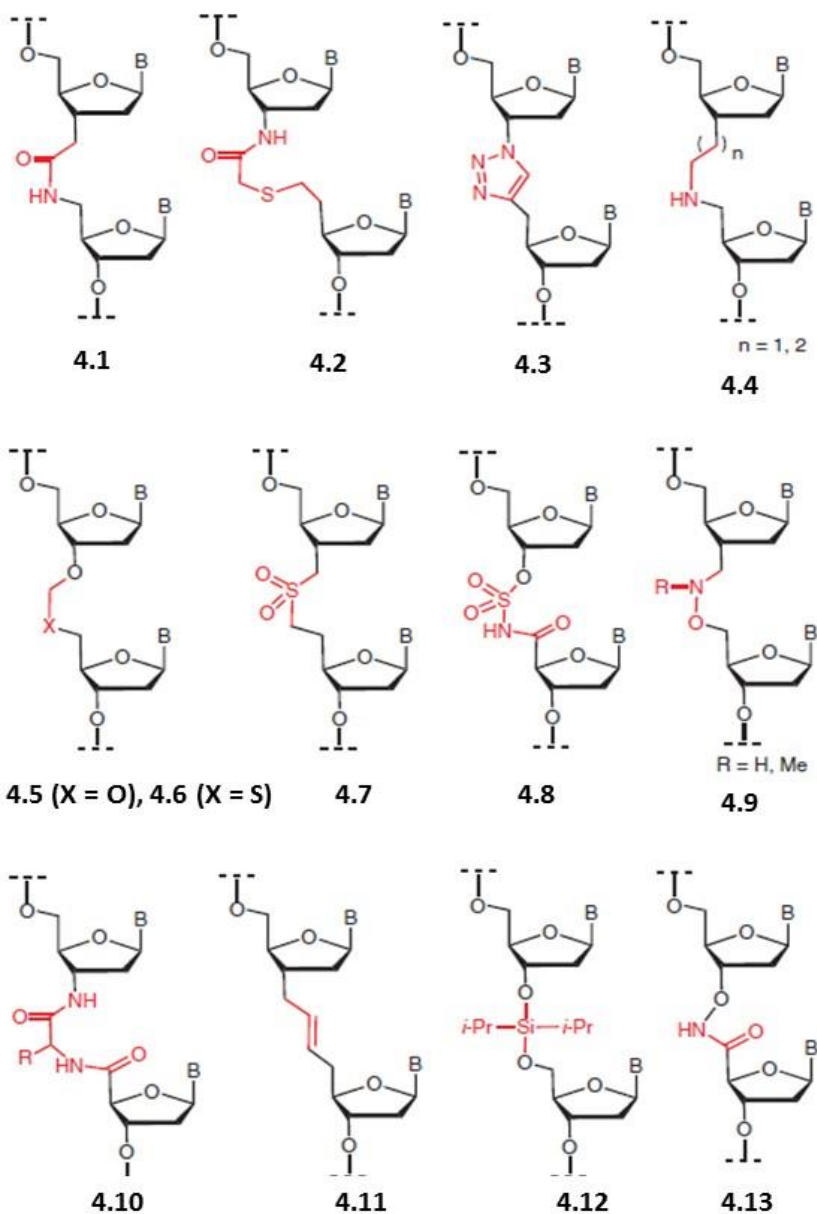


**Figure 4.2.** Structures of nonionic backbone modified oligonucleotides. Modifications include replacement of the native phosphodiester bond with: amide, **4.1**, thioacetamide, **4.2**, triazole, **4.3**, alkylamine, **4.4**, formacetal, **4.5**, thioformacetal, **4.6**, dimethylenesulfone, **4.7**, *N*-acylsulfamide,

**4.8**, oxyamine, **4.9**, or methylene(diamide), **4.10**, trans-butene, **4.11**, diisopropylsilyl, **4.12**, and *N*-oxyamide, **4.13** [8,9].

For example, the synthesis and structural properties of alkane-linked shDNA demonstrated hairpins possessing a stilbenediether linker, **4.14**, with greater structural stability when related to those that contained a C12 alkyl linker, **4.15**, and a hexa(ethylene glycol) linker, **4.16**, (*i.e.* stilbenediether > alkyl > glycol) [10]. These results indicated that hydrophobic interactions in between the linkers and the closing A:T base-pair were partially responsible for shDNA stability. Moreover, the stabilizing influence of the stilbenediether linker also suggested the importance of structural rigidity within the shDNA loop domain [10,12]. This privileged structure was found to pre-organize the putative turn conformation within shDNA via a cis-to-trans photoisomerization process that was detected by UV-Vis, CD and NMR spectroscopy. Similarly, a perylenediimide-linked DNA hairpin, **4.17**, was shown to stabilize monomeric shDNA structures in the absence of salt and dimerized sequences in >50 mM NaCl [11]. In comparison, increasing alkyl chains (C8-C14) led to an increase in shDNA thermal stability, however, with lengthier alkyl chains (>C14) a drop in melting temperature was observed [10]. Replacement of natural T<sub>4</sub> and T<sub>5</sub> loops with heptakis(ethylene glycol) and octakis(ethylene glycol), respectively, resulted in an enhancement in shDNA thermal stability [10,13]. Thus, replacement of the non-pairing nucleotides within the loop domain of shDNA with flexible and rigid alkyl linkers highlights the importance of hydrophobicity and conformation in dictating shDNA structural stability. The implications of stabilizing loop structures in shDNA not only provides greater insight into their structure and thermodynamic stabilities but also introduces modification that may improve their biological properties for applications in medicinal chemistry.

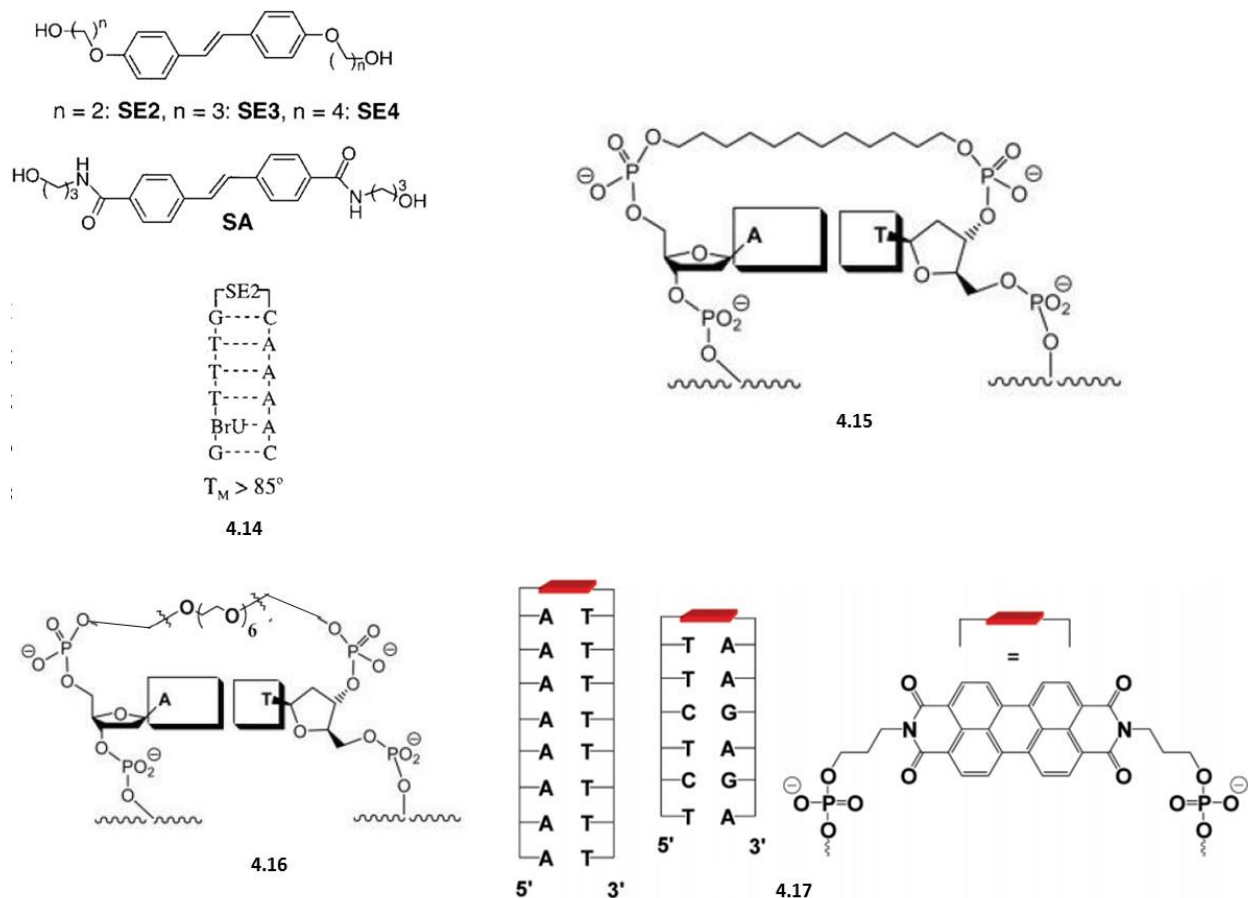


**Figure 4.3.** Structures of loop-modified shDNA [10-13].

## 4.2 CHAPTER OBJECTIVES

The aim of this thesis chapter is related to the synthesis and structural characterization of a novel backbone modified dinucleoside. The putative diacylhydrazine-linked T:A dimer is proposed to mimic shDNA by conferring a stable turn structure which orients the T:A base-pair in a favorable trajectory for H-bonding interactions (**Figure 4.6**). As such, the diacylhydrazine linkage is anticipated to mimic the structure and function of the loop domain, facilitating the

formation of the closing T:A base-pair. In this manner the diacylhydrazine-linked dinucleoside would form the smallest shDNA mimic reported to date. The solution-phase synthesis strategy is based on generating the 5'-semicarbazide-derived deoxyadenosine and the 3'-carboxy-derived thymidine as building blocks for the ensuing coupling reaction which generates the desired diacylhydrazine-linked T:A dimer. A synthetic strategy is outlined in this chapter and progress towards its synthesis is reported. Niki Rana, a graduate student in Dr. David Sabatino's group is currently pursuing the total synthesis of the coveted diacylhydrazine-linked T:A dimer for structure-activity relationship studies. Structure analyses by molecular modeling provides a preliminary insight on the nature and stability of the turn conformation induced by the diacylhydrazine linkage. Moreover, the dinucleoside bend is also expected to align the T:A base-pair for favorable Watson-Crick H-bonding interactions. With the ultimate goal of generating high affinity and selective small molecule inhibitors of the Glucose Regulated Protein of 78 kilodalton (GRP78) molecular docking is explored. The generation of potent GRP78 inhibitors has potential anti-cancer implications. Thus, the diacylhydrazine-linked dinucleoside reported for the first time in this thesis represents an exciting new class of shDNA mimics that may be useful for pre-organizing important DNA secondary structures that are related to their biological and therapeutic activity.

## **4.3 STABILIZING TURN CONFORMATIONS IN DNA HAIRPINS BY DIACYLHYDRAZINE-LINKED NUCLEIC ACIDS**

### **4.3.1 ABSTRACT**

The hairpin secondary structure is a prevalent motif found in naturally occurring DNA and RNA. DNA hairpins have been associated with the regulation of gene expression, modulating protein function and dictating the activity of mobile genetic elements. Thus, the study of DNA hairpins and their related analogs may provide greater insight into their evolution, function and potential in medicinal chemistry applications. The latter forms the basis of this thesis chapter, which aims to develop short hairpin DNA (shDNA) mimics as regulators of protein function for therapeutic applications. Our target is the Glucose Regulated Protein 78 (GRP78), which is overexpressed and exclusively found on the cell surface of tumors. Cell surface GRP78 has thus been classified as a clinically relevant biological marker for tumor therapy. Therefore, potent inhibitors of GRP78 may formulate the basis of effective anti-cancer strategies. The fruitful applications of shDNA in medicinal chemistry applications must address its poor pharmacokinetic properties and improve its ‘drug-like’ behavior. To this effect, the replacement of the native 3',5'-phosphodiester bond with a novel 3',5'-diacylhydrazine linkage is proposed to improve shDNA structural stability and pre-organize the turn-like loop geometry. Based on our preliminary molecular docking studies, the proposed diacylhydrazine-linked shDNA exhibits tight GRP78 binding at the active site that is also occupied by ATP. This observation is partly due to the folded geometry of the diacylhydrazine-linked shDNA which pre-organizes a turn conformation due to the repulsive hydrazine nitrogen lone-pair interactions. This bio-active structure is anticipated to supply a new class of potent and selective GRP78 competitive inhibitors.

### 4.3.2. INTRODUCTION

The DNA hairpin may differ in structure and function based on the length of the stem, the size of the loop and in actual nucleotide sequence. It can function to guide DNA folding events that are associated with protection from degradation, recognition sites for DNA binding proteins or for controlling gene expression in bacterial and mammalian cells [1]. Although relatively stable, shDNAs sometimes have the tendency to unfold [2], undergo hydrolysis [14] and nuclease digestion [15], limiting their overall efficacy as therapeutic agents and as useful ligands for controlling oncogene expression *in-vivo* [16,17]. Therefore, structural modifications that may stabilize hairpin conformation and provide resistance to degradation may improve the structure-function properties of shDNA. To this effect, alkyl and/or aromatic modifications of the loop domain found within shDNA have displayed varying effects on hairpin thermodynamic stability, limiting their potential in medicinal chemistry applications [10-13]. In an effort to improve DNA hairpin structural stability without compromising function and activity, the design of a 3',5'-diacylhydrazine backbone linkage as replacement of the native 3',5'-phosphodiester bond is proposed (**Figure 4.4**).



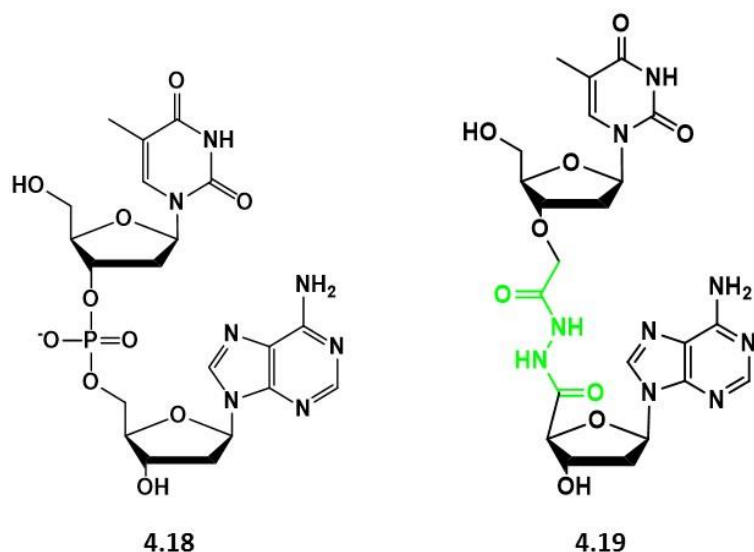


**Figure 4.4.** Structures of phosphodiester, **4.18** and diacylhydrazine, **4.19**, linked T:A dimer

The anticipated turn structure in 3',5'-diacylhydrazine-linked DNA, **4.19**, is based on the conformational analyses of diacylhydrazines [18-22] and their incorporation within bio-active peptide sequences, *i.e.* azapeptides [23-26]. Diacylhydrazine structural analyses by NMR spectroscopy has indicated a twisted energy minimum conformation, with a large torsional barrier (>20 kcal/mol in some cases) that locks the turn geometry in a ground state energy minimum [19,20]. Furthermore, steep rotational barriers (~10 kcal/mol) for the inter-conversion of *E,E* and *E,Z*-configurations about the N-N<sub>α</sub> hydrazine bond have been determined by computational analyses and underscore the stable turn geometries induced by the diacylhydrazine moiety [18]. These conformational preferences have been attributed to the lone pair repulsion interactions of the adjacent hydrazine nitrogen atoms which favor a twisted geometry [18-20]. Moreover, a natural bond orbital (NBO) analysis of *N,N'*-diformylhydrazine suggests that exchange of delocalization energy about the hydrazine functional group is partly involved in the pre-organized diacylhydrazine structure [21]. Furthermore, the rigid urea has

been found to stabilize the twist structure found within diacylhydrazine containing pseudopeptides [22]. The incorporation of diacylhydrazines within bio-active peptide sequences (*i.e.* azapeptides) have been shown to restrict the backbone torsion angles ( $90^\circ$  for  $\varphi$  and  $0^\circ$  or  $180^\circ$  for  $\psi$ ) for stabilizing peptide turn secondary structures [23-26]. In light of the diacylhydrazine twist and urea planarity, a turn-like geometry is expected to facilitate the thymine:adenine (T:A) loop closing interactions in the proposed shDNA mimic, **4.19**. This analog represents a new entry point into privileged shDNA structures that may be useful in a variety of biological and medicinal applications.

The Glucose Regulated Protein 78 (GRP78) has been classified as a biological target for therapeutic use due to its involvement in the unfolded protein response (UPR) and cell surface signaling activity in tumors [27]. GRP78 was first discovered as a 78,000 Da protein whose expression was enhanced in glucose deprived tissue cultures [28]. Subsequently, GRP78 was determined to be an ER resident protein, assisting in protein folding events due to a variety of environmental and physiological stress conditions that perturb ER function and homeostasis [29]. In cancer, GRP78 is overexpressed and exclusively found on the cell surface where it signals tumor initiation, replication and metastatic spread [30]. Therefore, potent inhibitors of cell surface GRP78 may formulate the basis of effective and selective anti-cancer strategies.

Small molecule GRP78 inhibitors have been prepared for anti-cancer applications (**Figure 4.5**). The natural products, epigallocatechin gallate, (**4.20**, EGCG), and honokiol, (**4.21**, HNK), extracted from green tea leaves and magnolia grandiflora, respectively, have been shown to induce ER stress leading to potent cell death effects in melanoma, glioblastoma and neuroblastoma by binding to the GRP78 ATPase domain and inhibiting its activity [31]. A library of synthetic adenosine-based inhibitors have been prepared by combinatorial chemistry

and screened against the GRP78 ATP binding domain [32]. The lead inhibitor, **4.22**, maintained potent ( $K_D$ : 60 nM) and selective GRP78 binding affinity when screened against homologous heat shock proteins leading to potent cell death across a panel of 10 human cancer cell lines [32,33]. A fungal metabolite, Verrucosidin (**4.23**, VCD) with putative GRP78 inhibition, solicited cytotoxicity in breast cancer cell lines by eliminating cellular mitochondrial energy production [34]. This finding has generated conjecture that other claimed GRP78 inhibitors (arctigenin, biguanides, deoxyverrucosidin, efrapeptin, JBIR, piericidin, prunustatin, pyrvinium, rottlerin, valinomycin, versipelostatin) might act in a GRP78-independent manner. The small molecule GRP78 inhibitors, **4.20-4.23**, may form the basis for the rational design of novel GRP78 inhibitors for potent and selective anti-cancer activity.

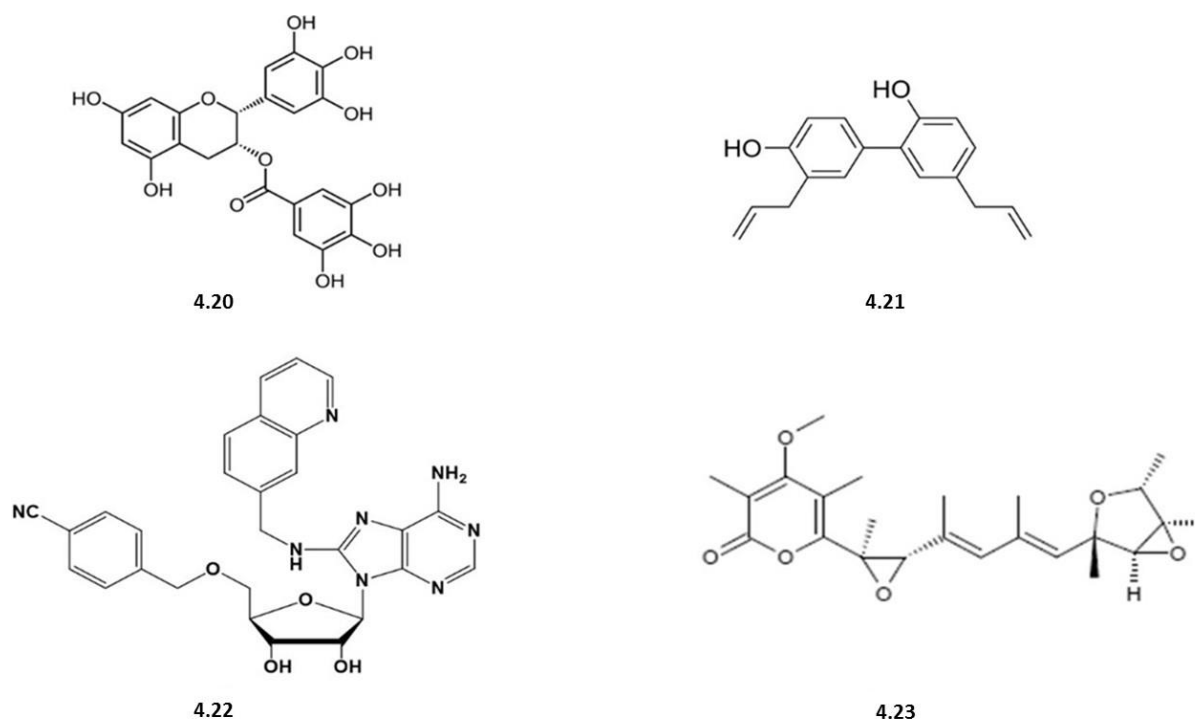


**Figure 4.5.** Small molecule GRP78 inhibitors [31-34].

**4.3.3. RESULTS AND DISCUSSION**In order to explore the putative turn-like geometry within diacylhydrazine-linked shDNA, **4.19**, molecular modeling and docking simulation studies were respectively performed using Chem3D molecular mechanics and Autodock Vina [35]. The energy minimized structures were then visualized using PyMOL [36]. A comparative energy minimization study was initially performed in between the native phosphodiester, **4.18** and diacylhydrazine, **4.19** linked T:A dimers (**Figure 4.6**) to explore the influence of the backbone modification on molecular structure. Based on the preliminary energy minimization data, the native T:A dimer exhibits a stacked orientation that is most likely stabilized by the hydrophobic aromatic interactions of the non-pairing nucleobases (**Figure 4.6, A**). In comparison, the 3',5'-diacylhydrazine linkage functions to pre-organize the molecular structure into a turn-like geometry that is reminiscent of the non-pairing loop domain found within shDNA (**Figure 4.6, B**). The observed turn structure in **4.19**, is most likely pre-organized by the repulsive hydrazine nitrogen lone-pair interactions and the rigid, planar urea which tends to favor a perpendicular geometry by bending the diacylhydrazine in a (*Z,E*)-conformation [18-22]. Furthermore, the turn-like geometry is also stabilized by the intramolecular H-bonding T:A base-pairing interactions. These have been found to occur within optimal spatial distances (<5 Å) in the diacylhydrazine-linked T:A dimer and not within the native sequence (>10 Å). Therefore, the turn-type conformation in shDNA mimic, **4.19**, has been found to be energetically stabilized by a combination of favorable stereoelectronic and bonding interactions. These effects are typically significant in minimizing the free energy ( $\Delta G_B^\ddagger$ ) associated with ligand binding to target receptor for fruitful medicinal chemistry applications [32,33].

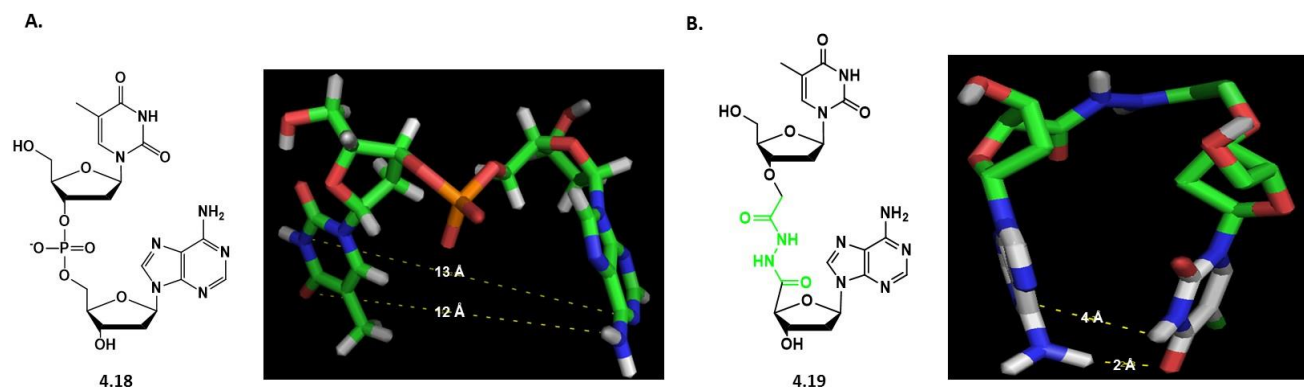


**Figure 4.6.** Structures and models of A. (ApT), native DNA, **4.18** and B. 3',5'-diacylhydrazine linked T:A, **4.19**. Molecular models were calculated using Chem3D molecular mechanics software and represented as energy minimized structures using the MM2 force field with a minimum RMS gradient of 0.01. The energy minimized structures were analyzed and the H-bonding distances were determined using PyMol.

AutoDock Vina [35] was next employed as computer docking simulations program to predict the GRP78:**4.19** binding interactions. The co-crystal structure of ATP bound to the ATPase domain of GRP78 was freely downloaded from RCSB PDB (PDB ID # 3LDL) [32,33,37]. An interface between the molecular graphics system PyMOL and the molecular docking suite AutoDock Vina was used to demonstrate the combination of docking and visualization models in between the ligand **4.19** and the GRP78 binding domain. The energy minimized structure of **4.19** was imported into AutoDock Vina and docked onto the ATPase binding domain of GRP78. The energy minimum conformation responsible for GRP78 binding (root mean square deviation; rmsd = 0) was selected from the output file (**Table 4.1**).

Mode	Affinity (kcal/mol)	Distance from best mode	
		Rmsd l.b.	Rmsd u.b
1	-9.3	0	0
2	-9.3	2.61	5.95
3	-9.2	2.699	6.743
4	-8.8	2.767	5.226
5	-8.8	3.208	6.807
6	-8.7	2.556	3.58
7	-8.7	1.419	2.057
8	-8.7	3.271	8.731
9	-8.5	2.667	6.21

**Table 4.1.** Energy minimized conformations of **4.19** bound to GRP78. Lamarckian genetic algorithms, as implemented in AutoDock Vina [35], were employed to perform the docking simulation studies. All other parameters were retained as default settings. By default, AutoDock Vina generate 10 best binding mode at receptor site. For each of the docking cases, the lowest energy docked conformation, according to the AutoDock scoring function, was selected as the binding mode.

Significantly, ligand **4.19** demonstrated comparable GRP78 binding affinity when compared to the literature reported adenosine-derived inhibitors, **4.22** [32,33]. Moreover, ligand **4.19** was found to occupy the ATPase binding site of GRP78, supporting its potential as a potent and selective GRP78 inhibitor (**Figure 4.7**). Comparison of the co-crystal structures of GRP78 and its related homologue HSP70 in the presence of their bound ligands indicated a conserved ATPase binding domain, with the exception of a single amino acid residue (GRP78 : Ile61 and HSP70 Thr37) [32,33,38]. This single amino acid substitution is sufficient in discriminating between the two chaperone proteins. Moreover, this structural feature has been exploited in the design of GRP78 selective inhibitors [32,33]. The non-polar Ile61 in GRP78 creates a

hydrophobic binding pocket that can accommodate ligands with non-polar and small electron-rich groups (*eg.* NH-, OH-, SH-). This interaction has facilitated the binding of ligand **4.19** within the same proximity ( $<6 \text{ \AA}$ ) as the naturally occurring ATP ligand (**Figure 4.8**). Thus, a combination of conformational pre-organization and non-polar interactions has enabled tight binding of ligand **4.19** to the GRP78 ATPase active site, making it a potential lead in the development of high affinity and selective GRP78 inhibitors.

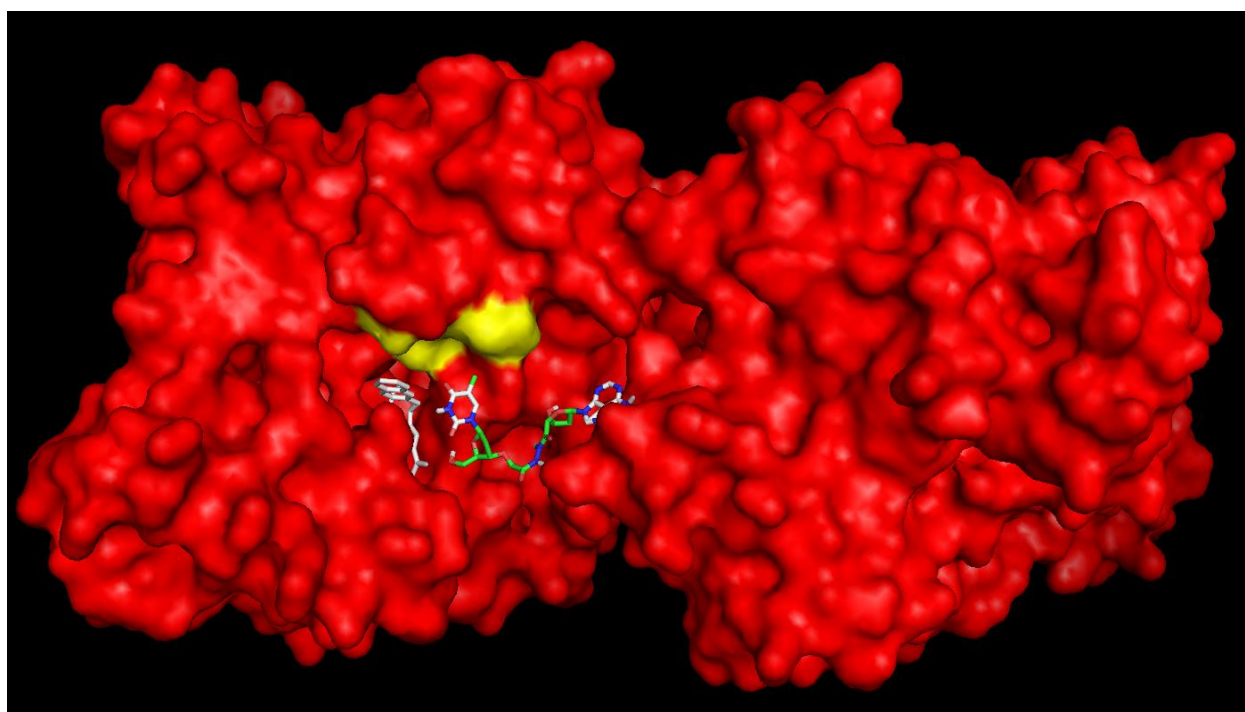


**Figure 4.7.** Docking of diacylhydrazine linked T:A dimer, **4.19** on the GRP78:ATP complex (PDB: 3LDL) (GRP78: Red, ATP: White, 4.19: multicolor, ATPase binding site: yellow).

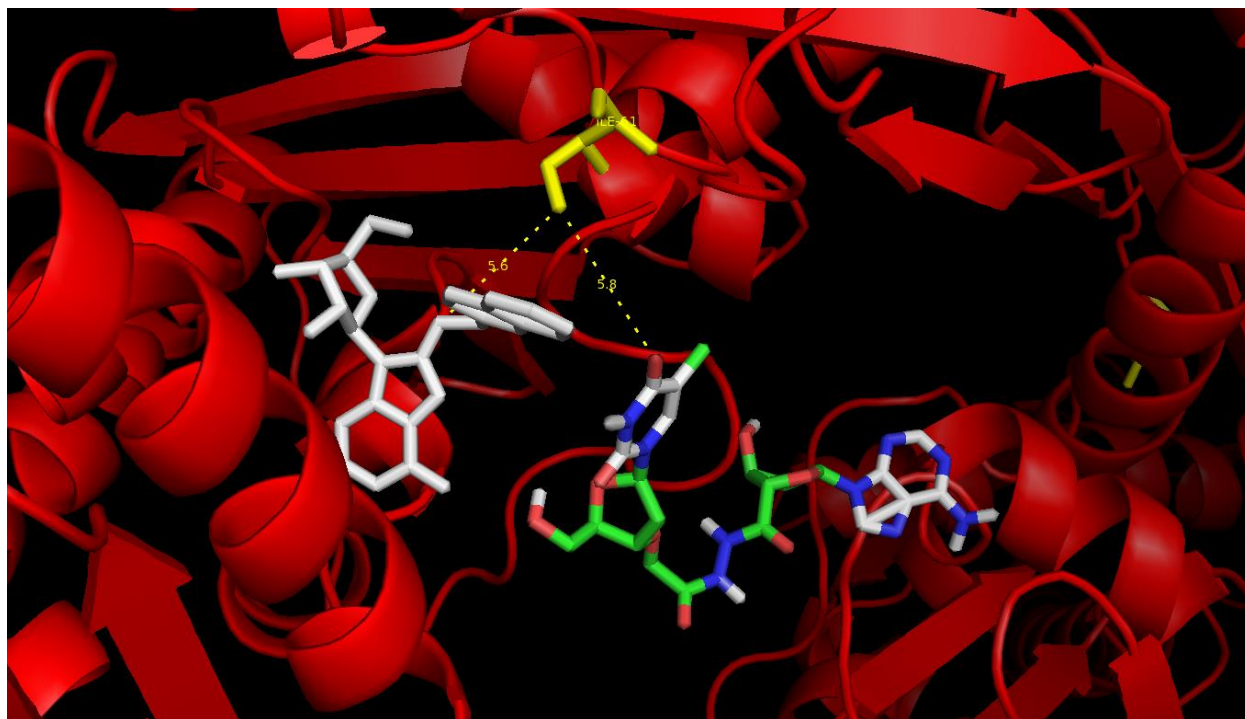
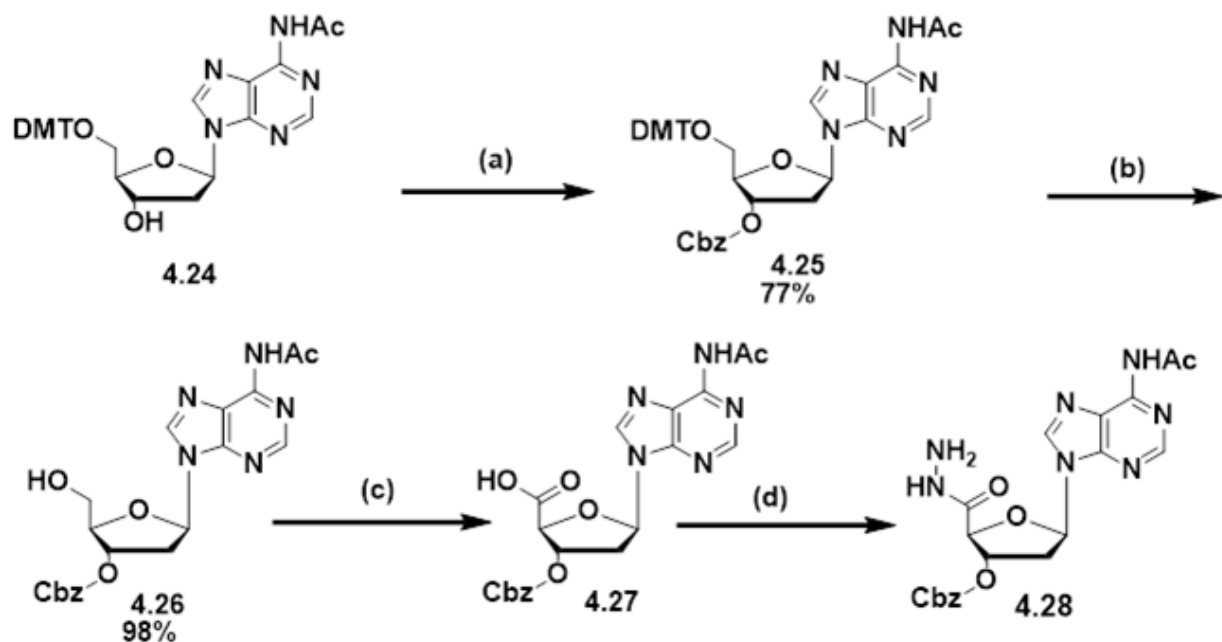


**Figure 4.8.** Expansion of the docking interaction of diacylhydrazine linked T:A dimer, **4.19** on the GRP78:ATP complex (PDB: 3LDL) (GRP78: Red, ATP: White, 4.19: multicolor, ATPase binding site: yellow). ATP and **4.19** are positioned within a 6 Å distance from the Ile61 residue located at the ATPase active site.

The synthesis strategy for the production of the diacylhydrazine-linked T:A dimer, **4.19**, is currently on-going in collaboration with Niki Rana, a graduate student in Dr. David Sabatino's research group. The proposed synthesis method is outlined, with a detailed description of the synthetic steps that have been successfully completed. The synthesis of the desired ligand **4.19** is contingent on the generation of a 3'-carboxy derived thymidine, **4.32**, and a 5'-semicarbazide-derived deoxyadenosine, **4.28**, that may be coupled to form the target diacylhydrazine-linked T:A dimer, **4.19** (Scheme 4.3).

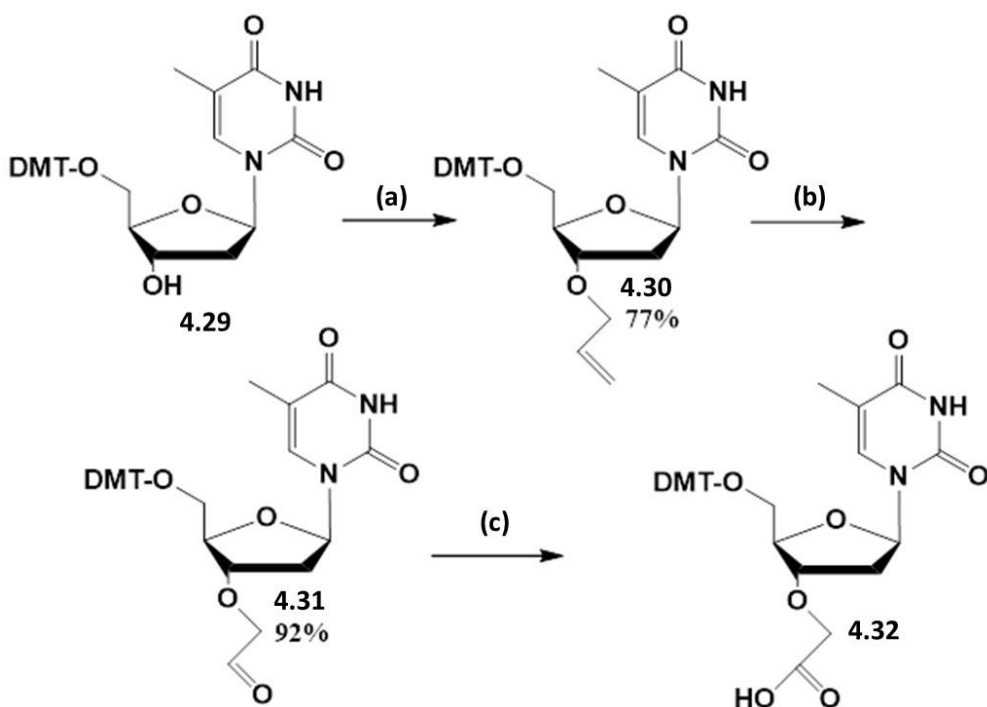


The synthesis of the 5'-semicarbazide derived deoxyadenosine, **4.28** begins with the attachment of a carboxybenzyloxy (Cbz) protecting group at the 3-position of commercially available *N*-acetyl-5'-*O*-(4-dimethoxytrityl) deoxyadenosine, **4.24**. (**Scheme 4.1**). The Cbz protecting group was easily installed using benzylchloroformate and DMAP in DCM [39]. Following carbonylation, **4.25** was detritylated using 3% trichloroacetic acid giving **4.26** in 98% yield. The 5'-alcohol was next oxidized to the corresponding carboxylic acid, **4.27**, using a BAIB-TEMPO oxidation reaction [40]. Due to difficulty in purification and very high polarity of carboxylic acid, this product was coupled to Boc-carbazate using conventional peptide coupling conditions [41]. Finally, attempts to remove BOC protecting group on carbazate to liberate free NH<sub>2</sub> using conventional TFA:DCM (50:50) led to a series of degradation products. Currently, we are optimizing the reaction and purification conditions for the synthesis of **4.28**.



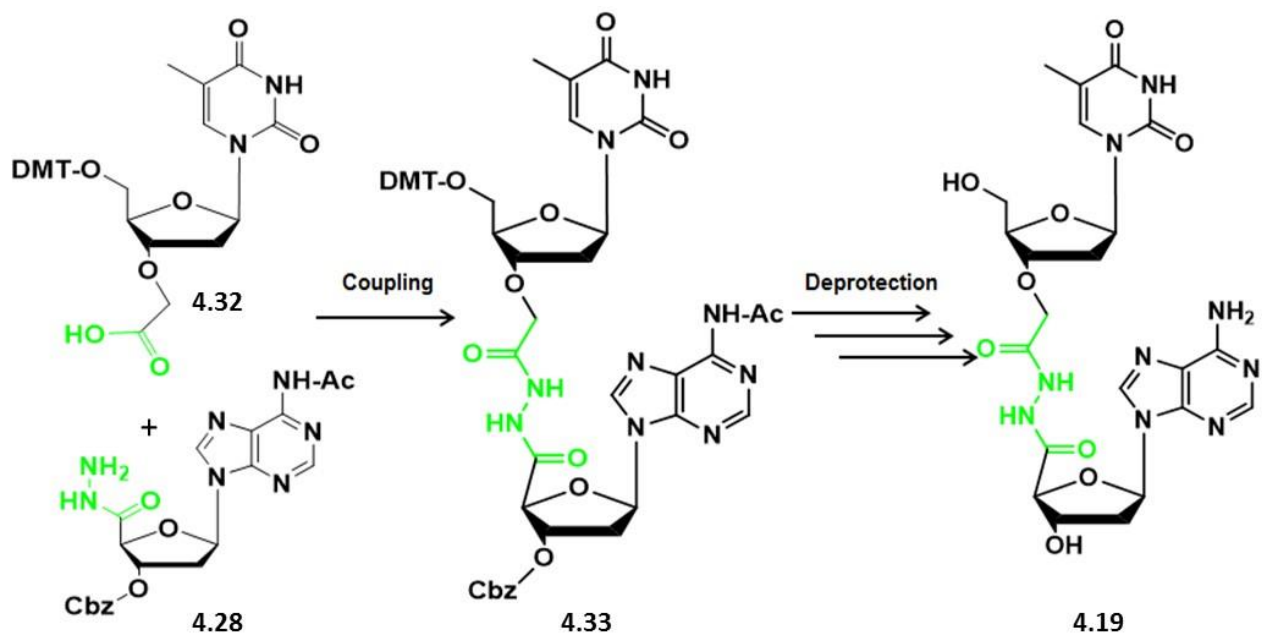
**Scheme 4.1.** Synthesis of *N*-acetyl 5'-semicarbazide 3'-carboxybenxyloxy deoxyadenosine, **4.28**. Reactions and Conditions. (a) DMAP, benzyl chloroformate, DCM, 0 °C - rt, 72 h, (b) 3% TCA:DCM, rt, 15 min, (c) TEMPO, BAIB, MeCN:H<sub>2</sub>O (50:50 v/v), rt, 15 h, (d) i. *t*-butyl carbazate, EDC, Oxyma, DIEA, DCM, rt, 12 h, ii. 50% TFA:DCM, rt, 2 h.

The synthesis of a 3'-carboxy-derived thymidine **4.32**, also proved challenging (**Scheme 4.2**). The first attempted *O*-alkylation reactions of commercially available 5'-*O*-(4-dimethoxytrityl) thymidine **4.29** with ethyl bromoacetate, methyl bromoacetate, phenyl bromoacetate and Boc-bromoacetate failed to yield the desired product. In spite of the alkylating reagent and reaction conditions, the *N*-alkylated nucleosides were isolated as major products due to enhanced nucleophilicity at the N3 position of thymine. Following literature precedence, an allylation strategy was adopted to circumvent *N*-alkylation and afford the desired 5'-*O*-(4-dimethoxytrityl) 3'-*O*-allyl thymidine **4.30** [42]. In our hands, the reaction of thymidine **4.29** with allyl bromide under ultrasonic conditions gave the desired product **4.30** in 77% yield. Oxidative cleavage of the allyl group using OsO<sub>4</sub> then allowed for the formation of aldehyde **4.31** in 92% yield. Radical oxidation conditions [40] (TEMPO-BAIB) were next employed to convert the 3'-aldehyde to the corresponding carboxylic acid **4.32**. Considering the difficulty associated with the purification of carboxylic acid **4.32** using normal phase silica gel chromatography and the acid sensitivity of the dimethoxytrityl (DMT) group, carboxylic acid **4.32** was not isolated and characterized. A modified protecting group strategy is currently being investigated for the stable production of building block **4.32**.



**Scheme 4.2.** Synthesis of 5'-*O*-(4-dimethoxytrityl) 3'-*O*-(carboxymethylene) thymidine, **4.32**. Reactions and Conditions. (a) allyl bromide, NaH, THF, rt, 3 h, (b) OsO<sub>4</sub>, NMO, NaIO<sub>4</sub>, Na<sub>2</sub>S<sub>2</sub>O<sub>5</sub>, acetone:phosphate buffer (3:1 v/v) pH 7, rt, 5 h, (c) TEMPO, BAIB, MeCN:H<sub>2</sub>O (50:50 v/v), rt, 2 h.

With isolated building blocks in hand, the coupling reaction in between the 5'-semicarbazide derived deoxyadenosine, **4.28** and the 3'-carboxy derived thymidine, **4.32** will be next attempted. Conventional coupling reagents such as EDC/Oxyma, HATU and EEDQ will be tried to afford the protected 3',5'-diacylhydrazine linked T:A dimer, **4.33**. The ensuing steps will consist of the selective removal of the protecting groups to afford the anticipated 3',5'-diacylhydrazine linked T:A dimer, **4.19**, (**Scheme 4.3**).



**Scheme 4.3.** Proposed synthesis of the 3',5'-diacylhydrazine linked T:A dimer, **4.19**.

#### 4.3.4. CONCLUSIONS

In summary, a novel class of backbone modified DNA has been introduced within this chapter. The 3',5'-diacylhydrazine linked T:A dimer is proposed to mimic shDNA structure and activity. The diacylhydrazine pre-organizes a turn-type geometry which favors the closing T:A base-pairing interactions according to computational analyses. This privileged structure was docked onto the GRP78 oncoprotein and demonstrated tight binding at the ATPase active site also occupied by the ATP ligand. These *in silico* studies demonstrate the potential for shDNA mimic **4.19** to bind and inhibit cell surface GRP78 activity. This is an essential requirement for the development of potent and selective GRP78 inhibitors for anti-cancer applications. Thus, diacylhydrazine-linked nucleic acids represent a new class of privileged structures that may mimic biologically active turn conformations for structure-activity relationship studies.

#### 4.3.5. EXPERIMENTAL SECTION

**Methods.** All reactions were carried out in oven dried (120 °C) glassware and purged with nitrogen. Syringes and needles were stored in an oven overnight and allowed to cool in desiccators with anhydrous calcium sulfate prior to use. Reactions were stirred with Teflon coated magnetic stir bars. Reactions were monitored using Thin Layer Chromatography (TLC) on aluminum-backed silica gel plates (Merck 60 F254). TLC plates and were visualized under UV light (260 nm) and by staining with 10% H<sub>2</sub>SO<sub>4</sub> in MeOH. Compound purification using silica gel chromatography was performed on a 230-400 mesh silica (Sorbent Technologies). Anhydrous solvents and reagents were purchased from Aldrich (St. Louis, MO) and VWR (Bridgeport, NJ). Melting points were measured on a Thermo Melt apparatus. Specific rotations measurements were recorded on a DigiPol 781 Automatic Polarimeter (Rudolph Instruments, Fairfield, NJ, USA) as averages of five measurements. Data are reported as follows:  $[\alpha]_{\lambda}$  temp, concentration (c in g/100 mL), in Ace, MeOH, DCM or CHCl<sub>3</sub>. Molecular weights were measured as direct injections on a Hewlett Packard series 1100 MSD equipped with ESI as ion-source in positive mode using 50/50 v/v MeOH/H<sub>2</sub>O at a flow-rate of 1 mL/min. Infrared (IR) spectra were obtained on a Nicolet 4700 FT-IR (ThermoElectron Co.) coupled with OMNIC software (driver version: 7.1). Samples were prepared on a KBr plate using a cast film technique and the spectrum was recorded by monitoring the change in sample transmittance as a function of wavenumbers (cm<sup>-1</sup>). IR spectra were collected in triplicate to ensure reproducibility. Nuclear magnetic resonance spectra (<sup>1</sup>H, <sup>13</sup>C, COSY NMR) were recorded on an OXFORD NMR AS500 spectrophotometer with sample dissolved in deuterated chloroform (CDCl<sub>3</sub>), dichloromethane (CD<sub>2</sub>Cl<sub>2</sub>), acetone (acetone-d<sub>6</sub>) and dimethylsulfoxide (DMSO-d<sub>6</sub>). The NMR spectra were obtained at ambient temperature using an indirect pulse-field gradient (ID-PFG) probe. The

obtained data was processed using VNMRJ software (version 2.2). The  $^1\text{H}$  and  $^{13}\text{C}$  assignments were based on gCOSY and gHMQC NMR correlation experiments.

***N*-Acetyl-5'-*O*-(4-dimethoxytrityl)-3'-*O*-(carboxybenzyloxy) deoxyadenosine, 4.25.** *N*-Acetyl-5'-*O*-(4-dimethoxytrityl) deoxyadenosine (2g, 3.36 mmol) was suspended in dichloromethane (20 mL) and DMAP (1.36 g, 11.13 mmol) was added. After cooling at 0 °C, benzyl chloroformate (1.39 mL, 9.24 mmol) was added dropwise and the suspension was stirred at room temperature overnight. The next day, the solution was diluted in dichloromethane (10 mL) and evaporated to a viscous oil. The product was purified by silica gel chromatography (Acetone/DCM 1:9 v/v) giving **4.25** (1.90 g) as a white solid. Yield: 77%. m.p. 89 °C.  $R_f = 0.55$  (CH<sub>2</sub>Cl<sub>2</sub>-Acetone, 9:1),  $[\alpha]_D^{22} -3.709$  ( $c$  0.80, DCM).  $^1\text{H}$  NMR (500 MHz, CD<sub>2</sub>Cl<sub>2</sub>):  $\delta$  1.45 (d,  $J = 0.9$  Hz, 3 H), 2.39 (ddd,  $J = 6.0, 8.5, 14.2$  Hz, 1 H), 2.50 (ddd,  $J = 2.3, 6.0, 14.2$  Hz, 1 H), 3.41–3.43 (m, 2 H), 3.79 (s, 6 H), 4.20–4.22 (m, 1 H), 4.27 (s, 2H), 4.46–4.48 (m, 1 H), 6.33 (dd,  $J = 6.0, 8.5$  Hz, 1 H), 6.90–6.92 (m, 4 H), 7.25–7.37 (m, 7 H), 7.48–7.50 (m, 2 H), 7.60 (d,  $J = 0.9$  Hz, 1 H), 9.64 (s, 1 H), 10.01 (s, NH).

$^{13}\text{C}$  NMR (500 MHz, DCM-*d*6):  $\delta = 12.2$  (CH<sub>3</sub><sup>T</sup>), 38.0 (C-2'), 55.5 (OCH<sub>3</sub><sup>DMT</sup>), 64.8 (C-5'), 75.4 (OCH<sub>2</sub>), 81.7 (C-3'), 84.7 (C-4'), 87.5 (Cq), 87.6 (C-1'), 111.1 (C-5), 114.0, 127.8, 128.8, 129.0 and 131.0 (5 × C-Ar), 136.4 (C-6), 145.9 (Cq), 151.3 (C-2), 159.6 (Cq), 164.2 (C-4), 200.6 (CHO)

ESI MS ( $m/z$ ) calculated for C<sub>40</sub>H<sub>37</sub>N<sub>5</sub>O<sub>9</sub> [M-H], 730.26; found 730.00

IR (KBr)  $\nu_{\text{max}}$  (cm<sup>-1</sup>) 3267.9, 3055.3, 2930.3, 2359.9, 1745.4, 1700.8, 1609.1, 1509, 1461, 1373.8, 1295.7, 1247.7, 1178.6, 1074.9, 1034.4, 942.3, 831, 790.5, 730.6, 701.5, 645.3.

***N*-Acetyl-3'-*O*-(carboxybenzyloxy) deoxyadenosine, 4.26.** To compound **4.25** (1.8 g, 2.4 mmol) was added 3% trichloroacetic acid in dichloromethane (134 mL, 3.6 mmol) at room temperature. The reaction was continued for an additional 15 minutes until TLC indicated reaction completion. The solution was diluted in dichloromethane (10 mL) and concentrated to a dark yellow residue. The pure product was isolated following purification by silica gel column chromatography (Acetone/DCM 2:8 v/v) giving **4.26** (500 mg) as a white solid. Yield: 87% TLC (Acetone/DCM 2:8)  $R_f$ : 0.23. m.p. 79 °C.  $^1\text{H}$  NMR (499.84 MHz, DMSO- $d_6$ ):  $\delta$  10.84 (s, NH), 11.61 (s, NH), 8.7-8.6 (s, 2H), 7.3-7.4 (m, 6H), 6.47 (d,  $J = 8.7$  Hz, 1H), 5.37 (dd,  $J = 5.49, 5$  Hz, 1H), 5.2 (t,  $J = 5$  Hz, 1H), 5.14 (d,  $J = 11$  Hz, 2H), 5.07 (d,  $J = 2$  Hz, 2H), 4.18 (brs, 1H), 3.7 (dd,  $J = 10, 5$  Hz, 2H), 3.07 (dd,  $J = 17.89$  Hz), 2.63 (m, 1H),  $^{13}\text{C}$  NMR (125.699 MHz, DMSO- $d_6$ ):  $\delta$  169.5, 165.5, 154.2, 152.1, 152.0, 151.9, 150.0, 143.2, 135.7, 128.8, 85.6, 84.2, 79.35, 70.6, 69.74, 61.90, 61.820, 40.0. IR(KBr)  $\nu_{\text{max}}$  ( $\text{cm}^{-1}$ ) 3572.1, 3400.3, 1736.0, 1700.5, 1658.3, 1649.7, 1641.3, 1631.0, 1620.0, 1612.7, 1555.7, 1537.9, 1462.6, 1381.7, 1331.3, 1266.9, 1101.0, 938.8, 787.9, 698.4.

MS: [M-H] found 426.26 found 427.0

***N*-Acetyl-5'-carboxy-3'-*O*-(carboxybenzyloxy) deoxyadenosine, 4.27.** *N*-Acetyl-3'-*O*-(carboxybenzyloxy) deoxyadenosine, **4.26** (0.4 g, 0.84 mmol), TEMPO (27 mg, 0.17 mmol) and bis(acetoxy)iodobenzene (BAIB) (547 mg, 1.70 mmol) were dissolved in MeCN/H<sub>2</sub>O (1:1 v/v, 8 mL) and stirred for an additional 3 h at room temperature (22 °C). Following complete reaction, the mixture was diluted in EtOAc (15 mL), washed with brine (2 x 15 mL) and extracted with EtOAc (2 x 15 mL). The combined organic extracts were dried over MgSO<sub>4</sub> and concentrated to

a yellow solid (325 mg, 79%) without the need for purification. TLC (MeOH/DCM 1:9 v/v)  $R_f$ : 0.1. IR(KBr)  $\nu_{\max}$  ( $\text{cm}^{-1}$ ) 3591.1, 3571.7, 3452.0, 1658.1, 1641.2, 1631.0, 488.4. ESI- MS M/Z Calculated for [M-H] 443. Found [M-H] 443 g/mol

**5'-O-(4-dimethoxytrityl) 3'-O-allyl thymidine, 4.30.** To a suspension of 60% NaH (182 mg, 4.55 mmol) in anhydrous THF (10 mL) was added 5'-O-(4-dimethoxytrityl) thymidine, **4.29** (988 mg, 1.82 mmol) under argon at 0 °C. The mixture was sonicated for 20 min, and allyl bromide (400  $\mu\text{L}$ , 9.1 mmol) was added to the reaction mixture which was stirred for an additional 3 h at room temperature (22 °C). The mixture was poured into saturated  $\text{NaHCO}_3$  (20 mL) and extracted with EtOAc (3  $\times$  20 mL). The combined organic extracts were washed with brine (30 mL), dried over  $\text{MgSO}_4$ , filtered and concentrated *in vacuo*. Purification by flash column chromatography (EtOAc–petroleum ether, 1:1 v/v, 1%  $\text{Et}_3\text{N}$ ) afforded **4.30** as a white solid; Yield: 954 mg, 90%;

m.p. 83 °C.  $[\alpha]_D^{22} +16.2$  (c 0.90, acetone).  $R_f = 0.55$  (EtOAc–petroleum ether, 7:3 v/v).

$^1\text{H}$  NMR (500 MHz, acetone- $d_6$ ):  $\delta$  1.47 (d,  $J = 1.4$  Hz, 3 H), 2.35 (ddd,  $J = 5.5, 7.8, 13.5$  Hz, 1H), 2.41 (ddd,  $J = 2.5, 6.0, 13.5$  Hz), 3.39 (d,  $J = 3.7$  Hz, 2 H), 3.79 (s, 6 H), 4.02 (dd,  $J = 5.5, 13.3$  Hz, 1 H), 4.07 (dd,  $J = 5.5, 13.3$  Hz, 1 H), 4.12–4.14 (m, 1H), 4.37–4.39 (m, 1H), 5.14 (m, 1H), 5.26 (m, 1H), 5.85–5.98 (m, 1H), 6.31 (dd,  $J = 6.0, 7.8$  Hz, 1 H), 6.89–6.93 (m, 4 H), 7.24–7.39 (m, 7 H), 7.47–7.50 (m, 2 H), 7.61 (d,  $J = 1.4$  Hz, 1 H), 10.0 (s, NH).  $^{13}\text{C}$  NMR (126 MHz, acetone- $d_6$ ):  $\delta$  12.2, 38.2, 55.5, 64.8, 70.6, 79.9, 84.6, 85.3, 87.5, 111.0, 114.0, 116.9, 127.7, 128.7, 129.0, 131.0, 135.8, 136.5, 145.9, 151.2, 159.7, 164.2. ESI MS (m/z) calculated for  $\text{C}_{34}\text{H}_{36}\text{N}_2\text{O}_7$  [M+Na], 607.2; found 607.2. IR (KBr)  $\nu_{\max}$  ( $\text{cm}^{-1}$ ) = 3182.1, 3059.1, 2929.9,



2836.8, 1693.4, 1607.7, 1582.3, 1508.9, 1464.5, 1364, 1273.5, 1251.1, 1177.1, 1105.4, 1063.1, 1033.5, 915.8, 829.1, 791.1, 755.8, 727.0, 702.1.

**5'-O-(4-dimethoxytrityl)-3'-O-(formylmethylene) thymidine, 4.31.** 5'-O-(4-dimethoxytrityl) 3'-O-allyl thymidine, **4.30** (1.63 g, 2.79 mmol) was dissolved in a mixture of acetone–H<sub>2</sub>O (3:1 v/v, 12 mL). NMO (0.65 g, 5.58 mmol) and 2% OsO<sub>4</sub> in H<sub>2</sub>O (1.8 ml, 7.0 mmol) was added and the mixture was stirred for 2 h at room temperature (22 °C) until TLC indicated complete consumption of starting material. Na<sub>2</sub>S<sub>2</sub>O<sub>5</sub> (0.98 g, 1.6 mmol) was then added and the reaction mixture was stirred for 30 min. The reaction was quenched with H<sub>2</sub>O (50 mL) and the aqueous layer was extracted with EtOAc (3 × 50 mL). The combined organic extracts were washed with brine (100 mL), dried over MgSO<sub>4</sub>, filtered and concentrated *in vacuo*. The residue was dissolved in a mixture of acetone–phosphate buffer pH 7 (3:1 v/v, 22 mL), and NaIO<sub>4</sub> (1.50 g, 7.02 mmol) was added. The mixture was stirred at room temperature for 2 h, filtered, and the precipitate was washed with EtOAc (50 mL). The aqueous layer was extracted with EtOAc (2 × 50 mL) and the combined organic extracts were washed with brine (100 mL), dried over MgSO<sub>4</sub>, filtered and concentrated. The crude product **4.31** (off white solid; 1.64 g, >90%) was isolated without further purification. m.p. 123 °C;  $[\alpha]_D^{22} +3.61$  (c 0.80, acetone);  $R_f = 0.55$  (CH<sub>2</sub>Cl<sub>2</sub>–MeOH, 9:1 v/v).

<sup>1</sup>H NMR (500 MHz, acetone-*d*<sub>6</sub>):  $\delta$  1.45 (d,  $J = 0.9$  Hz, 3 H), 2.39 (ddd,  $J = 6.0, 8.5, 14.2$  Hz, 1H), 2.50 (ddd,  $J = 2.3, 6.0, 14.2$  Hz, 1H), 3.41–3.43 (m, 2H), 3.79 (s, 6 H), 4.20–4.22 (m, 1 H), 4.27 (s, 2H), 4.46–4.48 (m, 1 H), 6.33 (dd,  $J = 6.0, 8.5$  Hz), 6.90–6.92 (m, 4H), 7.25–7.37 (m, 7H), 7.48–7.50 (m, 2 H), 7.60 (d,  $J = 0.9$  Hz, 1 H), 9.64 (s, 1H), 10.0 (s, NH). <sup>13</sup>C NMR (500 MHz, acetone-*d*<sub>6</sub>):  $\delta = 12.2, 38.0, 55.5, 64.8, 75.4, 81.7, 84.7, 87.5, 87.6, 111.1, 114.0, 127.8,$

128.8, 129.0 and 131.0, 136.4, 145.9, 151.3, 159.6, 164.2, 200.6; ESI MS (m/z) calculated for  $C_{33}H_{34}N_2O_8$  [M+H], 586.23; found 585.2; IR (KBr)  $\nu_{\max}$  ( $cm^{-1}$ ) = 3307, 3066.8, 3007.3, 2953.4, 2929.6, 2856.5, 1736.7, 1698.6, 1660.3, 1610.8, 1557.2, 1509.6, 1485.4, 1445.8, 1382.6, 1300.8, 1253.5, 1217.4, 1176.1, 1109.9, 1072, 1034.8, 1002.6, 968.5, 936.6, 890.7, 863.6, 755.8, 704.6, 667.9

**Molecular modeling.** MGL tools 1.5.4 with Autodock tools and AutoDock Vina [35] were used to create and perform blind docking calculations between the GRP78 ATPase binding domain in complex with ATP (PDB: 3LDL) and the 3',5'-diacylhydrazine linked T:A dimer, **4.19**. The molecular models were prepared using AutoDock Tools in PDBQT format. The GRP78 protein was enclosed in a box with the number of grid points located in the  $x \times y \times z$  directions,  $70 \times 86 \times 120$  and with a grid spacing of  $0.375 \text{ \AA}$ . The center of the grid was set to 14.719, 20.979, and  $8.824 \text{ \AA}$ . Lamarckian genetic algorithms, as implemented in AutoDock Vina [35], were employed to perform the docking simulation studies. All other parameters were retained as default settings. For each of the docking cases, the lowest energy docked conformation, according to the AutoDock scoring function, was selected as the binding mode. The output from AutoDock Vina was analyzed using PyMol [36].

#### 4.4. REFERENCES

- [1] Bikard, D.; Loot, C.; Baharoglu, Z.; Mazel, D. *Microbiol. Mol. Biol. Rev.* **2010**, *74*, 570-588.
- [2] Kuznetsov, S.V.; Ren, C.C.; Woodson, S.A.; Ansari, A. *Nucleic Acids Res.* **2008**, *36*, 1098-1112.
- [3] Nakano, M.; Moody, E.M.; Liang, J.; Bevilacqua, P.C. *Biochemistry* **2002**, *41*, 14281-14292.
- [4] Moody, E.M.; Bevilacqua, P.C. *J. Am. Chem. Soc.* **2003**, *125*, 2032-2033.
- [5] Moody, E.M.; Bevilacqua, P.C. *J. Am. Chem. Soc.* **2004**, *126*, 9570-9577.
- [6] Moody, E.M.; Bevilacqua, P.C. *J. Am. Chem. Soc.* **2003**, *125*, 16285-16293.
- [7] Moody, E.M.; Feerrar, J.C.; Bevilacqua, P.C. *Biochemistry* **2004**, *43*, 7992-7998.
- [8] Peyrat, S.; Xie, J. *Synthesis* **2012**, *44*, 1718–1724.
- [9] Micklefield, J. *Curr. Med. Chem.* **2001**, *8*, 1157-1179.
- [10] Hariharan, M.; Siegmund, K.; Lewis, F.D. *J. Org. Chem.* **2010**, *75*, 6236-6243.
- [11] Hariharan, M.; Zheng, Y.; Long, H.; Zeidan, T.A.; Schatz, G.C.; Vura-Weis, J.; Wasielewski, M.R.; Zuo, X.; Tiede, D.M.; Lewis, F.D. *J. Am. Chem. Soc.* **2009**, *131*, 5920-5929.
- [12] Lewis, F.D.; Liu, X. *J. Am. Chem. Soc.* **1999**, *121*, 11928-11929.
- [13] Rumney, S.; Kool, E.T. *J. Am. Chem. Soc.* **1995**, *117*, 5635-5646.
- [14] Xodo, L.E.; Manzini, G.; Quadrifoglio, F.; van der Marel, G.; van Boom, J. *Nucleic Acids Res.* **1991**, *19*, 1505-1511.
- [15] Baumann, U.; Frank, R.; Blöcker, H.; *Eur. J. Biochem.* **1986**, *161*, 409-413.
- [16] Woo, H.M.; Kim, K.S.; Lee, J.M.; Shim, H.S.; Cho, S.J.; Lee, W.K.; Ko, H.W.; Keum, Y.S.; Kim, S.Y.; Pathinayake, P.; Kim, C.J.; Jeong, Y.J. *Antiviral Res.* **2013**, *100*, 337-345.
- [17] Hofmann, M.H.; Heinrich, J.; Radziwill, G.; Moelling, K. *Mol. Cancer Res.* **2009**, *7*, 1635-1644.
- [18] Reynolds, C.H.; Hormann, R.E. *J. Am. Chem. Soc.* **1996**, *118*, 9395-9401.

- [19] Bishop, G.J.; Price, B.J.; Sutherland, I.O. *J. Chem. Soc. Chem. Commun.* **1967**, *14*, 672-674
- [20] Fletcher, J.R.; Sutherland, I.O. *J. Chem. Soc. Chem. Commun.* 1969, *13*, 706-708.
- [21] Lee, H.J.; Lee, M.H.; Choi, Y.S.; Park, H.M.; Lee, K.B. *J. Mol. Struct. (Theochem)*. **2003**, *631*, 101-110.
- [22] Semetey, V.; Hemmerlin, C.; Didierjean, C.; Schaffner, A.P.; Giner, A.G.; Aubry, A.; Briand, J.P.; Marraud, M.; Guichard, G. *Org. Lett.* **2001**, *3*, 3843-3846.
- [23] Lee, H.J.; Ahn, I.A.; Ro, S.; Choi, K.H.; Lee, K.B. *J. Pept. Res.* **2000**, *56*, 35-46.
- [24] Lee, H.J.; Jung, H.J.; Kim, J.H.; Park, H.M.; Lee, K.B. *Chem. Phys.* **2003**, *294*, 201-210.
- [25] Lee, H.J.; Park, H.M.; Lee, K.B. *Biophys. Chem.* **2007**, *125*, 117-126.
- [26] Proulx, C.; Sabatino, D.; Hopewell, R.; Spiegel, J.; Garcia Ramos, Y.; and Lubell, W.D. *Future Med. Chem.* **2011**, *3*, 1139-1164.
- [27] Ni, M.; Zhang, Y.; Lee, A.S. *Biochem J.* **2011**, *434*, 181-188.
- [28] Shiu, R.P.; Pouysségur, J.; Pastan, I. *Proc. Natl. Acad. Sci. USA* **1977**, *74*, 3840-3844.
- [29] Kozutsumi, Y.; Segal, M.; Normington, K.; Gething, M.J.; Sambrook, J. *Nature* **1988**, *332*, 462-464.
- [30] Dong, D.; Stapleton, C.; Luo, B.; Xiong, S.; Ye, W.; Zhang, Y.; Jhaveri, N.; Zhu, G.; Ye, R.; Liu, Z.; Bruhn, K.W.; Craft, N.; Groshen, S.; Hofman, F.M.; Lee, A.S. *Cancer Res.* **2011**, *71*, 2848-2857.
- [31] Martin, S.; Lamb, H.K.; Brady, C.; Lefkove, B.; Bonner, M.Y.; Thompson, P.; Lovat, P.E.; Arbiser, J.L.; Hawkins, A.R.; Redfern, C.P. *Br. J. Cancer* **2013**, *109*, 433-443.
- [32] Williamson, D.S.; Borgognoni, J.; Clay, A.; Daniels, Z.; Dokurno, P.; Drysdale, M.J.; Foloppe, N.; Francis, G.L.; Graham, C.J.; Howes, R.; Macias, A.T.; Murray, J.B.; Parsons, R.; Shaw, T.; Surgenor, A.E.; Terry, L.; Wang, Y.; Wood, M.; Massey, A.J. *J. Med. Chem.* **2009**, *52*, 1510-1513.
- [33] Macias, A.T.; Williamson, D.S.; Allen, N.; Borgognoni, J.; Clay, A.; Daniels, Z.; Dokurno, P.; Drysdale, M.J.; Francis, G.L.; Graham, C.J.; Howes, R.; Matassova, N.; Murray, J.B.;

Parsons, R.; Shaw, T.; Surgenor, A.E.; Terry, L.; Wang, Y.; Wood, M.; Massey, A.J. *J. Med. Chem.* **2011**, *54*, 4034-4041.

[34] Thomas, S.; Sharma, N.; Gonzalez, R.; Pao, P.W.; Hofman, F.M.; Chen, T.C.; Louie S.G.; Pirrung, M.C.; Schönthal, A.H. *PLoS One* **2013**, *8*, e65695.

[35] Trott, O.; Olson, A.J. *J. Comp. Chem.* **2010**, *31*, 455-461.

[36] Grell, L.; Parkin, C.; Slate, L.; Craig, P.A. *Biochem. Mol. Biol. Educ.* **2006**, *34*, 402-407.

[37] Berman, H.M.; Westbrook, J.; Feng, Z.; Gilliland, G.; Bhat, T.N.; Weissig, H.; Shindyalov, I.N.; Bourne, P.E. *Nucleic Acids Res.* **2000**, *28*, 235-242.

[38] Schlecht, R.; Scholz, S.R.; Dahmen, H.; Wegener, A.; Sirrenberg, C.; Musil, D.; Bomke, J.; Eggenweiler, H.M.; Mayer, M.P.; Bukau, B. *PLoS One* **2013**, *8*, e78443.

[39] Johnson, D.C.; Widlanski, T.S. *Org. Lett.* **2004**, *6*, 4643-4646.

[40] Foitzik, R.C.; Devine, S.M.; Hausler, N.E.; Scammells, P.J. *Tetrahedron* **2009**, *65*, 8851-8857.

[41] Luo, P.; Leitzel, J.C.; Zhan, Z.Y.J.; Lynn, D.G. *J. Am. Chem. Soc.* **1998**, *120*, 3019-3031.

[42] (a) Wu, J. C.; Xi, Z.; Gioeli, C.; Chattopadhyaya, J. *Tetrahedron* **1991**, *47*, 2237-2254, (b) Teste, K.; Colombeau, L.; Hadj-Bouazza, A.; Lucas, R.; Zerrouki, R.; Krausz, P.; Champavier, Y. *Carbohydr. Res.* **2008**, *343*, 1490-1495, (c) Seio, K.; Terada, T.; Mizuta, M.; Ohkubo, A.; Taguchi, H.; Sekine, M. *Helv. Chim. Acta* **2007**, *90*, 1946-1965.

## CHAPTER 5: CONCLUSIONS AND CONTRIBUTIONS TO KNOWLEDGE

### 5.1 CONCLUSIONS AND CONTRIBUTIONS TO KNOWLEDGE MADE IN THIS THESIS

#### 5.1.1 Aminoacyl Nucleolipids as DNA Binding Molecules with Anti-Leukemic Activity

The second chapter of this thesis focused on the synthesis and characterization of a series of nucleic acid bioconjugates. The goal of this work was to explore the ability of an aminoacyl nucleolipid bioconjugate to bind to oncogenic DNA sequences and exhibit anti-cancer activity. Towards this research aim, a small library of nucleoside bioconjugates with amino acyl, alkyl amino, alcohol and glycol groups were prepared by a simple, yet versatile synthetic procedure. This included the preparation of a novel *N*-isobutyryl 5'-carboxy 2',3'-bis-*O*-(carbobenzyloxy) guanosine, which served as a useful building block for further diversification. Among the synthesized nucleoside bioconjugates, the aminoacyl nucleoside, with a suitably protected lysine group was extended to the putative aminoacyl nucleolipid following the attachment of the palmitoyl groups. Following selective lysine deprotection under acidic conditions, a highly functionalized cationic nucleolipid was tested for its ability to bind to a GRP78 oncogene and trigger potent cell death activity in cancer. Firstly, the promoter region of GRP78 DNA was synthesized using an ABI 3400 DNA synthesizer. Following GRP78 DNA isolation, binding experiments using gel shift assays, thermal denaturation, CD spectroscopy and dynamic light scattering validated the DNA binding capabilities of the aminoacyl nucleolipid synthesized in this study. In order to assess its anti-cancer activity, the molecule was selected in the NCI's 60 cancer cell line screen (<http://dtp.nci.nih.gov/>). Its bioactivity profile was investigated among a panel of 60 cancer cell types at a single dose (10  $\mu$ M) experiment. Results showed greater than 90% cell death in a single human leukemia cell line (SR-91) from the panel of 60 different

cancer cell types tested. The reported aminoacyl nucleolipid thus represents a useful model for building DNA binding molecules and for the development of potent and selective anti-cancer agents. The significance of this work has been recognized by a recent publication in Bioorganic Medicinal Chemistry Letters and sets the stage for future work on the aminoacyl nucleolipid scaffold and its unprecedented anti-cancer activity.

### **5.1.2 A Fluoroalkyl Phthalocyanine-Cancer Targeting Oligonucleotide Bioconjugate and its Oncogene Photocleavage Activity**

The third thesis chapter reported for the very first time, a chemically robust photosensitizer, the fluoroalkyl phthalocyanine, conjugated with a cancer targeting oligonucleotide (CTO) to seek and destroy oncogenes in the presence of light and oxygen. This feat was accomplished by the preparation of an asymmetric perfluorophthalocyanine (Pc) bearing a carboxylic acid group for bioconjugation with a CTO. The preparation of the Pc was performed by a zinc-promoted macrocyclization reaction of phthalonitrile precursors under microwave radiation. Following exhaustive silica gel chromatographic purification, analyses by NMR, UV-Vis and HRMS, this Pc catalyst demonstrated long-lasting ( $t_{1/2} = 43$  min) singlet oxygen generation without self-decomposition in the photooxidation of  $\beta$ -citronellol. This Pc photosensitizer was then coupled to an antisense oligonucleotide targeting the GRP78 oncogene for applications in cancer-targeted photodynamic therapy (PDT). The complex demonstrated the ability to hybridize to the sense strand of GRP78 DNA and mRNA sequences to afford the putative PcDNA:DNA and PcDNA:mRNA hybrids. These complexes demonstrated good solubility in physiologically relevant phosphate buffer leading to the formation of stable hybrid duplexes ( $T_m$ : 75, 72 °C, respectively) as discerned from thermal denaturation experiments. In a

photooxidation and piperidine cleavage assay, PcDNA and PcDNA:mRNA hybrids demonstrated time-dependent (12 h) oligonucleotide degradation, highlighting their potential in cleaving oncogenes in a sequence specific manner. The photoactive and chemically robust fluorophthalocyanine-CTO bioconjugates thus encompass a new class of potential anti-cancer agents. The impact of this work has been recognized by a featured article in the journal of Chemical Communications. Our publication was selected as the journal cover story, which featured a depiction of our infamous McNulty Atom Wall shedding light and oxygen into a Pc substrate which induced potent degradation of an oncogene target (**Figure 3.3**).

### 5.1.3 The Diacylhydrazine DNA Turn

In chapter four of this thesis, a new class of DNA backbone modification is presented. The replacement of the native 3',5'-phosphodiester bond for a 3',5'-diacylhydrazine linkage is proposed to stabilize the turn-type conformation found within the loop domain of short hairpin DNA, shDNA. Considering the hairpin is a prevalent secondary structure found within DNA and RNA, mimics that may stabilize hairpin structure and function may have widespread utility in biology and medicine. The *N,N'*-diacylhydrazine functional group is especially useful in stabilizing turn-type geometries in small molecules and peptides. Our goal is to establish structural trends that may lead to important biological applications for diacylhydrazine containing nucleic acids.

The molecular modeling for a diacylhydrazine linked T:A dimer indicated a turn-type geometry that was contingent on the influence of the diacylhydrazine moiety. The diacylhydrazine tends to favor a turn-type geometry due to the repulsive stereoelectronic effects of the nitrogen lone pairs which bends the nucleic acid backbone into a turn geometry.



Moreover, this turn geometry is stabilized by the rigid urea which places the T:A base-pairs within hydrogen bonding distances ( $<5 \text{ \AA}$ ). Furthermore, molecular docking studies of the diacylhydrazine linked T:A dimer onto the GRP78 oncoprotein demonstrated tight binding at the ATPase active site also occupied by the ATP substrate. These *in silico* studies demonstrate the potential for shDNA mimic **4.19** to bind and inhibit cell surface GRP78 activity. Inhibition of GRP78 signaling in cancer has shown anti-proliferative effects in malignant tumors en route towards the development of effective anti-cancer strategies. Intrigued by its promising structure-activity profile, the synthesis of the diacylhydrazine linked T:A dimer was attempted. Progress towards the synthesis of the pre-requisite A and T building block nucleic acids for the generation of the target shDNA mimic **4.19** have been reported in this thesis. The synthesis strategy is currently being developed for structure-function studies of the coveted diacylhydrazine linked T:A dimer. In sum, this diacylhydrazine-linked nucleic acid represents a novel class of structures that may mimic biologically active turn conformations for important SAR studies.

## **5.2 PUBLICATIONS, INVENTION DISCLOSURES AND CONFERENCE PRESENTATIONS**

- ***Manuscripts accepted for publication***

1. Patel, P.; Patel, H.; Borland, E.; Gorun, S.M.; Sabatino, D. Chemically robust fluoroalkylphthalocyanine-oligonucleotide bioconjugates and their GRP78 oncogene photocleavage activity. *Chem. Comm.* **2014**, *50*, 6309-6311.

2. Patel, P.; Hanawa, E.; Yadav, R.; Samuni, U.; Marzabadi, C.; Sabatino, D. Synthesis, DNA binding and anti-leukemic activity of an aminoacyl nucleolipid. *Bioorg. Med. Chem. Lett.* **2013**, *23*, 5086-5090.

- ***Manuscripts in preparation***

1. Patel, P.; Rana, R.; Cultrara C.; Sabatino; D. Stabilizing turn-like conformations in short hairpin DNA by the Design, Synthesis and Structural Characterization of Diacylhydrazine-linked T:A Dimers.

- ***Patent Disclosures***

1. Patel, P.; Patel, H.; Borland, E.; Sabatino, D.; Gorun, S. Perfluorophthalocyanine Bioconjugates for Cancer Therapy. SETON 3.8-006 II; U.S. Provisional Patent Application No. 61/875,987; filed September 10, 2013.

- ***Poster Presentations***

1. Patel, P., Patel, M., Rana, N., Goldman, D., Maina, A., Carrion, E., Kozuch, S., Patel, H., Borland, E., Cultrara, C., Yadav, R., Hanawa, E., Blackman, B., Samuni, U., Marzabadi, C., Blake, A., Gorun, S.M., Sabatino, D. Modifying the sizes and shape of nucleic acids by chemical synthesis. June 5, (2014), The New York Academy of Sciences
2. Patel, P., Rana, N., Patel, H., Borland, E., Gorun, S.M., Sabatino, D. Nucleic acid bioconjugates in anti-cancer applications. Bioorthogonal Chemistry in Biology and Medicine' symposium. December 11, (2013), The New York Academy of Sciences.

3. Patel, P.; Maina, A.; Morozko, E.; Joseph, S.; Martinez, I.; Blackman, B.; Blake, A.D.; Sabatino, D. Targeting the glucose regulated protein 78 in cancer therapy. 245th ACS National Meeting & Exposition, New Orleans, LA, United States, April 7-11, 2013 (2013), MEDI-265.
4. Patel, P.; Sabatino, D. Applications of an Aminoacyl Nucleolipid Bio-conjugate in Medicinal Chemistry. 245th ACS National Meeting & Exposition, New Orleans, LA, United States, April 7-11, 2013 (2013), MEDI-134.
5. Patel, P.; Sabatino, D. Applications of an Aminoacyl Nucleolipid Bio-conjugate in Medicinal Chemistry. 17th Annual Petersheim Academic Expositions, Seton Hall University, April 18, 2013.
6. Patel, P.; Sabatino, D. Synthesis and characterization of 5'-modified nucleoside building block. 57th NJ academy of Science Symposium, Seton Hall University, April 21, 2012.
7. Patel, P.; Sabatino, D. Synthesis and characterization of modified nucleoside building block. 16th Annual Petersheim Academic Expositions, Seton Hall University, April 17, 2012.
8. Patel, P.; Mondello, V.; Sabatino, D. Synthesis Making RNA the solid phase synthesis way. 15th Annual Petersheim Academic Expositions, Seton Hall University, April 12, 2011.